

https://dspace.org/

Characterising partially coherent optical fields

Mredlana, Prince Maswazi

2019
https://hdl.handle.net/10539/28190

Downloaded from a DSpace repository. https://dspace.org/

University of the Witwatersrand

Masters of Science

Characterising partially coherent optical fields

Author:
Prince Maswazi
Mredlana

Supervisors:
Dr. Darryl Naidoo
Dr. Cosmas Mafusire
Prof. Andrew Forbes



Structure Light Lab
School of Physics

Declaration of Authorship

I, Prince Maswazi MREDLANA, declare that this thesis titled, "Characterising partially coherent optical fields" and the work presented in it are my own. I confirm that:

- This work was done wholly or mainly while in candidature for a research degree at the CSIR National laser center.
- Where any part of this thesis has previously been submitted for a degree or any other qualification at this University or any other institution, this has been clearly stated.
- Where I have consulted the published work of others, this is always clearly attributed.
- Where I have quoted from the work of others, the source is always given. With the exception of such quotations, this thesis is entirely my own work.
- I have acknowledged all main sources of help.
- Where the thesis is based on work done by myself jointly with others, I have made clear exactly what was done by others and what I have contributed myself.

Signed:

Date:

UNIVERSITY OF THE WITWATERSRAND

Abstract

Faculty of Science
School of Physics

Master of Science

Characterising partially coherent optical fields

by Prince Maswazi MREDLANA

The characterisation of optical fields is an essential task in understanding propagation and interaction with optical elements. The coherence of an optical field is an important factor in the consideration of a suitable characterisation method and traditional characterisation methods are unsuitable for characterisation for some fields across the coherence spectrum. Partially coherent beams have an unstable intensity distribution that changes randomly over time and an averaging function is more suitable to represent them. The Wigner Distribution Function (WDF) is a phase-space function that employs the mutual coherence function and can be used to represent and characterise beams across the entire coherence spectrum. Using theoretical and experimental simulations, we employ the WDF in characterising both coherent beams and partially coherent beams. The simulations yield comparable characterisation parameters and the parameters are also determined from a physical WDF generation experiment.

Acknowledgements

First off, I would like to give honour and thanks to God for giving me the strength to start and finish this dissertation. I would like to thank my supervisor Darryl Naidoo for all his efforts in making sure that I complete this work, my sincere gratitude for your guidance, advices and help throughout the entire process. Even at times when I wasn't at my best, you always had faith in me and treated me the best way a big brother would. I would like to also thank my co-supervisors Dr Cosmas Mafusire and Andrew Forbes. Thank you Cosmas for all the times I spent at UP, the conversations we had and your efforts in making sure I understand the work and I can produce the best work possible. Prof. Andrew, thank you for your guidance and offering your assistance whenever I needed help.

To the CSIR and Dr. Hencharl Strauss, thank you for giving me the opportunity to enrol and complete my MSc. Thank you for the financial support and all the resources you made available to me during this time. I would also like to thank my colleagues at the National Laser Centre for their support and making me feel at home from my first day. A special thanks to Mosima Kgomo, Dr. Monnamme Tlotleng, Lucas Gailele, Dr. Shashi Prabhakar and Dr. Teboho Bell. A well reserved acknowledgement to Chemist Mabena, thank you mfana for being there for me from the first day we met, you were always eager to help me understand concepts and always took time out of your schedule to make sure I was up to par with everything I needed to understand.

I would also like to thank my family for their support. Lastly I would like to thank my fiancée Dineo Molefe and her family for their constant encouragement, care and love. I wouldn't have done this without all your efforts in making sure I am always happy and feeling supported.

Contents

Declaration ii

Abstract iii

Acknowledgements iv

1 Paraxial wave approximation 1

1.1 Paraxial wave equation 1

1.2 Lasers 3

1.3 Paraxial wave propagation 7

1.3.1 Fundamental Gaussian field 10

1.4 Higher order solutions 13

1.4.1 Hermite-Gaussian modes 14

1.4.2 Laguerre Gaussian beams 18

1.5 Summary 20

2 Characterisation 22

2.1 Introduction 22

2.2 Ray optics and ray transfer matrices 22

2.2.1 Gaussian beam 25

Beam width 27

Divergence and curvature 28

Gouy phase 29

2.3 Higher order modes 30

2.3.1 Hermite-Gaussian modes 30

2.3.2 Laguerre Gaussian modes . . . 32
2.4 Beam moments . . . 33
2.4.1 First order moments . . . 33
2.4.2 Second order moments . . . 34
2.5 Characterisation methods . . . 37
2.5.1 Beam width . . . 37
Divergence . . . 38
2.5.2 Beam quality factor . . . 39
2.6 Summary . . . 40

3 Coherence theory **42**
3.1 Introduction . . . 42
3.2 Random light . . . 43
3.2.1 Random processes . . . 43
3.2.2 Random light and its sources . . . 46
3.2.3 The mutual coherence function . . . 47
Temporal coherence . . . 49
Spatial coherence . . . 50
Coherence degree . . . 51
3.3 Gauss-Schell beam . . . 52
3.4 Summary . . . 53

4 Wigner distribution function **55**
4.1 Phase-space optics . . . 56
4.1.1 Spatial and frequency domain . . . 56
4.2 Wigner distribution function . . . 58
4.3 WDF characterisation . . . 61
4.3.1 First order moments . . . 62
4.3.2 Second order moments . . . 64
4.4 Beam quality factor . . . 64

4.5 Summary 65

5 Simulations **66**

5.1 Simulations 66

5.1.1 Sampling 66

5.1.2 Field function 69

Simulation 70

5.2 WDF 75

5.2.1 1D WDF generation 75

5.2.2 2-dimensional WDF generation 77

5.2.3 Partially coherent beams 80

5.3 Summary 80

6 Experiments **84**

6.1 Introduction 84

6.2 Review of experimental methods 85

6.3 Experimental simulation 92

7 Experiment and future work **95**

7.1 Introduction 95

7.1.1 Interferometric set-up 96

7.2 Summary and discussion 99

8 Conclusion **100**

Bibliography **103**

List of Figures

1.1 Laser beam generation inside a laser cavity 5
1.2 The laser beam generation process 6
1.3 A paraxial beam travelling from the source plane $\mathbf{r}_0$ to the observation plane $\mathbf{r}$. 8
1.4 A demonstration of Huygens' wavelets 9
1.5 a) The evolution of the radius of curvature with propagation b) The sign convention of the radius of curvature 11

2.1 A ray propagating between two different media 23
2.2 A ray propagating through an optical system 24
2.3 The beam width is determined from a cross section of the fundamental Gaussian beam. 28
2.4 The change in the Gaussian beam width with propagation . . . 29
2.5 Hermite Gaussian beam intensity profiles 30
2.6 The propagation of the fundamental Gaussian beam against some higher order beam as a function of M^2 32
2.7 Laguerre Gaussian beam intensity profiles 32
2.8 Angular propagation of a wave 34
2.9 a) A symmetric beam centred on axis, b) A non-symmetric beam not centred on-axis 35
2.10 Determination of the standard deviation 36
2.11 Area integration of the cross-sections of a detected beam 38
2.12 A collimated beam focused by a thin lens 39
2.13 Beam width as a function of z 40

3.1 Sets that are contained in a sigma algebra. 44
3.2 Random results generated by a random experiment and approximated by the red Gaussian shaped line 45
3.3 Correlation of vectors $\mathbf{f}$, $\mathbf{v}_0$ and $\mathbf{v}_1$. 47
3.4 The functions $f(t)$ and $f(t+\tau)$ 48
3.5 A Michelson interferometer for the measurement of temporal coherence. 50
3.6 A shear interferometer for the measurement of spatial coherence. 51
3.7 Gaussian-Schell model beams of coherence degree a)$\sigma = 1$ and b)$\sigma = 0.5$ 53

4.1 The k-vector separated into its transverse components 58
4.2 An autocorrelation of the function $u(\mathbf{r})$ 59
4.3 The WDF distribution of a point source $\delta(x - x_0)$ 60
4.4 The WDF distribution of a spherical wave $\exp(i\pi a x^2)$ 61
4.5 Transformation of a 1-dimensional and a 2-dimensional function into 2-dimensional and 4-dimensional WDF distributions respectively. . . 62
4.6 Integration of the WDF. 63

5.1 The domain of points x with a spacing of δ 66
5.2 The function $f(x)$ and the Fourier transform $f(u)$ generated using MATLAB ® 70
5.3 Generated single mode beams, their beam width, divergence and beam quality factor. 73
5.4 Generated multi-mode mode beams, their beam width and beam quality factor which is given by $\mathrm{M}_e^2 = \sum_n c_n[2p + \mathrm{abs}(l) + 1]$ in both transversal directions. 74
5.5 1-dimensional LG beams transformed into 2-dimensional WDF plots 78

5.6 2-dimensional LG beams (left) and their corresponding 2-dimensional WDF centre section plots (right). 81
5.7 Gaussian-Schell model beams (left) and their corresponding WDF plots (right). 82

6.1 The scanning of a beam using a slit 86
6.2 The scanning transparency setup 86
6.3 a) The WDF of a slit. b) The WDF a. a cylindrical lens and b. half positive and negative lenses, both generated using a hologram as complex objects. Image courtesy of K. H. Brenner and A. W. Lohmann [89] 87
6.4 The Wigner distribution function whose section are obtained by several intensity distributions of the beam. Image courtesy of Jagus J. *et al* [87] 89
6.5 Generated WDF distributions. Image courtesy of Jagus J. *et al* [87] 89
6.6 Interferometric WDF generation setup 90
6.7 Interferometric WDF generation results. Image courtesy of Mukamel E. *et al* [90] 91
6.8 Sectional interferometric WDF generation. Image courtesy of Lee C. H. *et al et al* [72] 92
6.9 Results obtained from the experimental simulation and the expected theoretical results 93

7.1 The WDF generation experimental set-up 96
7.2 Position shifting the two Gaussian beams of opposite orientation at 0rad angular shift 97
7.3 Experimentally generated WDFs of a Gaussian beam for a positional and angular shift set size of a) 20 and 4, b) 40 and 11, respectively. 98

7.4 Position shifting the two vortex beams of opposite orientation at 0rad angular shift 98

7.5 a) The experimentally generated WDF of a vortex beam b) The expected WDF of a vortex beam. 99

List of Symbols

x, y, z	spatial coordinates (mm)
v_x, v_y, v_z	frequency coordinates (mm^{-1})
t	time (s)
τ	time delay (s)
∇	Laplace operator
k	wave-vector
r	radial coordinate (mm)
λ	wavelength (μm)
θ, φ, ψ	angle (rad)
N	population density ($\mathrm{atoms/mm}^2$)
$B_{ij}\rho(\nu)$	probability per unit frequency
A_{ij}	spontaneous transition probability
$\rho(\mathbf{r}_i, \mathbf{r}_j)$	radius (m)
P	power ($\mathrm{J\,s}^{-1}$)
ω	angular frequency (rad)
w_0	waist size (mm)
w	width (mm)
ℓ	azimuthal index
p	radial index

1 Paraxial wave approximation

The paraxial wave equation is derived from Maxwell's general wave equation [1, 2], that was developed as a means to describe optical fields which propagate close to the optical axis over relatively long distances. The paraxial wave equation is obtained from a wave-vector approximation called the paraxial approximation and it is particularly significant because it is the underlying approximation used to describe laser beams. The propagation of the paraxial fields is described using Huygen's principle. Lasers generate coherent beams inside the laser resonator in a process that involves absorption, stimulated emission and spontaneous emission. The process occurs when energy is injected into a crystal gain medium that is populated with atoms inside the cavity. In this chapter we explore the laser generation process. The Gaussian beam is the fundamental mode generated in a laser resonator, we explore its characteristics and also introduce higher order modes that are generated for specific resonator geometries.

1.1 Paraxial wave equation

Maxwell's equations were developed to describe an electromagnetic wave that is characterised by a high frequency and short wavelength [3]. According to Maxwell, given a continuous medium described by the spatial coordinates (x, y, z), an electromagnetic field E adheres to the simple *wave-equation* [4]:

$$[\nabla^2 + k^2]E(x, y, z) = 0, \tag{1.1}$$

where $k = \sqrt{k_x + k_y + k_z} = 2\pi/\lambda$ is the *wave-vector* which describes the propagation angle of the field with respect to the axis of propagation z, λ is the wavelength which describes periodicity. The symbol ∇^2 is the Laplace operator which describes how the field changes with reference to the spatial coordinates (x, y, z). For example $\frac{\partial E}{\partial x}$ describes an x change of the field $E(x, y, z)$ with propagation inside the medium in which the field exists [5]. The wave-equation can be simplified by expanding the Laplace operator [6]:

$$\frac{\partial^2 E}{\partial x^2} + \frac{\partial^2 E}{\partial y^2} + \frac{\partial^2 E}{\partial z^2} = -k^2 E, \tag{1.2}$$

where we have omitted the spatial coordinates on the term $-k^2 E$ for simplicity. The field $E(x, y, z)$ can be written as the complex function [7]:

$$E(\mathbf{r}, z) = a(\mathbf{r}) \exp[i\varphi(\mathbf{r}, z)], \tag{1.3}$$

where $a(\mathbf{r})$ is some $\mathbf{r} = (x, y)$ dependent amplitude function and $\varphi(\mathbf{r}, z)$ is some arbitrary phase.

In this work we are interested in light fields that propagate along some axis z and expand very slowly in size by some small angle θ along this propagation axis with respect to the transverse plane (x, y). We consider light fields whose direction vector k makes small angles θ with the optical axis, z, such that $\sin\theta \approx \theta$. This choice of small propagation angles is known as *paraxial approximation* [8, 3]. Given an electromagnetic field $E(\mathbf{r}, z)$ under the paraxial approximation, the spatial profile of the field in the (x, y) plane undergoes small changes when propagating along the z axis [6]. The change in the light field along the transverse direction is much smaller as compared to the change in the z direction and so we can isolate the z term of the wave-function and analyse the terms (x, y) and z separately. Under the paraxial-approximation

we can write Eq.1.3 as [7]:

$$E(\mathbf{r}, z) = u(\mathbf{r}, z)\exp(-ikz), \tag{1.4}$$

where $u(\mathbf{r}, z)$ is the field *amplitude* where the z dependence of the amplitude is a result of negligible diffraction effects. Substituting Eq.1.4 into Eq.1.2 results in the amplitude wave-equation:

$$\frac{\partial^2 u}{\partial x^2} + \frac{\partial^2 u}{\partial y^2} + \frac{\partial^2 u}{\partial z^2} - 2ik\frac{\partial u}{\partial z} = 0. \tag{1.5}$$

For large distances z we get the mathematical relationship between the spatial coordinates [6, 7]:

$$\left|\frac{\partial^2 u}{\partial z^2}\right| \ll \left|\frac{\partial u}{\partial z}\right|, \left|\frac{\partial u}{\partial x}\right|, \left|\frac{\partial u}{\partial y}\right|, \tag{1.6}$$

and thus Eq.1.4 reduces to:

$$\frac{\partial^2 u}{\partial x^2} - 2ik\frac{\partial u}{\partial z} + \frac{\partial^2 u}{\partial y^2} = 0. \tag{1.7}$$

Eq.1.7 is called the *paraxial wave-equation*. Since the paraxial wave-equation describes light that is propagating at almost parallel to the z-axis, it provides some basis for the mathematical description of laser light which remains confined within a small cross-sectional area over relatively long distances. We consider laser light in the next section and we explore its generation.

1.2 Lasers

Laser light is a form of light whose underlying wave function adheres to the paraxial wave-equation. The term LASER is short for "Light Amplification by the Stimulated Emission of Radiation". It is a monochromatic form of light

that is concentrated on a small cross-sectional area and generated by stimulated emission inside a resonant cavity.

The lasing process is based on energy transfer inside a crystal gain medium contained in the laser cavity (Fig.1.1). The crystal is populated with atoms and the atoms have defined and discrete energy levels. The atoms can be excited to a higher energy level from the ground state level by an injection of external energy and they also decay back to the ground state level by losing energy in the form of photons. There are 3 main processes that are involved in the generation of laser light and use the aforementioned energy transfer between atoms; absorption, spontaneous emission and stimulated emission each of which involves the transfer of photons between energy levels. To demonstrate the process of laser generation, we will denote the lowest energy level of the atoms present in the crystal by E_0 (Fig.1.2) and we also define a higher energy level E_1.

To facilitate the generation of laser light, energy in the form of photons is injected into the laser system by the pump process. An atom in the ground state E_0 in the populated crystal absorbs the energy and is elevated to E_1, this process is known as *absorption* (Fig.1.2a). The elevated atom is unstable and there is a probability that it decays and returns to the ground state by losing the absorbed energy in a process called *spontaneous emission*, this process occurs with no external stimuli. Achieving a beam of light requires amplification of the emitted energy and the amplification is achieved through *stimulated emission* (Fig.1.2b). The process of stimulated emission occurs when an atom in E_1 is further excited by external energy, the atom then emits a photon of identical frequency to that of the incident photon (Fig.1.2c) and whose energy level is between E_1 and E_0. The amplified photon completes a round trip inside the laser cavity by being reflected off the cavity mirrors back to the

gain medium and therefore giving rise to continuous re-amplification given the amplified photon meets some cavity condition. If mirror 2 is partially transmitting, a beam of photons is emitted as laser light [9].

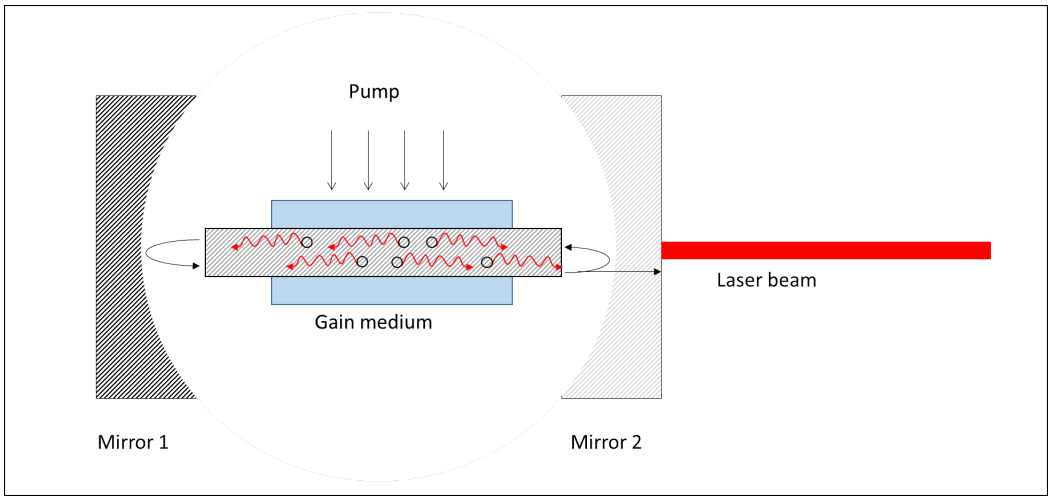


FIGURE 1.1: Laser beam generation inside a laser cavity

The laser generation process is dependent on the probability that the population of atoms present in the bulk medium will absorb and emit photons. There are three terms that describe this probability of decay and population of the energy levels by taking into account the total number of atoms per unit of energy level volume that are present at each time t, for a total number of energy levels $N_t = N_0 + N_1$, where N_0 is the population count of atoms in the ground level and N_1 the population count of atoms in E_1. Depending on the wave frequency ν, the population count of atoms in the ground level will gain energy and deplete at a rate given by [6]:

$$\frac{\partial N_0}{\partial t} = -B_{01}\rho(\nu)N_0, \tag{1.8}$$

where $B_{01}\rho(\nu)$ is the probability per unit frequency that each atom will get excited by the injection of energy. The rate at which the atoms at the level

E_1 will lose energy and decay to the ground level is given by [6]:

$$\frac{\partial N_1}{\partial t} = -A_{10}N_1, \tag{1.9}$$

where A_{10} is the spontaneous transition probability that an atom in E_1 will decay to E_0, A_{10} and B_{01} are formally related to Einstein's A and B coefficients. The occurrence of the spontaneous emission process is dependent on the time ($\tau_{10} = A_{10}^{-1}$) spent by the excited atom in E_1 from which we obtain the solution to Eq.1.9:

$$N_1(t) = N_1(0)\exp\left(\frac{t}{\tau_{12}}\right). \tag{1.10}$$

Stimulated emission is a process that combines both absorption and transmission, and so it combines both the Eqns.1.8 and 1.9:

$$\frac{\partial N_1}{\partial t} = -B_{10}\rho(\nu)N_1, \tag{1.11}$$

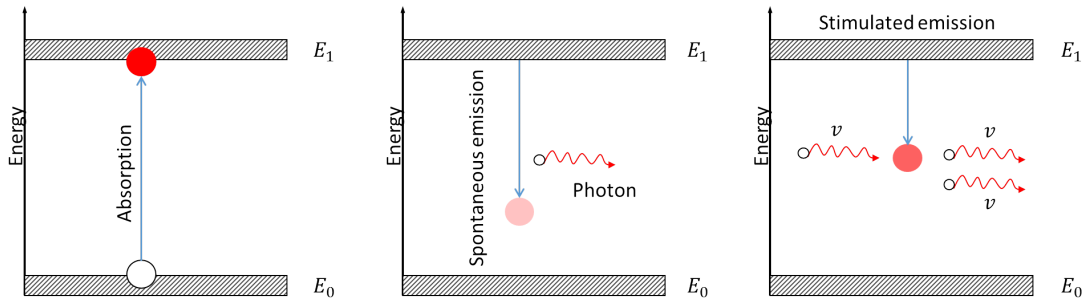


FIGURE 1.2: The laser beam generation process

In the next subsection we explore the propagation of the paraxial wave as it informs the propagation properties of laser light.

1.3 Paraxial wave propagation

Paraxial field propagation is dependent on the form of the phase $\exp(-ikz)$ of the wave. As an example we explore the propagation of a paraxial wave whose phase is quadratic and exhibits spherical attributes. Waves with spherical phases can be obtained from the laser resonator solutions to the paraxial wave-equation.

We consider a spherical wave that is propagating from a source plane $\mathbf{r}_0 = (x_0, y_0)$ to an observation plane $\mathbf{r} = (x, y)$ (Fig.1.3) by analysing changes in its phase function [10, 11]. A paraxial field $E(\mathbf{r})$ with a spherical phase can be described in the form [6]:

$$E(\mathbf{r}) = \frac{1}{\rho(\mathbf{r})}\exp[-ik\rho(\mathbf{r})]. \tag{1.12}$$

Eq.1.12 describes a paraxial wave field $E(\mathbf{r})$ emanating from a source plane $\mathbf{r}_0$ and observed at a plane $\mathbf{r}$. The quantity $\rho(\mathbf{r})$ describes the radial distance between the source and observation planes, and it is expanded as [6]:

$$\rho(\mathbf{r}) = \sqrt{(x - x_0)^2 + (y - y_0)^2 + (z - z_0)^2}. \tag{1.13}$$

The field $E(\mathbf{r}, z)$ can be estimated at the observation plane in various ways depending on the magnitude of $\rho(\mathbf{r})$. Fresnel's diffraction approximation [12] is used to estimate the propagation of the field where $\rho(\mathbf{r})$ is described at distances such that:

$$(z - z_0) \gg \sqrt{(x - x_0)^2 + (y - y_0)^2}. \tag{1.14}$$

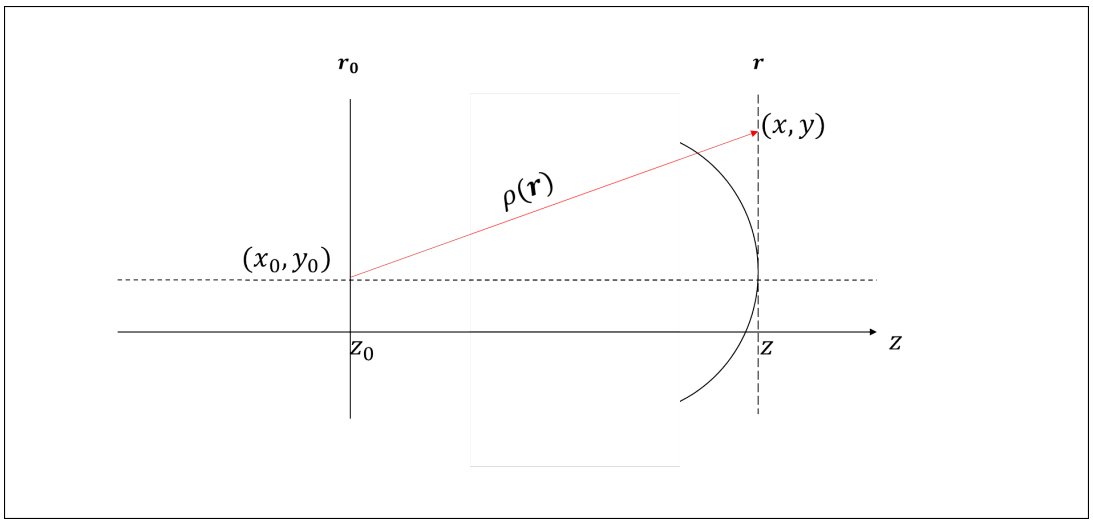


FIGURE 1.3: A paraxial beam travelling from the source plane $\mathbf{r}_0$ to the observation plane $\mathbf{r}$.

For Fresnel's approximation, the distance function $\rho(\mathbf{r})$ can be approximated and expanded by a Taylor series [13, 14]:

$$\rho(\mathbf{r}) \approx (z - z_0) + \frac{(x - x_0)^2 + (y - y_0)^2}{2(z - z_0)} - \frac{[(x - x_0)^2 + (y - y_0)^2]^2}{8(z - z_0)^3} + \frac{[(x - x_0)^2 + (y - y_0)^2]^6}{32(z - z_0)^5} + \cdots \tag{1.15}$$

The Fresnel diffraction approximation of the radial distance function renders all terms higher than the quadratic term negligible at least for the phase term $\exp[-ik\rho(\mathbf{r}]$ since the increase in the exponent of $(z - z_0)$ brings the terms very close to zero. For the term $1/\rho(\mathbf{r})$ however, we can ignore the quadratic term altogether as it also becomes negligibly small at and beyond the quadratic term. Using the Taylor series expansion (Eq.1.15), the paraxial field (Eq.1.12) can then be written as:

$$E(\mathbf{r}, z) \approx \frac{1}{z - z_0} \exp\left\{ - ik\left[(z - z_0) + \frac{(x - x_0)^2 + (y - y_0)^2}{2(z - z_0)}\right]\right\}. \tag{1.16}$$

The Fresnel approach is used to describe fields that are emitted by a single point source. Laser beams operate similarly to a source that emits at multiple

points simultaneously and so we also need an approach that considers paraxial fields as emitted by multiple point sources. The Huygens principle is best suited for this approach.

Huygens' principle is based on a theory that the propagation distribution of a light field that is defined on a closed source surface can be treated as a result of an infinite number of infinitesimal point sources on the surface that produces spherical waves or "Huygens' wavelets" (Fig.1.4). The total field is determined by summing over all the Huygens' wavelets at the source plane and beyond.

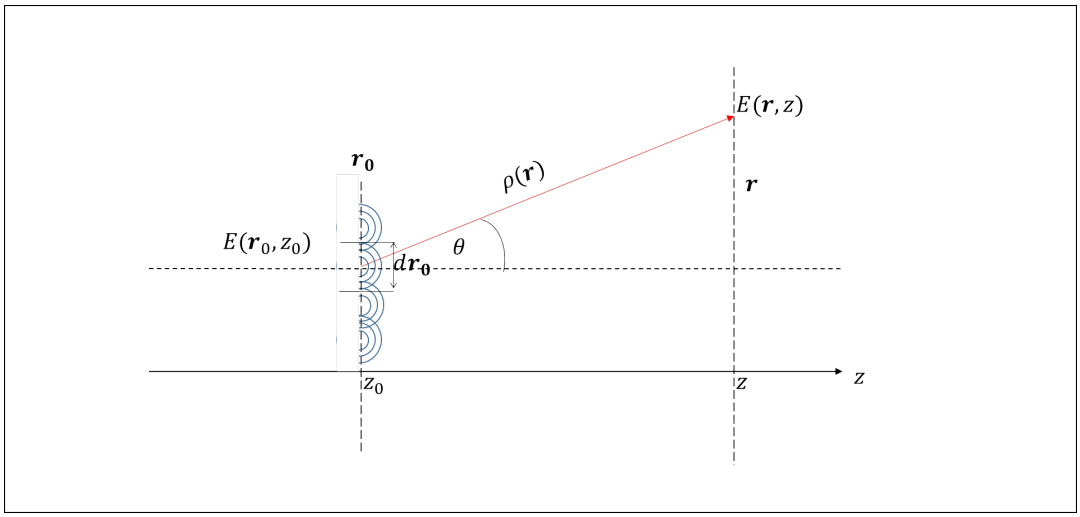


FIGURE 1.4: A demonstration of Huygens' wavelets

According to Huygens' principle, the total field as a result of Huygens' wavelets at a plane $\mathbf{r}_0$ is given by [6]:

$$E(\mathbf{r},z) = \frac{i}{\rho(\mathbf{r})\lambda}\int\int_{\mathbf{r}_0} E(\mathbf{r}_0,z_0)\exp[-ik\rho(\mathbf{r})]\cos[\theta(\mathbf{r})]d\mathbf{r}_0, \tag{1.17}$$

where $\mathbf{r}_0$ represents the source plane surface area, i/λ is a normalization factor and $\cos[\theta(\mathbf{r},\mathbf{r}_0)]$ is the obliquity factor which is a function of the angle of propagation of the resultant secondary wavelets with respect to the z-axis. For an input paraxial wave field emanating from a source plane at $z = z_0$, we employ the paraxial spherical phase approximation in Eq.1.16, Eq.1.17 then

becomes:

$$E(\mathbf{r},z) \approx \frac{i\exp[-ik(z-z_0)]}{\lambda(z-z_0)} \int\int E_0(x_0,y_0), \\ \times \exp\Bigg\{ -ik\Bigg[(z-z_0) + \frac{(x-x_0)^2+(y-y_0)^2}{2(z-z_0)}\Bigg]\Bigg\} dx_0 dy_0. \tag{1.18}$$

In the above equation, the obliquity factor is approximated to unity by making the angle $\theta \leq 0.5\ rad$ such that we are within paraxial approximation and the field propagates close to the z axis with little expansion in the transverse plane.

Since we can separate a paraxial field into a product of the amplitude and z dependent phase factor, we can write the Huygens' integral equation as:

$$E(\mathbf{r},z) = u(\mathbf{r},z)\exp(-ikz), \tag{1.19}$$

such that:

$$u(x,y,z) \approx \frac{i}{\lambda(z-z_0)} \int\int u_0(x_0,y_0,z_0) \\ \times \exp\Bigg\{ -ik\Bigg[(z-z_0) + \frac{(x-x_0)^2+(y-y_0)^2}{2(z-z_0)}\Bigg]\Bigg\} dx_0 dy_0. \tag{1.20}$$

The process that occurs inside the laser resonator/cavity generates paraxial wave solutions which are called transverse modes given specific boundary conditions of the resonator. The paraxial wave approximation of spherical phase waves informs the mathematical basis for the fundamental Gaussian mode. In the following section we explore the fundamental Gaussian mode and we study its properties. We also investigate higher order solutions of the wave-equation that are described in rectangular and circular symmetry.

1.3.1 Fundamental Gaussian field

The Gaussian field is the fundamental solution of the paraxial wave-equation that is extensively used as a basis for the description of laser beams. The

fundamental Gaussian beam equation is developed by considering an approximation of a field amplitude $u(\mathbf{r})$ at a plane $\mathbf{r}$, a distance z from the source plane $\mathbf{r}_0$. The distance z such that $z - z_0$ is sufficiently large compared to the quantities $x - x_0$ and $y - y_0$ as depicted in Fig.1.5. The field amplitude at the observation plane can be approximated using the paraxial approximation and is given by the function [6]:

$$\begin{aligned} u(x,y,z) &\approx \frac{1}{z-z_0}\exp\left\{-ik\left[(z-z_0)+\frac{(x-x_0)^2+(y-y_0)^2}{2(z-z_0)}\right]\right\} \\ &\approx \frac{1}{R(z)}\exp\left\{-ik\left[(z-z_0)+\frac{(x-x_0)^2+(y-y_0)^2}{2R(z)}\right]\right\}. \end{aligned} \tag{1.21}$$

In the above equation we have introduced the radial distance function $R(z) = z - z_0$ which is the *radius of curvature* and can also be written as $R(z) = R_0 + z - z_0$ where R_0 is the radius of curvature at the source plane and so $R = R_0(\approx 0) + z$ at $z_0 = 0$.

The radius of curvature can either be negative or positive depending on the nature of the propagation of the field, for a diverging field we select $R > 0$ (Fig.1.5a) and for a converging field $R < 0$ (Fig.1.5b).

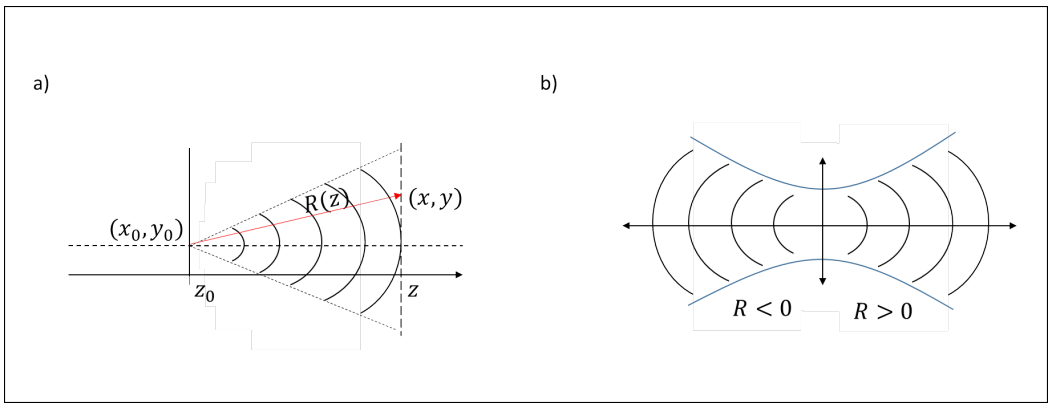


FIGURE 1.5: a) The evolution of the radius of curvature with propagation b) The sign convention of the radius of curvature

As much as Eq.1.21 describes the paraxial propagation of a spherical phased light field, it is not useful for the description of a real physical beam because

the transverse profile of a real physical beam does not evolve linearly as it propagates. The radius of curvature maintains a linear increase within some distance $z - z_0$ and then it gradually increases beyond $z - z_0$ [15]. Another anomaly with the description of the real radius of curvature is encountered at the source plane, when $z_0 = 0$ the spherical phase becomes ∞. To solve these two problems we explore the use of complex coordinates.

We set both x_0 and y_0 to zero and subtract a complex quantity q_0 from z_0. This subtraction does not affect the beam in the real plane as the shift is in the imaginary plane but allows us to have a continuous radius of curvature at and beyond the source plane. The complex radius of curvature can then be written as:

$$\begin{aligned} R(z) &= R_0 + z - (z_0 - q_0) \\ &= R_0 + q(z), \end{aligned} \tag{1.22}$$

where $q(z) = z - (z_0 - q_0)$ such that at the source plane $q(z_0) = q_0$. We substitute Eq.1.22 into Eq.1.21 and we get the function:

$$\begin{aligned} u(x, y, z) &= \frac{1}{z - (z_0 - q_0)} \exp\left[- ik \frac{x^2 + y^2}{2(z - (z_0 - q_0))} \right] \\ &= \frac{1}{q(z)} \exp\left[- ik \frac{x^2 + y^2}{2q(z)} \right]. \end{aligned} \tag{1.23}$$

We can separate the q-parameter $q(z)$ into its real $q_r(z)$ and imaginary $q_i(z)$ parts, such that:

$$\frac{1}{q(z)} = \frac{1}{q_r(z)} - i \frac{1}{q_i(z)}. \tag{1.24}$$

In real physical beams the term $q_r(z)$ is related to curvature and $q_i(z)$ is related to the transversal size of the beam. This can be incorporated into Eq.1.23 and

we obtain the amplitude equation [6]:

$$u(x,y,z) = \frac{1}{q(z)}\exp\left[-ik\frac{x^2+y^2}{2R(z)} - k\frac{x^2+y^2}{\omega^2(z)}\right], \tag{1.25}$$

where $w(z)$ is a transversal profile property that is a measure of the transversal "size" of the Gaussian amplitude. The q-parameter is then written as [3]:

$$\frac{1}{q(z)} = \frac{1}{R(z)} - i\frac{\lambda}{\pi\omega^2(z)}, \tag{1.26}$$

such that the Gaussian field becomes:

$$E(x,y,z) = \frac{1}{q(z)}\exp\left[-ik\frac{x^2+y^2}{2R(z)} - k\frac{x^2+y^2}{\omega^2(z)}\right]\exp(-ikz). \tag{1.27}$$

The Gaussian field (Eq.1.27) is used as a basis for the formulation of Gaussian beams that are generated by a laser. We also note that the complex parameter $q(z)$ describes a Gaussian field completely as it describes the variation in the radius of curvature with propagation and also the transversal size of the intensity profile. In the following section we explore higher order solutions to the wave paraxial equation.

1.4 Higher order solutions

Higher order soltions to the paraxial-wave equation depend on the geometry of the resonator and its boundary conditions, these solutions include the Laguerre-Gaussian and Hermite-Gaussian beams whose underlying basis functions are the Hermite and Laguerre functions, respectively. There are various ways in which we can derive these solutions, the fundamental Gaussian beam uses a direct geometrical approach and in this instance we use a differential trial solution method [3].

To derive the Gaussian beam wave-equation, we assume a trial solution to satisfy the amplitude paraxial equation [6]:

$$u(x,y,z) \quad = A(z)\exp\left[-ik\frac{x^2+y^2}{2q(z)}\right], \tag{1.28}$$

such that $A(z)$ and $q(z)$ are initially unknown, we want to find solutions to both of these parameters that fit the paraxial wave equation. If we substitute this trial solution into Eq.1.7 we get the following expression:

$$\left[\left(\frac{k}{z}\right)^2\left(\frac{dq}{dz}-1\right)(x^2+y^2)-\frac{i2k}{q}\left(\frac{q}{A}\frac{dA}{dz}+1\right)\right]\mathrm{A}(z)=0. \tag{1.29}$$

To obtain a solution that satisfies this equation for all x and y, we can set both the differential parts of this equation to zero which results in the solutions:

$$\begin{aligned}\frac{dq}{dz}&=1,\\ \frac{dA}{dz}&=-\frac{A}{q}.\end{aligned} \tag{1.30}$$

The solutions to Eq.1.30 are $q(z) = q_0 + z - z_0$ and $\frac{A(z)}{A_0} = \frac{q_0}{q(z)}$ which give us exactly the spherical wave given in Eq.1.25 for some constant A_0. We extend this trial solution method to obtain the Hermite Gaussian solution of rectangular symmetry.

1.4.1 Hermite-Gaussian modes

We assume that the paraxial wave equation is separable in rectangular coordinates [3, 7]:

$$u(x,y,z) = u_n(x,z)u_m(y,z), \tag{1.31}$$

which then allows us to find the solution in just one transverse coordinate and we can apply the solution to the other coordinate by substitution. We can

thus apply the same separation of the transverse coordinates to Eq.1.7 which in both coordinates is reduced to:

$$\begin{aligned}\frac{\partial^2 u(x,z)}{\partial x^2} - 2ik\frac{\partial u(x,z)}{\partial z} = 0,\\ \frac{\partial^2 u(y,z)}{\partial y^2} - 2ik\frac{\partial u(y,z)}{\partial z} = 0.\end{aligned} \tag{1.32}$$

For this derivation we pick a more general trial function that includes an unknown function $h_n(x)$ evaluated in rectangular coordinates. The trial function for the wave function $u(x,z)$ is given by:

$$u(x,z) = A[q(z)] \times h_n\left[\frac{x}{p(z)}\right]\exp\left[-ik\frac{x^2}{2q(z)}\right], \tag{1.33}$$

where A$[q(z)]$ and $h_n(x/p(z))$ are initially unknown quantities and we identify $p(z)$ as a distance dependent scaling factor. Using the conditions given in Eq.1.30, specifically the differential $dq/dz = 1$, we substitute Eq.1.33 into Eq.1.7 and obtain a differential equation of the function h_n given by:

$$h_n'' - 2ik\left[\frac{p}{q} - p'\right]xh_n' - \frac{ikp^2}{q}\left[1 + \frac{2q}{A}\frac{dA}{dq}\right]h_n = 0. \tag{1.34}$$

The above equation is similar to the differential equation for Hermite functions of order n:

$$\mathrm{H}_n'' - 2\left(\frac{x}{p}\right)\mathrm{H}_n' + 2n\mathrm{H}_n = 0. \tag{1.35}$$

We notice that the Eqns.1.34 and 1.35 have a similar structure and we can find a common solution that connects them if we can find solutions for $A(q)$

and $p(z)$ such that:

$$\begin{aligned} 2ik\left[\frac{p}{q}-\frac{dp}{dz}\right] &= \frac{2}{p}, \\ -\frac{ikp^2}{q}\left[1+\frac{2q}{\mathrm{A}}\frac{d\mathrm{A}}{dq}\right] &= 2n \end{aligned} \tag{1.36}$$

There are various solutions to the terms in Eqns.1.36 with each solution leading to a different class of higher order Hermite-Gaussian modes. For simplicity we explore a more widely used Hermite-Gaussian solution which we will use as an example in this text to describe the structure of rectangular symmetric solutions. We assume that $p(z)$ is a real quantity and is related to the Gaussian transversal width $w(z)$ by the equation [6]:

$$\frac{1}{p(z)} = \frac{\sqrt{2}}{w(z)}. \tag{1.37}$$

Taking into account that $w(z)$ depends on $p(z)$, it has to satisfy the q-parameter differential equation in Eq.1.36 which is used to obtain the equation [6]:

$$\begin{aligned} \frac{1}{w^2(z)} &= \frac{-ik}{2}\left[\frac{1}{q^*(z)}-\frac{1}{q(z)}\right], \\ &= \frac{ik}{2}\frac{q^*(z)-q(z)}{q(z)q^*(z)}. \end{aligned} \tag{1.38}$$

such that $q^*(z)$ is the complex radius of curvature and it satisfies:

$$\begin{aligned} \frac{dq^*}{dz} &= 1, \\ q^*-q &= q_0^*-q_0. \end{aligned} \tag{1.39}$$

The only equation we need to satisfy now is $A(q)$, we use the definition of the q-parameter and that $dq^* = dq$. We can then rewrite the A dependent differential of Eq.1.36 as:

$$\frac{d\mathrm{A}}{\mathrm{A}} = -\frac{1}{2}\frac{dq}{q}+\frac{n}{2}\left[\frac{dq^*}{q^*}-\frac{dq}{q}\right], \tag{1.40}$$

from which we integrate both sides to get the solution:

$$A(q) = A_0 \left[\frac{q_0}{q(z)}\right]^{1/2} \left[\frac{q_0}{q_0^*}\frac{q^*(z)}{q(z)}\right]^{1/2}. \tag{1.41}$$

We have derived solutions for both $A[q(z)]$ and $h_n[x/p(z)]$, we can then write the normalized Hermite Gaussian beam in free space propagation as:

$$\begin{aligned} u_n(x,z) = &\left[\frac{2}{\pi}\right]^{1/4} \left[\frac{1}{2^n n! w_0}\right]^{1/2} \left[\frac{q_0}{q(z)}\right]^{1/2} \left[\frac{q_0}{q_0^*}\frac{q^*(z)}{q(z)}\right]^{n/2}, \\ &\times \mathrm{H}_n\left[\frac{\sqrt{2}x}{w(z)}\right] \exp\left[-i\frac{kx^2}{2q(z)}\right], \end{aligned} \tag{1.42}$$

where the overall solution in 2-dimensions is given by:

$$\begin{aligned} u_{n,m}(x,y,z) = &\left[\frac{2}{\pi}\right]^{1/2} \left[\frac{1}{2^n n! w_0}\right] \left[\frac{q_0}{q(z)}\right] \left[\frac{q_0}{q_0^*}\frac{q^*(z)}{q(z)}\right]^{n}, \\ &\times \mathrm{H}_n\left[\frac{\sqrt{2}x}{w(z)}\right] \mathrm{H}_m\left[\frac{\sqrt{2}y}{w(z)}\right] \exp\left[-i\frac{k(x^2+y^2)}{2q(z)}\right]. \end{aligned} \tag{1.43}$$

Since the q-parameter is a complex quantity, like all complex numbers we can associate with it an angle which in this case is called a Gouy phase, we also associate with it an amplitude. The Gouy phase takes into account the evolution of the phase which is almost planar at the source plane and it becomes more spherical with propagation and this phase change is mitigated by the Guoy phase [7]. The complex q-parameter written in terms of an angle and amplitude is given by [7, 6]:

$$\begin{aligned} \frac{i}{q} &= \frac{\lambda}{\pi w^2(z)}\left[1 + i\frac{\pi w^2}{\lambda R(z)}\right], \\ &\equiv \frac{1}{|q|}\exp[i\psi(z)] \end{aligned} \tag{1.44}$$

such that $\tan[\psi(z)] = \pi w^2/\lambda R(z)$. Using this definition for q, it can be shown that the quantity $q_0/q(z)$ in Eq.1.43 can be written as:

$$\frac{1}{w_0}\frac{q_0}{q(z)} = \frac{1}{\omega(z)}\exp[i(\psi(z) - \psi_0)], \tag{1.45}$$

from which we can rewrite both the fundamental Gaussian and Hermite Gaussian paraxial approximations. The first order Gaussian beam is amended and written as:

$$u_n(x,z) = \left(\frac{2}{\pi}\right)^{1/4}\left[\frac{1}{\omega(z)}\exp[i(\psi(z) - \psi_0)]\right]^{1/2}\exp\left[-i\frac{kx^2}{2q(z)}\right], \tag{1.46}$$

and the higher order Hermite Gaussian function is written as:

$$\begin{aligned} u_{n,m}(x,y,z) = &\left[\frac{2}{\pi}\right]^{1/2}\left[\frac{1}{2^n n! w_0}\right]^{1/2}\left[\frac{1}{2^m m! w_0}\right]^{1/2}\left[\frac{q_0}{q(z)}\right]\mathrm{H}_n\left[\frac{\sqrt{2}x}{w(z)}\right] \\ &\mathrm{H}_m\left[\frac{\sqrt{2}y}{w(z)}\right] \times \exp\left[-i\frac{k(x^2+y^2)}{2q(z)}\right]\exp[i2(\psi(z) - \psi_0)]. \end{aligned} \tag{1.47}$$

It should also be noted that the first order Gaussian beam is the fundamental solution of Eq.1.47 for $n, m = 0$:

$$\begin{aligned} u_{0,0}(x,y,z) = &\left[\frac{2}{\pi}\right]^{1/2}\left[\frac{1}{w_0}\right]\left[\frac{\sqrt{2}x}{w(z)}\right]\left[\frac{q_0}{q(z)}\right] \times \exp\left[-i\frac{k(x^2+y^2)}{2q(z)}\right] \\ &\times \exp[i2(\psi(z) - \psi_0)]. \end{aligned} \tag{1.48}$$

We now explore higher order solutions of circular symmetry.

1.4.2 Laguerre Gaussian beams

The Laguerre Gaussian solution is obtained from the paraxial wave-equation written in radial coordinates (r, φ) [16]:

$$\frac{\partial^2 u}{\partial r^2} + \frac{1}{r}\frac{\partial u}{\partial r} - 2ik\frac{\partial u}{\partial z} = 0. \tag{1.49}$$

An appropriate trial function for the derivation is [6]:

$$u(r,\varphi,z) = A(z) \times \exp\left[-ik\frac{r^2}{2q(z)}\right] s(r)\exp(im\varphi) \tag{1.50}$$

where $S(r)$ is an unknown radial function. Substituting Eq.1.50 into Eq.1.49 results in the differential equation:

$$\begin{aligned} s^{''}(r) + s^{'}(r)\left[\frac{1}{r} - i2k\frac{r}{q(z)}\right] - s(r)\left[ik^2\frac{r^2}{q(z)^2} - 2ik\frac{1}{q(z)}\right. \\ \left. + ik^2r^2\frac{q^{'}(z)}{q(z)} + i2k\frac{A^{'}(z)}{A(z)}\right] = 0. \end{aligned} \tag{1.51}$$

To find the solutions for $A(z)$ and $q(z)$ in this instance we can compare Eq.1.51 to the Laguerre polynomial differential equation:

$$r\frac{d^2}{dr^2}L_p^\ell + (\ell + 1 - r)\frac{d}{dr}L_p^\ell + pL_p^\ell = 0 \tag{1.52}$$

Using the assumptions in Eq.1.30, Eq.1.51 reduces to:

$$s^{''}(r) + s^{'}(r)\left[\frac{1}{r} - i2k\frac{r}{q(z)}\right] - s(r)\left[i2k^2\frac{r^2}{q(z)^2}\right] = 0. \tag{1.53}$$

From Eq.1.52 and Eq.1.53, the solutions for $A(z)$ and $q(z)$ are obtained when:

$$\begin{aligned} \frac{1}{r} &= 1, \\ (\ell + 1 - r) &= \frac{1}{r} - i2k\frac{r}{q(z)}, \\ p &= i2k^2\frac{r^2}{q(z)^2}. \end{aligned} \tag{1.54}$$

where ℓ and p are the azimuthal and radial indices, respectively. Using Eq.1.54 and Eq.1.53, $s(r)$ is then given by:

$$s(r) = \left(\frac{\sqrt{2r}}{w_0}\right)^\ell L_p^\ell\left(\frac{2r^2}{w_0^2}\right). \tag{1.55}$$

Applying the same solution path as that applied in obtaining Eq.1.47, the solution for $s(r)$ is obtained by assuming $q(z)$ is real and related to the transversal Gaussian profile width $w(z)$ by the equation:

$$\frac{1}{q(z)} = \frac{\sqrt{2}}{w(z)} \tag{1.56}$$

Substituting Eq.1.56 into Eq.1.50 gives us:

$$u(r,\varphi,z) = A[q(z)] \times \exp\left[-ik\frac{r^2}{2}\frac{\sqrt{2}}{w(z)}\right] S(r)\exp(im\varphi) \tag{1.57}$$

Applying the same solution path as that applied into obtaining Eq.1.47, the normalized Laguerre Gaussian (LG) modes are then given by:

$$\begin{aligned} u_{p\ell}(r,\varphi,z) = \frac{1}{w(z)}\left[\frac{2p!}{\pi(|\ell|+p)!}\right]^{1/2} \exp[-i(2p+|\ell|+1)\psi_0] \\ \times \left(\frac{\sqrt{2}r}{w(z)}\right)^{|\ell|} L_p^{|\ell|}\left[\frac{2r^2}{w^2(z)}\right]\exp\left[-\frac{ikr^2}{2q(z)} + i\ell\varphi\right], \end{aligned} \tag{1.58}$$

Similar to the Hermite Gaussian case, the first order Gaussian mode is also the fundamental solution of the LG equation for $\ell = p = 0$:

$$u_{p\ell}(r,\varphi,z) = \frac{\sqrt{2}}{\pi w(z)}\left[\frac{2r^2}{w^2(z)}\right]\exp\left[-\frac{ikr^2}{2q(z)}\right]\exp[-i\psi_0], \tag{1.59}$$

1.5 Summary

In this chapter we introduced the fundamental theory of laser light and solutions to the paraxial wave equation generated in the laser resonator to understand the mathematical formulation and generation of modes in solid state lasers. Understanding the formulation of these paraxial fields is important for characterisation purposes. We studied that natural sources of light generate a type of light that spreads at relatively large angles with respect to the optical axis and paraxial waves operate under the paraxial operation and travel almost

parallel to the optical axis, this in effect informs the nature of real laser light that propagates as a beam that is confined within a small cross-sectional area over long distances. Various classes of solutions to the paraxial wave equation generated inside the laser resonator, in particular the low order fundamental Gaussian beam and higher order solutions of rectangular and cylindrical symmetry were explored. These solutions inform the structure and properties of laser beams and in the next chapter we explore how they are characterised.

2 Characterisation

2.1 Introduction

Beam moments are used as a general characterisation method to calculate beam parameters such as the beam width and the radius of curvature [17, 18]. Characterising laser light is an important task in optics in that it allows us to understand the interaction of light with optical elements. In this work we employ the beam quality factor (M^2) which is calculated from the beam width, divergence and radius of curvature. The beam quality factor is a parameter that is used as a measure of how the beam width of a higher order mode differs from that of the fundamental Gaussian beam ($M^2 = 1$) in free space propagation and it can be used to uniquely identify certain higher order modes. We begin this chapter by exploring ray optics which informs the theory of how parameters of paraxial beams change in interaction with optical elements. Beam parameters such as the beam width are introduced in the context of the fundamental Gaussian beam and higher order modes, we also explore the experimental and computational methods used to determine these parameters.

2.2 Ray optics and ray transfer matrices

Ray optics is an approximation of wave-theory and considers waves of very short wavelengths [19]. In ray optics, light is treated as a bundle of rays propagating in space. Rays reflect and refract when they interact with different media/material that are characterised by a refractive index n. The refractive index is a constant that represents a measure of how the surface of a specific medium changes the propagation direction of a ray [20, 21, 22, 23]. The medium in which rays propagate are classified

into two categories, homogeneous and non-homogeneous media. Homogeneous media have a uniform composition and so the refractive index is the same throughout the medium, non-homogeneous materials however have varying composition and the refractive index is a function of position $n(\mathbf{r})$ within the material.

The propagation of rays between media is described by *Snell's law* (Fig.2.1) [19, 24]:

$$\frac{n_0}{n_1} = \frac{\sin\theta_1}{\sin\theta_0}, \tag{2.1}$$

where n_0 and n_1 are the media refractive indices, θ_0 the angle of propagation of the incident ray and θ_1 is the resultant angle of propagation.

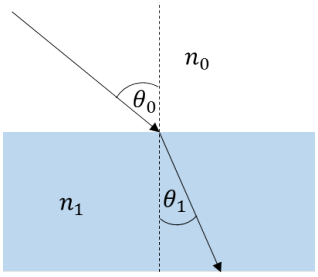


FIGURE 2.1: A ray propagating between two different media

Ray interaction with media can be further described by aid of a ray transfer matrix [25, 26, 27] as demonstrated in Fig.2.2. The ray emanates from a position $\mathbf{r}_0 = (x_0, y_0)$ and travelling at an angle θ_0 inside a medium of uniform refractive index n, after interaction of the ray with the optical system, the output position r_1 and angle θ_1 of propagation of the ray is given by [7, 3]:

$$\begin{aligned} \mathbf{r}_1 &= A\mathbf{r}_0 + B\theta_0, \\ \theta_1 &= C\mathbf{r}_0 + D\theta_0, \end{aligned} \tag{2.2}$$

where A, B, C and D are constants that describe properties of the optical system. Using a matrix notation, the Eqns.2.2 can be written as:

$$\begin{bmatrix} \mathbf{r}_1 \\ \theta_1 \end{bmatrix} = \begin{bmatrix} \mathrm{A} & \mathrm{B} \\ \mathrm{C} & \mathrm{D} \end{bmatrix} \begin{bmatrix} \mathbf{r}_0 \\ \theta_0 \end{bmatrix} \tag{2.3}$$

There are various optical elements whose interaction with rays can be described using the ray transfer matrix, we consider free space propagation by a distance L and propagation through a thin lens.

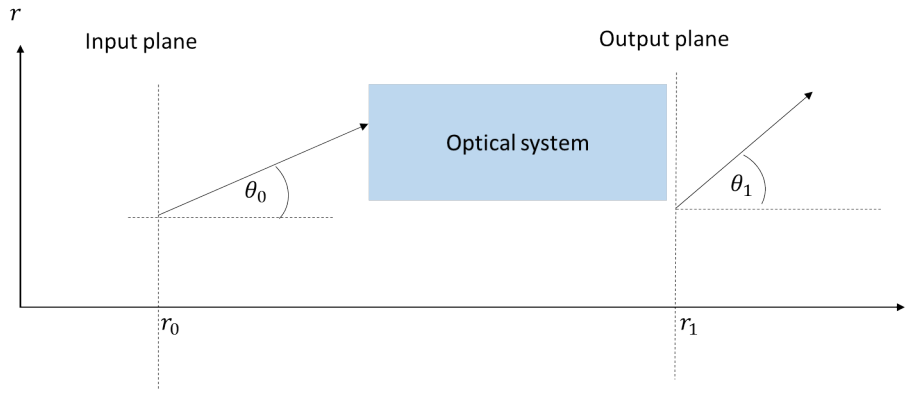


FIGURE 2.2: A ray propagating through an optical system

Free-space refers to ambient space with a refractive index of 1 such that $A = 1$, $B = L$, $C = 0$ and $D = 1$. A ray propagating through free space is then described by [3]:

$$\begin{aligned} \begin{bmatrix} \mathbf{r}_1 \\ \theta_1 \end{bmatrix} &= \begin{bmatrix} 1 & L \\ 0 & 1 \end{bmatrix} \begin{bmatrix} \mathbf{r}_0 \\ \theta_0 \end{bmatrix} \\ &= \begin{bmatrix} \mathbf{r}_0 + L\theta_0 \\ \theta_0 \end{bmatrix} \end{aligned} \tag{2.4}$$

Rays propagating in free-space only change in position and not direction since the refractive index of free-space ideally remains constant. A thin spherical lens of focal length f on the other hand affects the direction by a change in the angle of propagation. The lens is characterised by the constants $A = 1$, $B = 0$, $C = -1/f$ and

$D = 1$, the focal length f is the distance at which the lens focuses a beam of light and is given by [3]:

$$-\frac{1}{f} = \frac{n_1 - n_0}{n}\left(\frac{1}{\rho_1} - \frac{1}{\rho_0}\right), \tag{2.5}$$

where n_0 is the free-space refraction index, n_1 is the refractive index of the lens, ρ_0 and ρ_1 are the lens radii of curvature of the inner and outer surfaces. The output ray position and angle are given by:

$$\begin{aligned}\begin{bmatrix}\mathbf{r}_1\\ \theta_1\end{bmatrix} &= \begin{bmatrix}1 & 0\\ \frac{1}{f} & 1\end{bmatrix}\begin{bmatrix}\mathbf{r}_0\\ \theta_0\end{bmatrix}\\ &= \begin{bmatrix}\mathbf{r}_0\\ \frac{\mathbf{r}_0}{f} + \theta_0\end{bmatrix}\end{aligned} \tag{2.6}$$

Ray optics can be used as a basis to study the propagation and interaction of paraxial light with optical elements. The method of using ray transfer matrices to describe optical elements can be applied to paraxial Gaussian beams to determine changes in beam parameters when they interact with optical systems. In the next section we explore the application of the ray transfer matrix to Gaussian beams

2.2.1 Gaussian beam

We consider a Gaussian beam propagating in free space whose k-vector makes small angles θ_0 with the optical axis and whose radius of curvature is R_0:

$$E_0(x_0, y_0, z_0) = E_0 \exp\left[-\frac{ik}{2q_0}(x_0^2 + y_0^2)\right], \tag{2.7}$$

where E_0 is some amplitude factor. When the Gaussian beam is passed through an ABCD system, the radius of curvature is changed according to the equation [3]:

$$R_1 = \frac{AR_0 + B}{CR_0 + D}, \tag{2.8}$$

where $R \approx \mathbf{r}/\theta$ and $\mathbf{r}$ is the radial distance. For a complex radius of curvature we have the q-parameter equation:

$$q_1 = \frac{Aq_0 + B}{Cq_0 + D}. \tag{2.9}$$

Eq.2.9 is the *ABCD law* and it is the q-parameter solution for the resultant Gaussian mode that is obtained from evaluating the propagation integral [3]:

$$\begin{aligned} E_1(x_1, y_1, z_1) = \frac{i}{\lambda(B - z_0)} \exp(-ik(z - z_0)) \int\int E_0(x_0, y_0, z_0) \exp\left\{ -i\frac{\pi}{\lambda B} \right. \\ \left. \times \left[A(x_0^2 + y_0^2) + D(x^2 + y^2) - 2(x_0 x + y_0 y) \right] \right\} dx_0 dy_0. \end{aligned} \tag{2.10}$$

Inserting Eq.2.7 into Eq.2.10 gives us the output beam:

$$E_1(x_1, y_1, z_1) = \frac{E_0}{A - B/q_0} \exp\left[-\frac{ik}{2q_1}(x_1^2 + y_1^2) \right]. \tag{2.11}$$

In this work we characterise beams using the beam quality factor which is obtained from measurements of the beam divergence, width and radius of curvature. Using the ABCD-law, these parameters are related in the input and output plane for a Gaussian beam by the equations [3]:

$$\begin{aligned} w_1^2 &= A^2 w_0^2 + 2AB w_0^2/R_0 + B^2\theta_0, \\ \theta_1^2 &= C^2 w_0^2 + 2CD w_0^2/R_0 + D^2\theta_0, \\ R_1 &= \frac{w_1^2}{\sqrt{w_1^2\theta_1^2 - (\lambda/\pi)^2}} \end{aligned} \tag{2.12}$$

where w_0 is the beam waist, the smallest beam circumference along the propagation axis and z_0 the waist position.

To obtain the Gaussian expression and beam parameters for free-space propagation, Eq.2.11 can be approximated as [3]:

$$E_1(x_1, y_1, z_1) = E_0 \exp\left[-\frac{x_1^2 + y_1^2}{w_0^2} \right]. \tag{2.13}$$

The parameter q_0 can be obtained by comparing Eq.2.7 and Eq.2.13, which we determine as:

$$q_0 = i\frac{\pi w_0^2}{\lambda} = iz_0, \tag{2.14}$$

from which we can obtain $q(z)$ for a distance z:

$$q(z) = q_0 + z. \tag{2.15}$$

By direct calculation, the term $1/q(z)$ is obtained as:

$$\frac{1}{q(z)} = \frac{1}{z_0(z/z_0 + z_0/z)} - \frac{i\lambda}{\pi w_0^2[1 + (z/z_0)^2]}, \tag{2.16}$$

and the real and imaginary terms are respectively the phase and beam radius terms, we define the parameters:

$$\begin{aligned} w(z) &= w_0\sqrt{z + \left(\frac{z}{z_0}\right)^2}, \\ R(z) &= z + \frac{z_0^2}{z}, \\ \theta_0 &= \frac{\lambda}{w_0\pi}. \end{aligned} \tag{2.17}$$

The term $w(z)$ is the beam width, $R(z)$ the radius of curvature and θ_0 the divergence [7]. The Gaussian beam propagating in free-space propagation a distance z is then given by:

$$E_1(x_1, y_1, z_1) = \frac{E_0}{1 - iz/z_0}\exp\left[-\frac{x_1^2 + y_1^2}{w_0^2}\right]\exp\left[-\frac{ik(x_1^2 + y_1^2)}{R^2(z)}\right] \tag{2.18}$$

In the following sub-section we explore the beam width, divergence and radius of curvature according to Eqns.2.17.

Beam width

The beam width is the diameter of the beam cross-sectional area. For the fundamental Gaussian beam this area is circularly symmetric with high intensity in the centre

and so its size is measured using the radius. This radial size measure can be adapted to other beam profiles [28]. The beam width changes with propagation according to the properties of its curvature and is fundamental in describing propagation properties. In a practical setting, the beam width is determined from the transversal cross section of the intensity distribution given by [3]:

$$I(x, y, z) = |E(x, y, z)|^2, \tag{2.19}$$

as given in Fig.2.3. The beam width in this case is measured at a distance within which 86% of the total beam power is contained, the beam intensity decreases considerably as you move further from the centre.

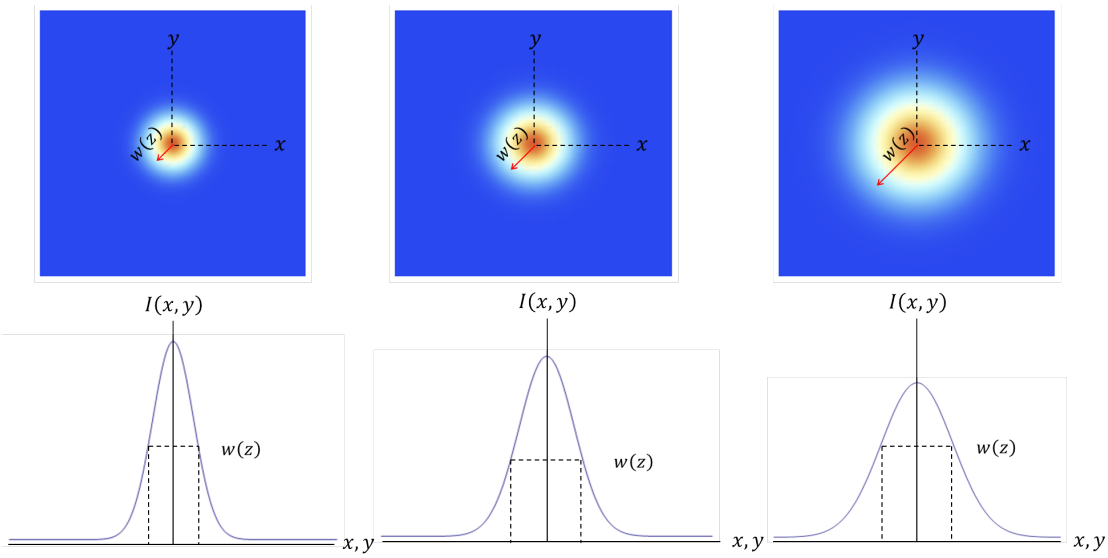


FIGURE 2.3: The beam width is determined from a cross section of the fundamental Gaussian beam.

The evolution of the Gaussian beam width is described by Eq.2.17 [6] which is derived from the beam geometry as in Fig.2.4.

Divergence and curvature

The divergence of a Gaussian beam, denoted by the angle θ_0 is a measure of the increase in the transverse size of the beam with propagation. The divergence is determined with reference to the propagation axis and it depends on the Rayleigh

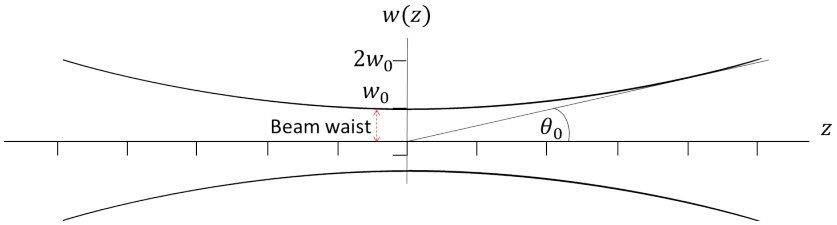


FIGURE 2.4: The change in the Gaussian beam width with propagation

range z_R which is the propagation distance from the waist within which the beam width increases linearly by a factor $\sqrt{2}$. At distances $z \gg z_R$ the beam width is described by [6]:

$$\begin{aligned} w(z) &\approx z\frac{w_0}{z_0} \\ &= \theta_0 z \end{aligned} \tag{2.20}$$

The beam waist is described by the equation $w_0 = \sqrt{\frac{\lambda z_0}{\pi}}$ [7] and thus the divergence can be written as:

$$\theta_0 = \frac{\lambda}{\pi w_0}. \tag{2.21}$$

The beam curvature for Gaussian beams is as defined for Gaussian fields (Fig.1.5)and in Eq.2.17 [7]. The radius of curvature is not linear and it changes with propagation. A spherical wave as the Gaussian beam assumes an approximately planar profile within the Rayleigh range and a more spherical profile as it propagates beyond the Rayleigh range, the change in Radius of curvature is described by the expressions:

$$R(z) = \begin{cases} \infty, z \ll z_R \\ 2z_R, z = z_R \\ z, z \gg z_R \end{cases}. \tag{2.22}$$

Gouy phase

The angle $\psi(z)$ in the Gaussian field (Eq.1.48) is called the Gouy phase. When we compare the propagation of a plane field and that of the Gaussian field by considering

the phase, the Gaussian beam acquires a phase shift with propagation because of the change in the phase structure beyond the Rayleigh range and this phase shift ranges from $-\pi$ to π [29, 30]. The shift is described by the equation [7]:

$$\psi(z) \quad = \text{atan}\left(\frac{z}{z_R}\right). \tag{2.23}$$

In the the next section we explore higher order Gaussian beams.

2.3 Higher order modes

The Gaussian beam explored in the previous section is the fundamental solution to higher order Gaussian modes. In this section we explore higher order beams in rectangular and circular coordinates whose basis are the Hermite and Laguerre functions, respectively.

2.3.1 Hermite-Gaussian modes

Hermite-Gaussian(HG) modes are as given in Eq.1.47. The constants n and m define each solution of the Hermite Gaussian class and the fundamental Gaussian mode is obtained when $n = m = 0$. Various Hermite Gaussian modes are demonstrated in Fig.2.5.

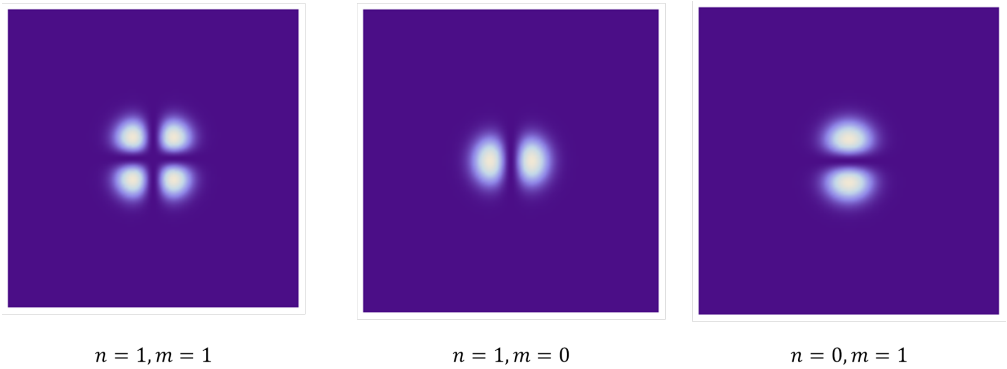


FIGURE 2.5: Hermite Gaussian beam intensity profiles

Hermite Gaussian modes have a beam width that is related to the fundamental mode

by the equations [3]:

$$\begin{aligned} w_n(z) &= w_0\sqrt{2n+1}\sqrt{1+\left(\frac{z}{z_R}\right)^2}, \\ w_m(z) &= w_0\sqrt{2m+1}\sqrt{1+\left(\frac{z}{z_R}\right)^2}. \end{aligned} \tag{2.24}$$

The beam width is expressed for each index n or m because the modes can have different widths in both directions. The waist and divergence are given by:

$$w_{0m,n} = w_0\sqrt{2(m,n)+1}, \tag{2.25}$$

$$\theta_{0m,n} = \theta_0\sqrt{2(m,n)+1}, \tag{2.26}$$

Another important parameter which is used to uniquely identify each pure mode from that of the fundamental Gaussian mode is the beam quality factor, M^2, which is a measure of how the beam width of some higher order mode deviates from that of the fundamental Gaussian mode in free space propagation [31, 32, 33]. M^2 for the fundamental mode is given by:

$$\begin{aligned} M^2 &= \theta_0 w_0 \frac{\pi}{\lambda}, \\ &= 1. \end{aligned} \tag{2.27}$$

The beam quality factor of each HG mode is then given by:

$$\begin{aligned} M_n^2 &= 2n+1, \\ M_m^2 &= 2m+1. \end{aligned} \tag{2.28}$$

The difference in beam quality factor for the fundamental mode and some higher order mode is demonstrated in Fig.2.6. Given two beams, a fundamental Gaussian beam and another beam i.e an HG beam with indices $m, n > 0$ such that they are both initially characterised by a beam width w_0. With propagation, the beam width of the higher order beam will expand at some relatively higher rate to that of the fundamental Gaussian beam.

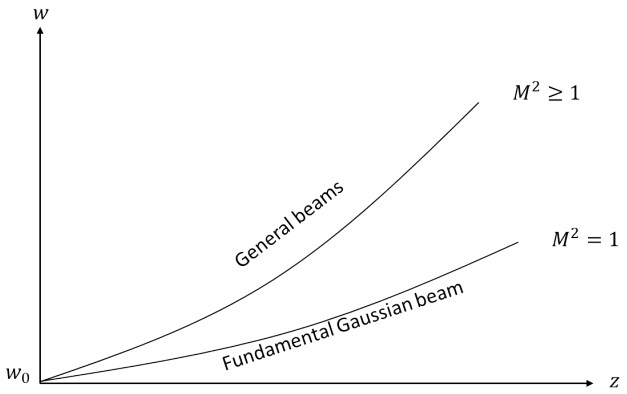


FIGURE 2.6: The propagation of the fundamental Gaussian beam against some higher order beam as a function of M^2

2.3.2 Laguerre Gaussian modes

The LG modes Fig.2.7 are as given in Eq.1.58.

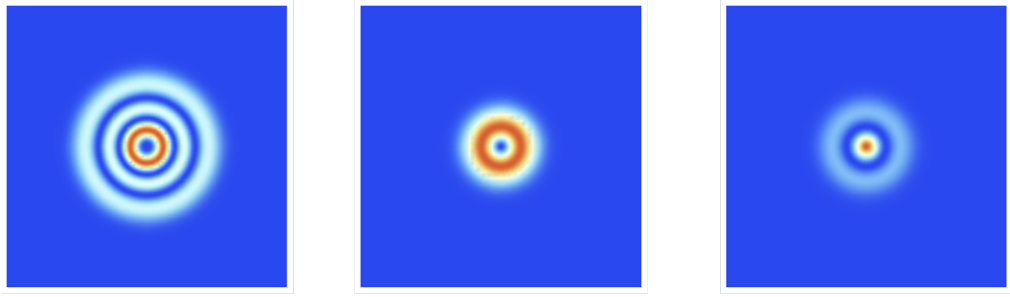


FIGURE 2.7: Laguerre Gaussian beam intensity profiles

The beam width of the Laguerre Gaussian modes is also similarly determined from the intensity distribution and is expressed as [3]:

$$w(z) = w_0\sqrt{2p+\ell+1}\sqrt{1+\left(\frac{z}{z_R}\right)^2}. \tag{2.29}$$

The waist and divergence are given by:

$$w_{0p\ell} = w_0\sqrt{2p+\ell+1}, \tag{2.30}$$

$$\theta_{0p\ell} = \theta_0\sqrt{2p+\ell+1}, \tag{2.31}$$

The beam quality factor of each LG mode is then given by:

$$M_{x,y}^2 = 2p + \ell + 1, \tag{2.32}$$

In the next chapter we explore the characterisation of general beams using beam intensity moments. Some of the parameters that can be extracted from beam moments include the beam width, divergence and curvature.

2.4 Beam moments

Beam moments are a statistical method used extensively in optics to deduce beam parameters such as the centre and the size of the beam.

2.4.1 First order moments

The first order beam moments are parameters used to obtain the centre of a beam. Symmetric beams such as the fundamental Gaussian beam have a defined average value [3, 10] which is the centre of the beam, this centre value is important in determining the beam width. For non symmetric beams, the first order moments allow us to find the centre of the beam which is used as a reference point for the determination of the beam width.

Measuring the first order beam moments is a measurement of the centre value of the intensity distribution. For simplicity, we explore the symmetric fundamental Gaussian profile in studying the determination of the beam centre which can be adapted to any general profile. The first order moments in the spatial domain are obtained from the equations [3]:

$$\begin{aligned} \langle x \rangle &= \frac{1}{P} \int_{\infty}^{\infty} \int_{\infty}^{\infty} x |u(x,y,z)|^2 dxdy, \\ \langle y \rangle &= \frac{1}{P} \int_{\infty}^{\infty} \int_{\infty}^{\infty} y |u(x,y,z)|^2 dxdy, \end{aligned} \tag{2.33}$$

and in the Fourier domain:

$$\begin{aligned}\langle v_x \rangle &= \frac{1}{P}\int_{\infty}^{\infty}\int_{\infty}^{\infty} v_x |\tilde{u}(v_x, v_y, v_z)|^2 dv_x dv_y, \\ \langle v_y \rangle &= \frac{1}{P}\int_{\infty}^{\infty}\int_{\infty}^{\infty} v_y |\tilde{u}(v_x, v_y, v_z)|^2 dv_x dv_y,\end{aligned} \tag{2.34}$$

where:

$$P = \int\int |u(x, y, z)|^2 dx dy, \tag{2.35}$$

which is the power distribution and $\mathbf{v} = (v_x, v_y)$ are Fourier coordinates. The Fourier coordinates are given as a function of the propagation angle ($v_x \approx \theta_x/\lambda$) (Fig.2.8) of a wave travelling at an angle θ_x [6]. The wave function $u(v_x, v_y, v_z)$ essentially represents a superposition of plane waves travelling at different directions each represented by a particular direction vector $\mathbf{v} = (v_x, v_y, v_z)$ that is a function of the angle of propagation.

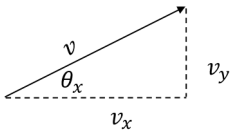


FIGURE 2.8: Angular propagation of a wave

The centre of the beam is represented by the coordinates $(\langle x \rangle, \langle y \rangle)$ in the near field and $(\langle v_x \rangle, \langle v_y \rangle)$ in the far field.

Fig.2.9a shows a symmetric Gaussian beam whose centre position (average) is well defined as the centre peak point, Fg.2.9b shows a beam whose centre point is not centred on the optical axis and so the first order moment is important in identifying the centre of the distribution.

2.4.2 Second order moments

The second order moments are used to calculate the beam width, radius of curvature and beam divergence. In statistics [34], the second order moments are used to

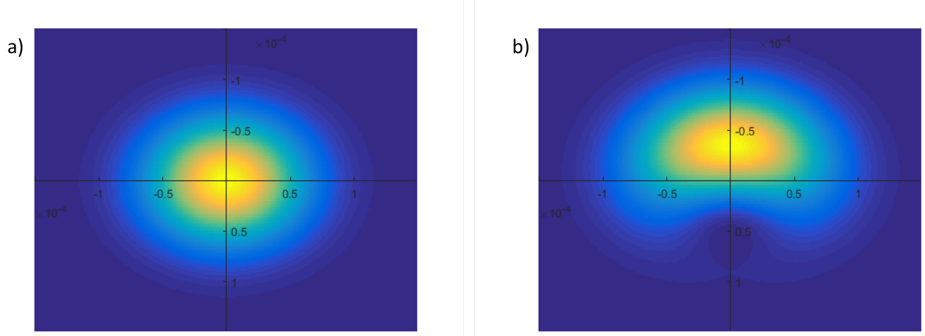


FIGURE 2.9: a) A symmetric beam centred on axis, b) A non-symmetric beam not centred on-axis

determine the standard deviation which is the average distance at which the distribution points lie away from the centre. The standard deviation is denoted by the σ in Fig.2.10 for the fundamental Gaussian beam, 4σ is the distance at which we determine the beam width. Using the second order moments we determine the beam width in both transverse directions[3]:

$$\begin{aligned}\langle w_x^2\rangle &= \frac{1}{P}\int_\infty^\infty\int_\infty^\infty [x-\langle x\rangle]^2|u(x,y,z)|^2dxdy,\\ \langle w_y^2\rangle &= \frac{1}{P}\int_\infty^\infty\int_\infty^\infty [y-\langle y\rangle]^2|u(x,y,z)|^2dxdy,\end{aligned} \tag{2.36}$$

the divergence:

$$\begin{aligned}\langle \theta_x^2\rangle &= \frac{4\lambda^2}{\pi P}\int_\infty^\infty\int_\infty^\infty [v_x-\langle v_x\rangle]^2|\tilde{u}(v_x,v_y,v_z)|^2dv_xdv_y,\\ \langle \theta_y^2\rangle &= \frac{4\lambda^2}{\pi P}\int_\infty^\infty\int_\infty^\infty [v_y-\langle v_y\rangle]^2|\tilde{u}(v_x,v_y,v_z)|^2dv_xdv_y,\end{aligned} \tag{2.37}$$

and the space-angular momentum:

$$\begin{aligned}\langle w_x\theta_x\rangle &= \frac{-i\lambda^2}{\pi P}\int_\infty^\infty\int_\infty^\infty x\left[u(x,y,z)\frac{\partial u^*(x,y,z)}{\partial x}-u^*(x,y,z)\frac{\partial u(x,y,z)}{\partial x}\right]dxdy,\\ \langle w_y\theta_y\rangle &= \frac{-i\lambda^2}{\pi P}\int_\infty^\infty\int_\infty^\infty y\left[u(x,y,z)\frac{\partial u^*(x,y,z)}{\partial x}-u^*(x,y,z)\frac{\partial u(x,y,z)}{\partial x}\right]dxdy,\end{aligned} \tag{2.38}$$

where $w_{x,y}$ is the beam width, $\theta_{x,y}$ the beam divergence and $w_{x,y}\theta_{x,y}$ is used to obtain the radius of curvature from the equations [3]:

$$\begin{aligned} R_x(z) &= \frac{\langle w_x^2 \rangle}{\langle w_x \theta_x \rangle}, \\ R_y(z) &= \frac{\langle w_y^2 \rangle}{\langle w_y \theta_y \rangle}. \end{aligned} \tag{2.39}$$

For simplicity, we set both $\langle v_x \rangle = 0$ and $\langle x \rangle = 0$ and assume the beam is centered

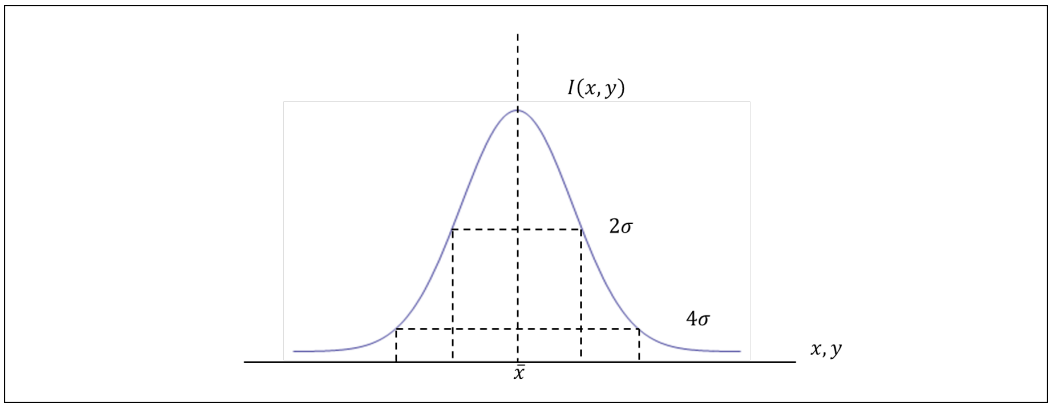


FIGURE 2.10: Determination of the standard deviation

in the optical axis. The beam width in the x is then given by [3, 35]:

$$\langle w_x^2 \rangle = \frac{1}{P} \int_\infty^\infty \int_\infty^\infty x^2 |u(x,y,z)|^2 dxdy, \tag{2.40}$$

and the divergence:

$$\langle \theta_x^2 \rangle = \frac{4\lambda^2}{\pi P} \int_\infty^\infty \int_\infty^\infty v_x^2 |\tilde{u}(v_x, v_y, v_z)|^2 dv_x dv_y. \tag{2.41}$$

The beam moments are measured at the distance 2σ as demonstrated in Fig.2.10, at which 86% of the total beam power is contained.

We also introduce an extra direction of measurement as we can not only rely on the transverse x, y directions to measure the beam parameters to characterise assymetrical beams. We introduce a diagonal measurement that combines the x and y

coordinates, the beam width is then given by [3]:

$$\langle w_{x,y}^2 \rangle \quad = \frac{1}{P} \int_\infty^\infty \int_\infty^\infty xy |u(x,y,z)|^2 dxdy, \tag{2.42}$$

and the divergence:

$$\langle \theta_{x,y}^2 \rangle \quad = \frac{4\lambda^2}{\pi P} \int_\infty^\infty \int_\infty^\infty v_x v_y |\tilde{u}(v_x,v_y,v_z)|^2 dv_x dv_y. \tag{2.43}$$

We can also extend the definition of the beam quality factor to include the radius of curvature for general optical beams:

$$\begin{aligned} M_x^2 &= \frac{k}{2}\sqrt{\langle w_x^2\rangle\langle\theta_x^2\rangle - \langle w_x\theta_x\rangle^2}, \\ M_y^2 &= \frac{k}{2}\sqrt{\langle w_y^2\rangle\langle\theta_y^2\rangle - \langle w_y\theta_y\rangle^2}. \end{aligned} \tag{2.44}$$

In the first few sections of the second chapter we have established the theoretical methods employed to characterise general beams of varying symmetry. Ray optics is important in understanding the interactions of paraxial beams with optical elements and we use the ray approach to study paraxial propagation. First order and second order moments are important in determining properties of beams with symmetric and also non-symmetric irradiation distribution profiles. In the next section we explore the methods used to physically measure beam parameters.

2.5 Characterisation methods

In this section we present various experimental methods currently in use to determine the beam width, beam divergence and curvature. These methods are outlined in the ISO standard (ISO 11146-2) [36, 37] and they are accepted as standard methods to measure and calculate the aforementioned parameters for all types of laser beams.

2.5.1 Beam width

Experimentally the beam width is measured using an intensity detector and employing the 4σ method for determining beam moments. As demonstrated in Fig.2.11,

the intensity of a laser beam is measured using an area detector and the detected intensity is analysed to determine the standard deviation which is the measure of the beam width. For both axis x and y, the area under the curve of each cross-section is estimated by dividing it into squares such that each square has an area given by $|u(x)|^2 \times dx$. The resulting areas from these squares are summed and their standard deviation is determined.

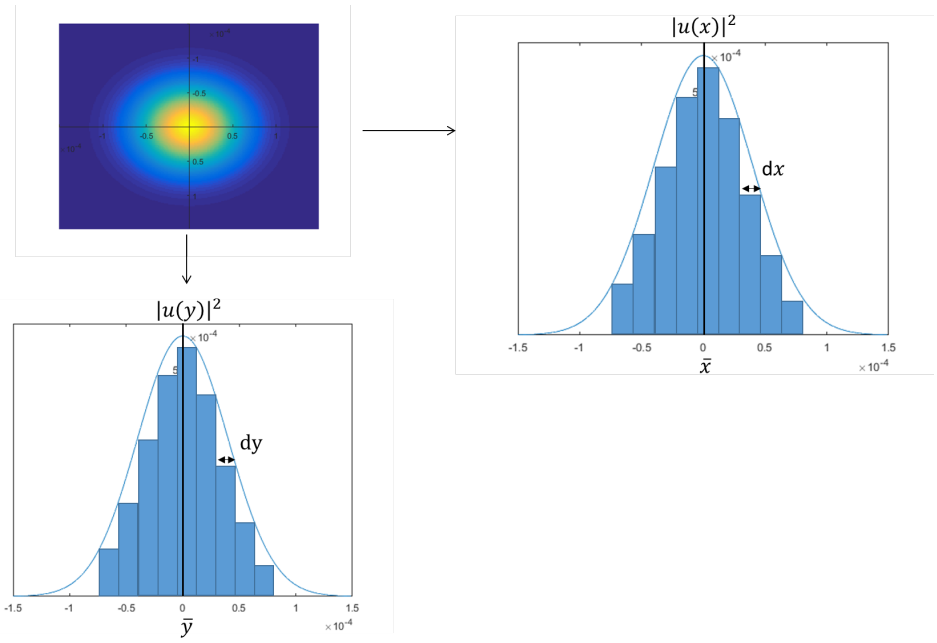


FIGURE 2.11: Area integration of the cross-sections of a detected beam

There are various other methods that one can use to obtain the beam width which are slightly inaccurate from diffraction effects compared to the 4σ method like the scan-slit method and the knife edge methods.

Divergence

Divergence is measured using the beam width in the far field (frequency domain). A simple setup for the measurement of divergence is demonstrated in Fig.2.12, the beam is collimated and passed through a focusing lens of focal length f. The waist w_0 is calculated from the recorded intensity distribution at the focal plane, the divergence

is then obtained from:

$$\theta_0 = \frac{w_0}{f}. \tag{2.45}$$

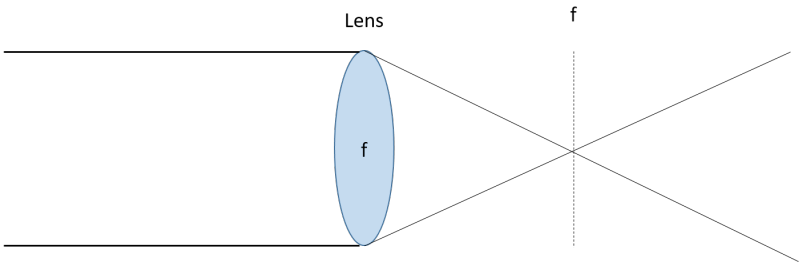


FIGURE 2.12: A collimated beam focused by a thin lens

Divergence can also be obtained from the above beam quality measurements by using the relation:

$$\theta_0^2 = \left(\frac{M}{w_0}\frac{\lambda}{\pi}\right)^2 \tag{2.46}$$

2.5.2 Beam quality factor

The beam quality factor can be obtained from beam width measurements over a range of intensity distributions at various locations z. The method is formalised by considering the fundamental Gaussian beam whose beam width changes with propagation over a distance z. The beam width expression (Eq.2.20) can be written as:

$$w^2(z) = w_0^2\left[1 + \left(\frac{z - z_0}{z_R}\right)^2\right] \tag{2.47}$$

where the Rayleigh range z_R takes the form:

$$z_R = \frac{\pi w_0^2}{M^2\lambda}. \tag{2.48}$$

Eq.2.48 is substituted into Eq.2.47 which is rearranged and we obtain:

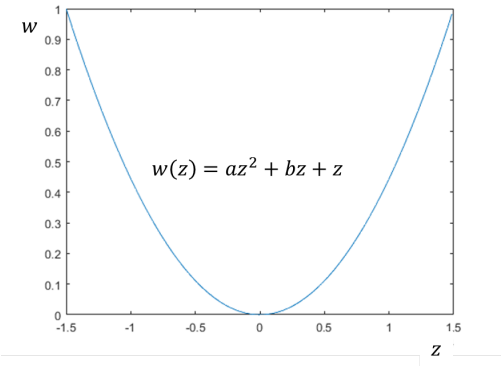


FIGURE 2.13: Beam width as a function of z

$$w^2(z) = \left(\frac{M^2\lambda}{\pi w_0}\right)^2 z^2 - 2z_0\left(\frac{M^2\lambda}{\pi w_0}\right)^2 z + \left(\frac{M^2\lambda}{\pi w_0}\right)^2 z_0^2 + w_0^2. \tag{2.49}$$

The coefficients (Fig.2.13) in the polynomial fit are determined by making the comparisons:

$$\begin{aligned} a &= \left(\frac{M^2\lambda}{\pi w_0}\right)^2, \\ b &= -2z_0\left(\frac{M^2\lambda}{\pi w_0}\right)^2, \\ c &= \left(\frac{M^2\lambda}{\pi w_0}\right)^2 z_0^2 + w_0^2, \end{aligned} \tag{2.50}$$

From which we can obtain the beam waist, its position and the beam quality factor. We can rearrange Eq.2.50 and obtain the expressions:

$$\begin{aligned} z_0 &= -\frac{b}{2a}, \\ w_0 &= \sqrt{c - \frac{b^2}{4a}}, \\ M^2 &= \frac{\pi}{\lambda}\sqrt{ac - \frac{b^2}{4}} \end{aligned} \tag{2.51}$$

2.6 Summary

In this chapter we explored the characterisation of general paraxial light fields that are generated in a laser resonator. We explored ray optics which is an important

concept in the characterisation of paraxial fields because it looks at how they propagate as rays inside the resonator. The ray concept is useful in describing the change in a paraxial field's phase and amplitude as it interacts with optical elements. The characterisation of paraxial light fields is the calculation of beam parameters such as the beam width and beam moments are useful in determining these parameters for beams whose irradiation distribution may not be symmetrical. From the first order beam moments we obtain the centre of the beam and from the second order moments we can obtain the beam width, beam divergence and curvature using the 2σ method. We use the parameters obtained from second order moments to determine the beam quality factor which is an important concept in uniquely identifying higher order modes. There are also various methods which can be used to determine these parameters from physical set-ups. The beam width can be calculated by various methods including the scan slit method although the 2σ method is the most accurate method from which we integrate over an irradiation distribution to obtain the beam width. We have established the fundamentals of paraxial waves and how they can be characterised, we have done this by assuming that the intensity distributions from which we determine these parameters remains constant with time. There are various instances where this assumption does not apply, in the next chapter we study light fields whose intensity distribution may change with time, we look at their representation and characterisation.

3 Coherence theory

The beam parameters in the previous chapter are obtained using intensity distributions that do not vary over time, they remain constant at each plane along the propagation axis. Beams that maintain a constant intensity profile are called *coherent* beams and they have a value of 1 in the coherence degree scale $(0-1)$ with 0 denoting an *incoherent beam* whose intensity profile changes constantly over a long time/space period. Between the scale's two extremes lies a class of beams that are *partially coherent* whose intensity profile is constant only over a specific time/spatial range. In this chapter we investigate the formulation of partially coherent light fields which is also applicable to coherent fields in a view to obtain a more general method of characterisation that applies for all beam types.

3.1 Introduction

Monochromatic waves are waves of a single frequency and until now we have been dealing with varieties of idealized monochromatic waves and light fields. Not all waves and light fields are monochromatic, some light emitted by real physical sources is polychromatic. These light sources consist of an array of point sources that generate polychromatic waves and if the phase relationship between the waves in the field is completely random within a long time and/or spatial range, the field is called *incoherent*. The idea of coherence can be understood as a constant phase relationship between the waves produced by a light source and a random relationship is characteristic of *partially coherent light*. Monochromatic waves can also be partially coherent when they are characterised by a random phase such as laser beams that are described using the Gauss-Schell model [38, 39]. Various light sources generate different types of beams and it is imperative to know the coherence of the light produced for characterisation and application purposes. A partially coherent beam is better

suited to transport information in optical communication [40, 41] as it is not affected significantly by turbulence compared to coherent light and coherent beams are better applicable in processes that require a constant beam profile. In this chapter we explore coherence theory and how it informs characterisation.

3.2 Random light

The description and characterisation of random light borrows its principles from random processes encountered in probability theory. In the following sections we look at random processes and how the theory of random processes translates to optics and random light. We look at the representation of random light by the mutual coherence function, examples of random light and characterisation using beam moments and the beam quality factor.

3.2.1 Random processes

The basic principle of a random process begins with the random variable. A random variable is a map/function that maps a random set to another set, specifically it maps values from a measurable set S to the set of real numbers $\mathbb{R}$ [42]. So in essence, a random variable is a function whose outcome is the result of a random occurrence, an unpredictable occurrence. A random variable can map a random event into a probability space that contains the set of outcomes in $[0, 1]$, this type of random variable is demonstrated in the coin flip experiment where each outcome *tale* or *head* is mapped into either 0 or 1.

Random variables are built with a specific structure, they consist of a set of outcomes S which could be outcomes of a random experiment and a measurable set E which the outcomes in S from the experiment are mapped to. The set E is measurable if it forms a measurable space $(E, \sum, X)$ with the $\sigma-$algebra $\sum$, a $\sigma-$algebra is a set of subsets of E such that [43]:

1. $\emptyset \in \sum$,
2. $\bar{A} \in \sum \; \forall A \in \sum$,

3. $A \cap B \in \sum \forall A, B \in \sum$,

4. $A \cup B \in \sum \forall A, B \in \sum$,

the empty set $\emptyset$ is contained in σ, a complement exists in σ for every set contained in σ, an intersection exists in σ for every two sets contained in σ and lastly, a union exists in σ for every two sets contained in σ (Fig.3.1).

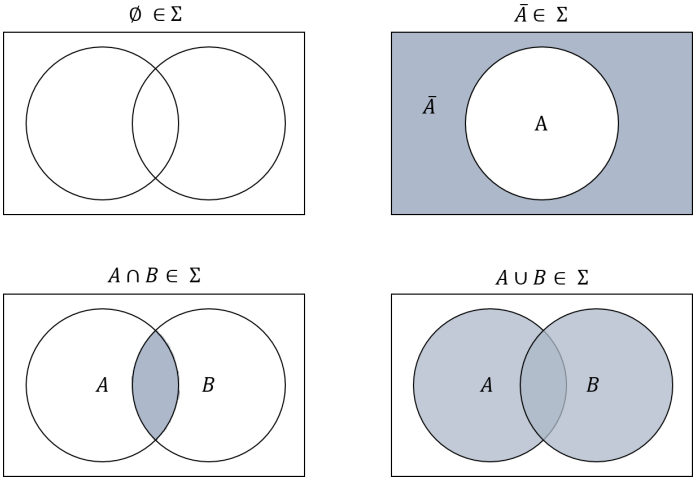


FIGURE 3.1: Sets that are contained in a sigma algebra.

So the random variable X returns real values for a set of outcomes S [44, 45]. An example of this would be drawing cards from a deck of cards that is shuffled randomly, each number on a card drawn lies in the real valued set $E = \{1, 2, \cdots, 9, 10\}$ if we don't count the Ace, Jack, King and Queen cards. The set of outcomes produces what we call a *random distribution* from which we can deduce important information about the random results from the experiment, for example, what is the average occurring outcome? and often how far from this average are the other outcomes?

To formally define a random variable [42, 46] let S denote a set that contains elements s such that

$$S = \{s_i | i = 1, ..., n\} \tag{3.1}$$

A *random variable* is a rule/function $X : S \longrightarrow E$ that assigns to each element of outcomes $s_i \in S$ a value u_j in a measurable set E such that $X(s_i) = u_j$.

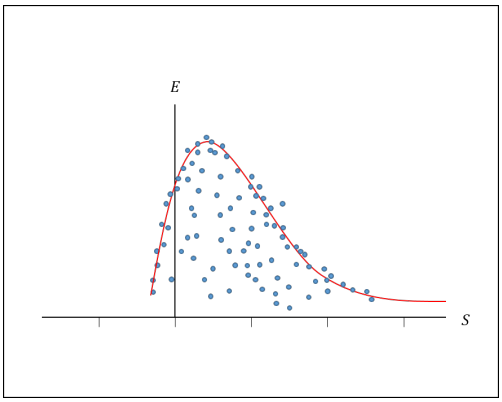


FIGURE 3.2: Random results generated by a random experiment and approximated by the red Gaussian shaped line

Fig.3.2 demonstrates a distribution generated by a random variable which is approximated by the red Gaussian line.

We can define a random light beam as a collection of random variables at planes $\mathbf{r}_i$ for $i = 1, 2, \cdots$ such that:

$$u(\mathbf{r}_i)_z = \{X(S_i)\} \tag{3.2}$$

where S_i is the set of inputs at the $i-th$ plane. Random variables are characterised by the expected value (mean), the standard deviation and a host of other parameters which can be deduced using the $4-\sigma$ method. For random variables, a more appropriate mean and standard deviation measure is the ensemble average which is an average at each plane over many realisations of the random variable [7]. The random variable expected value is denoted by [43]:

$$\mathrm{E}[X] = \lim_{t\to\infty} \frac{1}{2t} \int_{-t}^{t} S_i |X(S_i)|^2 dS_i \tag{3.3}$$

where t denotes the $t-th$ realisation of the random variable at the plane S_i and the standard deviation is given by:

$$\mathrm{E}[X^2] = \lim_{t\to\infty} \frac{1}{2t} \int_{-t}^{t} (\mathrm{E}[X] - S_i)^2 |X(S_i)|^2 dS_i \tag{3.4}$$

In the next section we analyse random light with respect to coherence in detail and how it is generated by exploring partially coherent sources.

3.2.2 Random light and its sources

A measure of randomness in light fields is the random/inconsistent phase relationship among the waves that make up a light field. In *Coherent* light, a fixed phase relationship is maintained between waves. This fixed phase relationship is also present in partially coherent light however within specific time or spatial boundaries.

Given an optical field $u(\mathbf{r}, t)$ defined for space $\mathbf{r} = (x, y)$ and time t, and propagating in the z-coordinate direction. Since coherent light fields maintain a constant phase difference among the constituent waves with propagation, the phase difference does not change with time and this makes it easy to determine parameters such as the expected value $\mathrm{E}[u]$ of the field since it remains constant at a particular transverse plane at varying times. Partially coherent light does not fully adhere to this, it resembles a random variable such that the phase differences change randomly with time and therefore parameters of the field are determined using time ensembles as in Eqn.3.3. Taking this into account, a generalized time average form of $u(\mathbf{r}, t)$ is needed for a generalized description of the distribution that accommodates partially coherent light and of course this has no effect on coherent fields since they are time independent. The time average of the irradiation distribution which represents the field is given by: [7]:

$$u(\mathbf{r}, t) = \lim_{t \to \infty} \frac{1}{2t} \int_{-t}^{t} |u(\mathbf{r}, t)|^2 d\mathbf{r}. \tag{3.5}$$

In the next section we explore the generally used ensemble function which is the *mutual coherence function* as it better represents the coherence properties of the light field.

3.2.3 The mutual coherence function

Mutual coherence is a concept that was developed as a vector mathematics tool to correlate functions for comparison and measuring similarity.

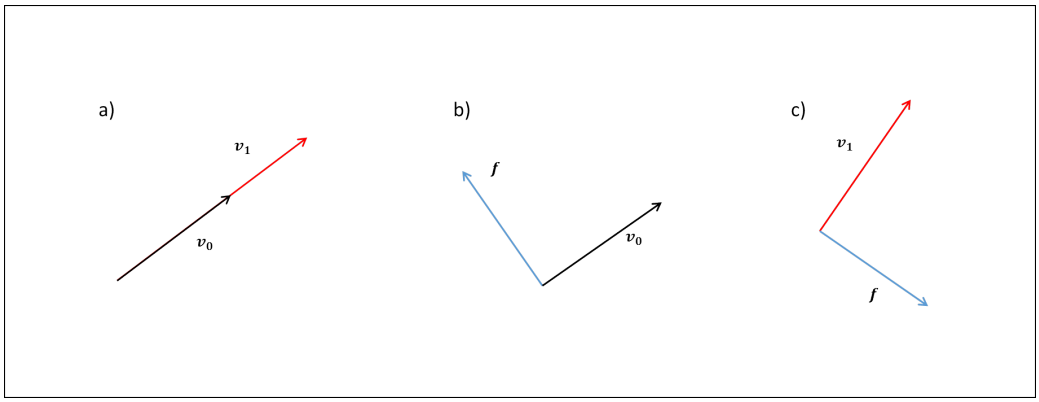


FIGURE 3.3: Correlation of vectors $\mathbf{f}$, $\mathbf{v}_0$ and $\mathbf{v}_1$.

As an example, suppose we are given the vectors $\mathbf{f}$, $\mathbf{v}_0$ and $\mathbf{v}_1$ such that $\mathbf{v}_1 = c\mathbf{v}_0$ and $\mathbf{f}$ is orthogonal to both $\mathbf{v}_0$ and $\mathbf{v}_1$ for some real constant c. The measure of similarity between the functions is given by the angle between the vectors [47]:

$$\begin{aligned} \cos\theta_0 &= \frac{\mathbf{v}_1.\mathbf{v}_0}{|\mathbf{v}_1||\mathbf{v}_0|}, \\ \cos\theta_1 &= \frac{\mathbf{f}.\mathbf{v}_0}{|\mathbf{f}||\mathbf{v}_0|}, \\ \cos\theta_2 &= \frac{\mathbf{f}.\mathbf{v}_1}{|\mathbf{f}||\mathbf{v}_1|}. \end{aligned} \tag{3.6}$$

From the above equations we get the results

$$\begin{aligned} \theta_0 &= 1, \\ \theta_1 &= 0, \\ \theta_2 &= 0 \end{aligned} \tag{3.7}$$

or

$$\begin{aligned} \theta_0 &= 0, \\ \theta_1 &= \pi/2, \\ \theta_2 &= \pi/2 \end{aligned} \tag{3.8}$$

where an angle of 0 (or $\cos\theta = 1$) represents similar vectors and $\pi/2$ (or $\cos\theta = 0$) dissimilar vectors [48, 49](Fig.3.3). We can use the concept of correlation in optical fields to test the similarity of wave functions, correlation is particularly important in evaluating partially coherent fields whose wave function changes randomly with propagation. We can take a partially coherent field and autocorrelate it to itself to measure the extent (angle) to which the field is partially coherent. The random variation of the field is to a specific extent, the correlation of these variations at a specific point in space(autocorrelation) can measure the extent to which the wave-function changes with propagation.

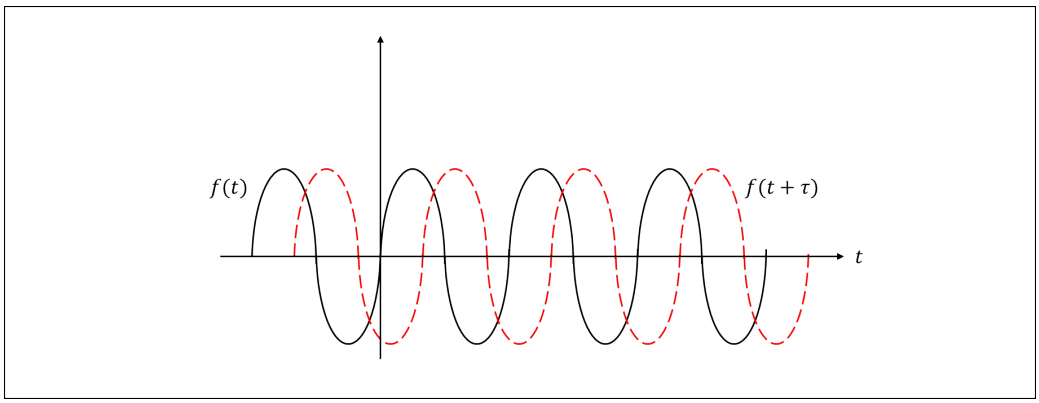


FIGURE 3.4: The functions $f(t)$ and $f(t+\tau)$

Given a wave-function $f(t)$, the degree of autocorrelation [48] of $f(t)$ is given by (Fig.3.4):

$$c_n = \frac{1}{I_f(t)} \int_{-\infty}^{\infty} f(t) f(t+\tau) dt \tag{3.9}$$

where τ is a time shift and $I_f(t)$ is the intensity. The two signals $f(t)$ and $f(t+\tau)$ are similar when $c_n = 1$ and dissimilar when $c_n = 0$. The constant c_n can also lie between 0 and 1, in that case we say $f(t)$ and $f(t+\tau)$ are partially similar, a concept that is closely related to the partial coherence of paraxial wave-functions.

Using the mutual coherence function for a paraxial wave-function given as $u(\mathbf{r}, t)$ over a spatial domain $\mathbf{r}$ and time domain t, we can correlate the field in either the

time of spatial domain. For example, the temporal (time) autocorrelation of $u(\mathbf{r},t)$ is given by:

$$\begin{aligned}\Gamma(t,t+\tau) &=< u^*(\mathbf{r},t)u(\mathbf{r},t+\tau) >,\\ &= \lim_{t\to\infty}\frac{1}{2t}\int_{-t}^{t} u^*(\mathbf{r},t)u(\mathbf{r},t+\tau)dt.\end{aligned} \tag{3.10}$$

When we are looking solely at the time coherence of a function, we can drop the spatial dependence and write the mutual coherence function as:

$$\Gamma(t_1,t_0) = \lim_{t\to\infty}\frac{1}{2t}\int_{-t}^{t} u^*(t_1)u(t_2)dt. \tag{3.11}$$

where $t_1 = t$ and $t_2 = t+\tau$.

Temporal coherence

A simple demonstration for measuring temporal autocorrelation is carried out using a Michaelson interferometer [16, 3]. The beam $u(t)$(Fig.3.5) is sent through a beam splitter that separates it into two beams $u_0(t)$ and $u_1(t)$. The beam $u_1(t)$ travels an extra time δt which is achieved by shifting the mirror m_1, and the two beams are recombined as $u_0(t)$ and $u_1(t+\delta t)$ at the observation plane. The recombined beams are given at the observation plane by:

$$\begin{aligned}u(t)_{obs} &= u_0(t) + u_1(t+\triangle t),\\ &= u(t) + u(t+\triangle t)\end{aligned} \tag{3.12}$$

We obtain the mutual coherence function by taking the ensemble average/intensity of $u(t)_{obs}$ at the observation plane:

$$\begin{aligned}< u(t)_{obs}u^*(t)_{obs} > &= \lim_{T\to\infty}\frac{1}{2T}\int_{-T}^{T} u(t)_{obs}u^*(t)_{obs}\mathrm{d}t,\\ &= \lim_{T\to\infty}\frac{1}{2T}\int_{-T}^{T}\big[u(t)+u(t+\triangle t)\big]\big[u(t)+u(t+\triangle t)\big]^*\mathrm{d}t,\\ &= \lim_{T\to\infty}\frac{1}{2T}\int_{-T}^{T}\big[u(t)u^*(t)+u(t)u^*(t+\triangle t)+u(t+\triangle t)u^*(t)\\ &\quad + u(t+\triangle t)u^*(t+\triangle t)\big]\mathrm{d}t\\ &= I(t)+\big\langle u(t)u^*(t+\triangle t)\big\rangle+\big\langle u(t+\triangle t)u^*(t)\big\rangle+I(t+\triangle t).\end{aligned} \tag{3.13}$$

The **mutual coherence function** is then given by the term $\langle u(t)u^*(t+\triangle t)\rangle$ such that:

$$\Gamma(t, t+\triangle t) = \langle u(t)u^*(t+\triangle t)\rangle, \tag{3.14}$$

where the term $\langle u(t+\triangle t)u^*(t)\rangle$ is the conjugate of $\Gamma(t, t+\triangle t)$.

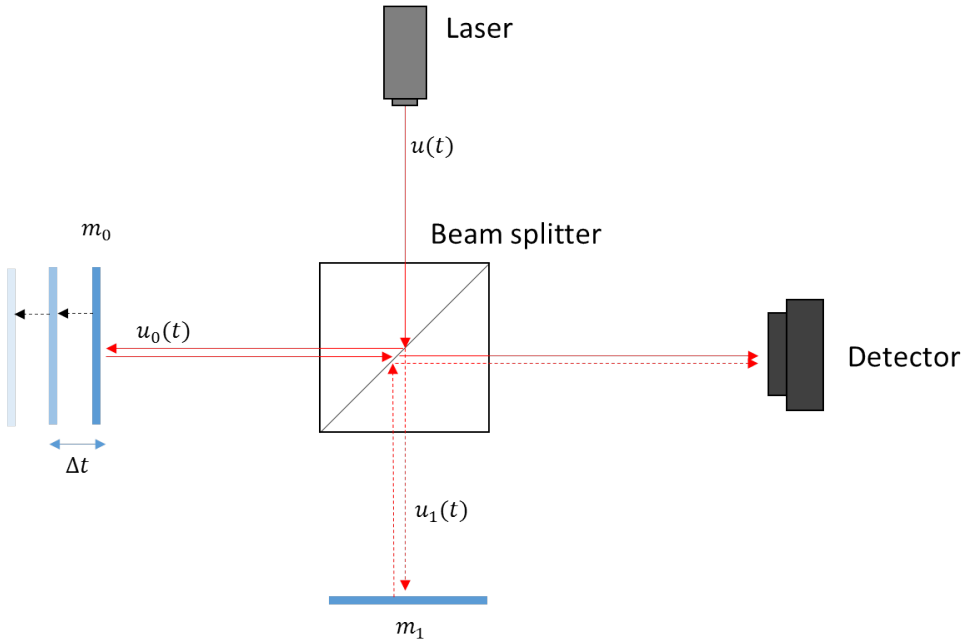


FIGURE 3.5: A Michelson interferometer for the measurement of temporal coherence.

Spatial coherence

The spatial mutual coherence function which is significant in evaluating real beams is given by a product of the beam and its space-shifted version. The beam $u(\mathbf{r})$ is divided into $u_0(\mathbf{r})$ and $u_1(\mathbf{r})$ as depicted in Fig.3.6[3]. Shifting the mirror m_1 results in a spatial shift m_1 and both beams are recombined and detected by a camera. Following a similar formulation to that of Eq.3.14, we obtain the spatial mutual

coherence function:

$$\begin{aligned}\Gamma(\mathbf{r}_1,\mathbf{r}_2) &= \langle u_1(\mathbf{r}_1,t)u_0^*(\mathbf{r}_2,t)\rangle, \\ &= \lim_{T\to\infty}\frac{1}{2T}\int_{-T}^{T} u_1(\mathbf{r}_1,t)u_0^*(\mathbf{r}_2,t)\mathrm{d}t\end{aligned} \tag{3.15}$$

where $\mathbf{r}_1 = \mathbf{r}$ and $\mathbf{r}_2 = \mathbf{r} + \triangle\mathbf{r}$.

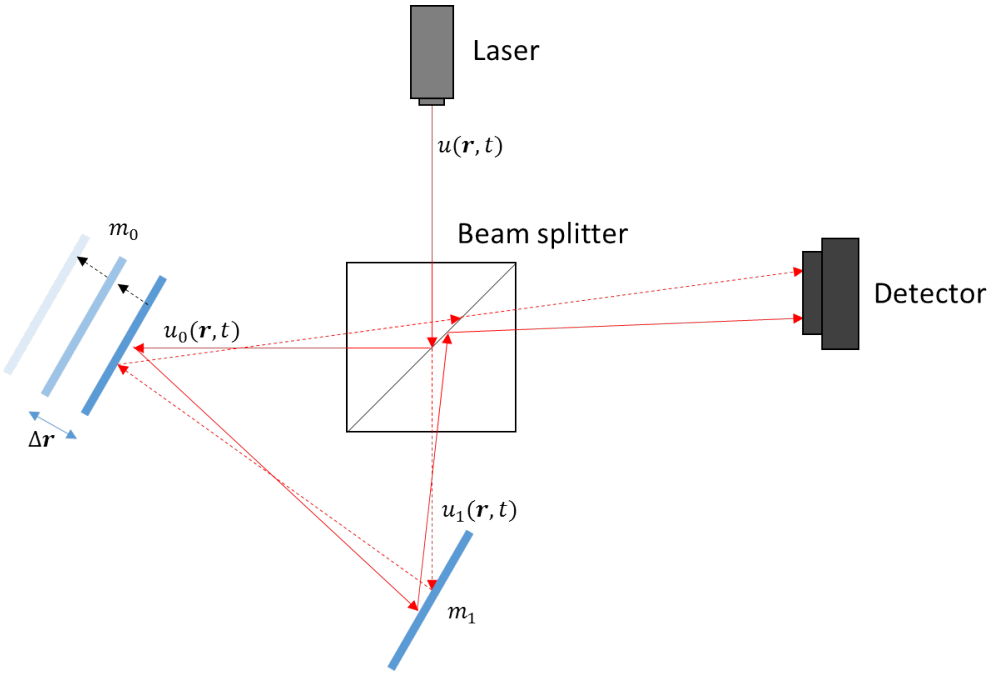


FIGURE 3.6: A shear interferometer for the measurement of spatial coherence.

Coherence degree

The degree of coherence is a measure of how coherent a light beam is. If we consider the fluctuations in the intensity profile of the beam $u(\mathbf{r})$ at a position $\mathbf{r}$ at varying times t, we observe that the fluctuations are correlated in some way within a specified time period τ_c and beyond this period the fluctuations are random. This correlation between the fluctuations is the measure of coherence and is quantified by the degree of coherence [7]:

$$\mu = \frac{\langle u(\mathbf{r},t)u^*(\mathbf{r},t+\triangle t)\rangle}{\langle u(\mathbf{r},t)u^*(\mathbf{r},t)\rangle}, \tag{3.16}$$

such that:

$$0 \leq |\sigma| \leq 1, \tag{3.17}$$

where $|\sigma| = 1$ denotes complete correlation exhibited by coherent light, $|\sigma| = 0$ is total non-correlation which is found in incoherent light and partially coherent light is in the region $|\sigma| \in (0, 1)$.

In the next section we investigate a model that is used to describe partially coherent light that exhibits Gaussian properties, the Gauss-Schell model.

3.3 Gauss-Schell beam

Gaussian Schell-model (GSM) beams are a class of beams that are Gaussian in nature and are produced by Schell model sources, they exhibit partial coherence behaviour. GSM beams are defined by a mutual coherence function whose complex degree of coherence can be varied and hence can be explored as either a coherent, partially coherent or an incoherent field.

GSM beams are produced by Schell-model sources which are characterised by the mutual coherence function [50, 39]:

$$\Gamma(\mathbf{r}_1, \mathbf{r}_2) = \sqrt{S(r_1)}\sqrt{S(r_2)}\mu(\mathbf{r}_1 - \mathbf{r}_2). \tag{3.18}$$

We consider Schell-model sources whose intensity is Gaussian where:

$$s(\mathbf{r}_i) = A_i \exp\left[-\frac{\mathbf{r}_i^2}{2\sigma_i}\right], \tag{3.19}$$

and:

$$\mu(\mathbf{r}_1 - \mathbf{r}_2) = \exp\left[-\frac{(\mathbf{r}_1 - \mathbf{r}_2)^2}{2\delta_i^2}\right]. \tag{3.20}$$

where δ_i is some constant. The mutual coherence function is then given by:

$$\Gamma(\mathbf{r}_1, \mathbf{r}_2) = A \exp\left[-\frac{\mathbf{r}_1^2}{4\sigma_1}\right] \exp\left[-\frac{\mathbf{r}_2^2}{4\sigma_2}\right] \times \exp\left[-\frac{(\mathbf{r}_1 - \mathbf{r}_2)^2}{2\delta_i^2}\right]. \tag{3.21}$$

We obtain a Gaussian beam when $\delta_i \to \infty$ and σ is some constant. As an example (Fig.3.7) we generated a Gaussian Schell-model beam given by the equation:

$$\Gamma(\mathbf{r}, s, \sigma) = \frac{1}{2} ce \left|\sqrt{\frac{2}{\pi w_0^2}}\right|^2 \exp\left(-\frac{2\mathbf{r}^2}{w_0^2} - \frac{2\mathbf{s}^2}{2\sigma^2 w_0^2}\right) \tag{3.22}$$

where $\mathbf{r} = (\mathbf{r}_1 + \mathbf{2})/2$ and $\mathbf{s} = \mathbf{r}_1 - \mathbf{r}_2$. The constants are $c = 3\times10^{11}$mm/s, $w_0 = 1$mm and $e = 8.85 \times 10^{-9}$F/mm.

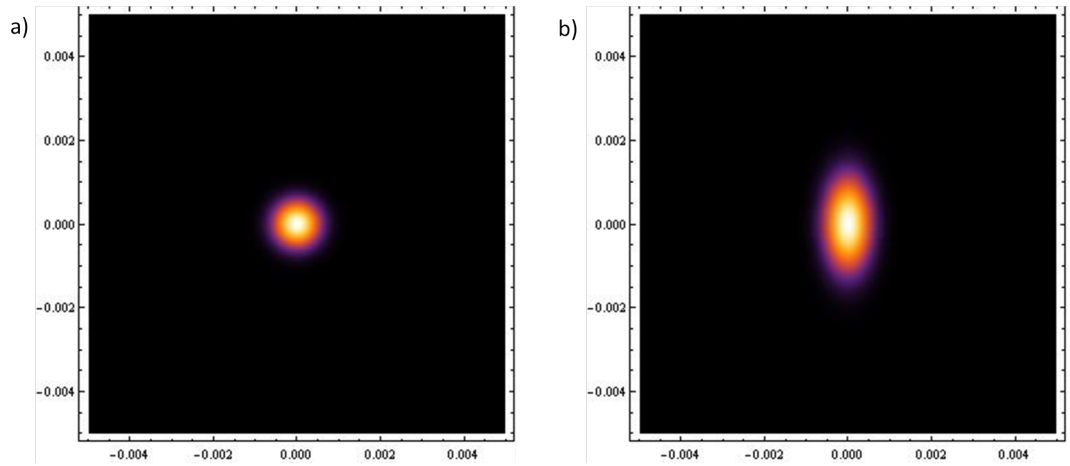


FIGURE 3.7: Gaussian-Schell model beams of coherence degree a)$\sigma = 1$ and b)$\sigma = 0.5$

3.4 Summary

In this chapter we have explored the theory of coherence using a statistical approach and how it translates to partially coherent light. A distribution of points that change randomly are characterised by using statistical measures such as the expected value and standard deviation, these measures are determined by considering averages over specific period of the domain. The theory is applied to the subject of coherent

and partially coherent light. The mutual coherence function is important in coherence theory as it allows us to characterise unstable beams and it can be generated physically. In the next chapter we study the Wigner distribution function which is a function that uses the mutual coherence function and is used to characterise partially coherent beams.

4 Wigner distribution function

The general characterisation of light beams must take into account the coherence properties of the source and so finding a general method to characterise beams of varying coherence is an important task. The characterisation process often requires multiple independent experimental methods and in this work we seek a more efficient and generalized method that takes into account coherence effects and reduces the need for multiple experiments in the characterisation process. In this chapter we introduce a phase-space function, the Wigner distribution function(WDF) which employs the mutual coherence function and is a dual function in the spatial and spatial frequency domains. The WDF is a general description of light such that it allows us to describe light beams of varying degrees of coherence which simplifies characterisation. Phase-space optics [51, 52, 53] explores the simultaneous description of signals. The WDF was first introduced as a concept in mechanics to correct for the Boltzman probability distribution at low temperatures by E. Wigner [54]. It was then introduced to optics by A. Wilther [55] using coherence theory for photometry which inspired wide application in the field of phase-space optics as a dual optical field representation. The first applications inspired by the WDF in optics were largely in time-frequency analysis [53] and its applications in coherence theory [52]. Several authors have explored how the WDF of known beams evolve and interact with optical systems, the WDF adheres to the propagation properties of the underlying field and is also similarly transformed by ABCD systems [56, 57, 57] and thus it can be used for characterisation purposes. Since the WDF employs the mutual coherence function, it has also proved to be important in the description of partially coherent beams [58, 51]. The WDF has also been applied in optical signal analysis research including image processing for in depth image analysis [59, 60, 61, 62] and optical communication [57].

4.1 Phase-space optics

Phase-space optics is a model that simplifies the description of propagating light beams by unifying various propagation concepts while preserving their unique features. The WDF along with the ambiguity function (AF) and the Wigner-Ville distribution are part of a family of functions that demonstrate the phase-space model and are applied vastly in varying signal analysis work [63, 64, 65].

4.1.1 Spatial and frequency domain

The frequency domain is used to describe the propagation properties of the beam. Given a beam $u(x, y)$, the far-field(frequency) representation of the beam is obtained from the inverse of the Fourier transform [7]:

$$\begin{aligned} \tilde{u}(v_x, v_y) &= \mathcal{F}\{u(x, y)\}, \\ &= \int\int u(x, y)\exp[-i2\pi(xv_x + yv_y)]dxdy. \end{aligned} \tag{4.1}$$

The inverse Fourier transform is given by:

$$\begin{aligned} u(x, y) &= \mathcal{F}^{-1}\{u(v_x, v_y)\}, \\ &= \int\int u(v_x, v_y)\exp[i2\pi(xv_x + yv_y)]dv_xdv_y. \end{aligned} \tag{4.2}$$

The spatial frequency domain provides an angular propagation distribution of a light beam and it is useful in measuring divergence. To demonstrate the description of a wave-function in the spatial frequency domain, we consider the plane-wave as a building block of a spherical phase beam [6]. A plane-wave is a wave described by the wave-equation:

$$\begin{aligned} u(x, y, z) &= \exp[-i\mathbf{rk}], \\ &= \exp[-i(k_x x + k_y y + k_z z)]. \end{aligned} \tag{4.3}$$

where the k-vector in each transverse direction is interpreted as in Fig.4.1 with the transverse components:

$$\begin{aligned} k_x &= k \sin\theta_x \\ &= 2\pi v_x, \\ k_y &= k \sin\theta_y \\ &= 2\pi v_y. \end{aligned} \tag{4.4}$$

The terms v_x and v_y are the spatial frequency coordinates for each plane-wave propagating at angles θ_x and θ_y at each transverse direction. The spatial frequency coordinates are simplified under paraxial approximation to:

$$\begin{aligned} v_x &= \frac{k_x}{2\pi} \sin\theta_x \\ &\approx \frac{\theta_x}{\lambda} \\ v_y &= \frac{k_y}{2\pi} \sin\theta_y \\ &\approx \frac{\theta_y}{\lambda}. \end{aligned} \tag{4.5}$$

The component $k = \sqrt{k_x^2 + k_y^2 + k_z^2}$ can be rewritten in spatial frequency coordinates as:

$$\begin{aligned} k_x &= \sqrt{k^2 - (k_x^2 + k_y^2)} \\ &\approx k - \frac{(k_x^2 + k_y^2)}{2k} \\ &= k - \lambda\pi(v_x^2 + v_y^2), \end{aligned} \tag{4.6}$$

and therefore we can write the plane wave in terms of the spatial frequency coordinates with each plane in the phase represented by the corresponding coordinates (v_x, v_y) and hence a unique angle of propagation (θ_x, θ_y) along the z-axis such that:

$$u(x, y, z) = u(x, y, 0) \times \exp[-ikz + i\lambda\pi(k_x^2 + k_y^2)z]. \tag{4.7}$$

Each plane thus travels with a different propagation constant in the z-axis given by:

$$\lambda\pi(k_x^2 + k_y^2)z \tag{4.8}$$

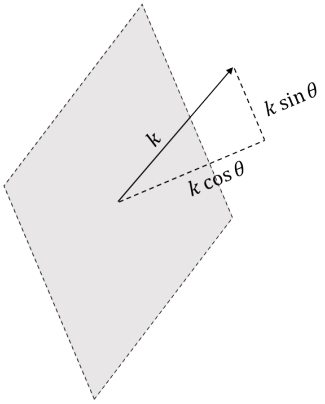


FIGURE 4.1: The k-vector separated into its transverse components

The inverse Fourier transform in Eq.4.2 gives us an expression of $u(x, y, z)$ as a superposition of plane waves in the spatial frequency domain and therefore we can write a paraxial light beam as a superposition of plane waves propagating at slightly different directions that form an angular propagation/divergence distribution.

4.2 Wigner distribution function

The WDF is widely employed in optics as a phase-space representation. The WDF is formulated using the mutual coherence function and can be employed on light fields across the coherence degree spectrum of $0 - 1$. The mutual coherence function is a statistical function that is used to correlate two functions or a function with itself (autocorrelation) to measure similarity [66, 67], it is highly useful in the representation of partially coherent light.

Given a paraxial wave function $u(\mathbf{r}, t)$, the mutual coherence function is given by:

$$\begin{aligned} \Gamma(\mathbf{r}_1, \mathbf{r}_2) &= \big\langle u(\mathbf{r}_1, t) u^*(\mathbf{r}_2, t) \big\rangle, \\ &= \lim_{T \to \infty} \frac{1}{2T} \int_{-T}^{T} u(\mathbf{r}_1, t) u^*(\mathbf{r}_2, t) \mathrm{d}t \end{aligned} \tag{4.9}$$

where the angle brackets denote an ensemble average which is an average of the intensity distribution over a long time period over many realisations of the field [68,

69]. Eq.4.9 is an autocorrelation (Fig.4.2) of the wave-function $u(\mathbf{r},t)$ at the planes $\mathbf{r}_1$ and $\mathbf{r}_2$. It is also important to note that Eq.4.9 is simply an intensity distribution for fully coherent beams since:

$$\lim_{T\to\infty}\frac{1}{2T}\int_{-T}^{T}u(\mathbf{r}_1,t)u^*(\mathbf{r}_2,t)\mathrm{d}t = u(\mathbf{r},t)u^*(\mathbf{r},t) \tag{4.10}$$

The WDF of a paraxial beam $u(r)$ is given by the equation [70, 71]:

$$\begin{aligned} W(\mathbf{r},\mathbf{v}) &= \int \Gamma\left(\mathbf{r}+\frac{1}{2}\mathbf{s},\mathbf{r}-\frac{1}{2}\mathbf{s}\right)\exp(-ik\mathbf{v}\mathbf{s})d\mathbf{s}, \\ &= \int \langle u\left(\mathbf{r}+\frac{1}{2}\mathbf{s}\right)u^*\left(\mathbf{r}-\frac{1}{2}\mathbf{s}\right)\rangle\exp(-ik\mathbf{v}\mathbf{s})d\mathbf{s}, \\ &= \int\int \langle u\left[(x,y)^t+\frac{1}{2}(s_x,s_y)^t\right]u^*\left[(x,y)^t-\frac{1}{2}(s_x,s_y)^t\right]\rangle \\ &\times \exp[-ik(v_x,v_y)^t(s_x,s_y)^t]ds_x ds_y. \end{aligned} \tag{4.11}$$

where $\mathbf{r}=(x,y)$ is the space vector and $\mathbf{v}=(v_x,v_y)$ is the spatial frequency vector. Although it can take negative values, the WDF has important physical attributes

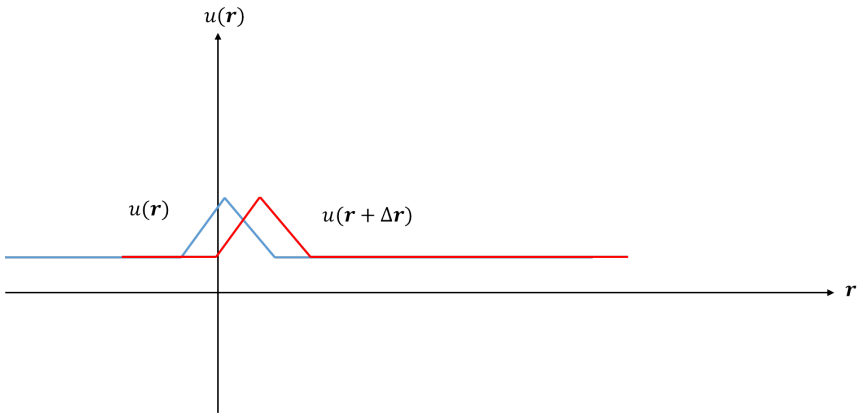


FIGURE 4.2: An autocorrelation of the function $u(\mathbf{r})$

which can be used in the characterisation of light beams [72, 73, 74, 75]. We explore various examples of WDFs obtained from various beams given by Alieva T. *et. al* in [56].

The first example is the generation of the WDF of a point source which is a source of radiation and whose function assumes a value only at the source point and it is

zero everywhere else. For simplicity we analyse a 1D point source that is given by:

$$u(x) = \delta(x - x_0). \tag{4.12}$$

The WDF of the point source is obtained as:

$$W(x, v_x) = \delta(x - x_0). \tag{4.13}$$

The WDF of the point source is also a point source at a position x_0 that irradiates uniformly at all angles of propagation in the spatial frequency domain v_x as depicted in Fig.4.3.

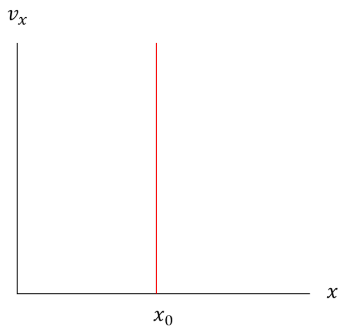


FIGURE 4.3: The WDF distribution of a point source $\delta(x - x_0)$

Another example is a spherical wave whose intensity profile is Gaussian. Given a paraxial spherical wave $u(\mathbf{r}) = \exp(i\pi a x^2)$, its WDF is given by the equation:

$$W(x, v_x) = \delta(v_x - ax). \tag{4.14}$$

The WDF of $u(x)$ implies that at every point in the domain x at which the spherical wave exists, there exists a corresponding spatial frequency point in the domain $v_x = ax$ (Fig.4.4).

The WDF transforms an n-dimensional function into a $2n$-dimensional function. This presents difficulty in the experimental and computational generation of the WDF for some beams because of the increase in dimension. Take for example a 2-dimensional function $u(x, y)$, its WDF is given by the 4-dimensional function

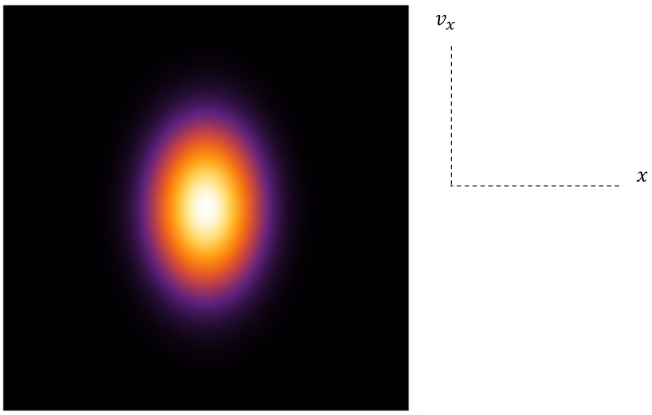


FIGURE 4.4: The WDF distribution of a spherical wave $\exp(i\pi a x^2)$

$W(x, y, v_x, v_y)$ which is difficult to visualize (Fig.4.5). For a simplified visualization, the WDF of a 2D function is generated by evaluating sections of the beam [76, 77] and so 1-dimensional functions of symmetrical beams are often preferred in WDF generation since they are easier to generate both experimentally and computationally. Given a 1D function $u(x)$, the WDF is given by:

$$W(x, v_x) = \int u\left(x + \frac{1}{2}s_x\right)u^*\left(x - \frac{1}{2}s_x\right)\exp(-i2\pi v_x s_x)ds_x. \tag{4.15}$$

In the following section we study the characterisation of the WDF.

4.3 WDF characterisation

For symmetric/stigmatic beams, the WDF is a perfect characterisation tool because we only need one dimension to extract the parameters of the beam and we can then adapt these parameters to the other dimension [78]. On the other hand, general astigmatic/non-symmetric beams present the difficulty of expanding the dimensions of the beam by a factor of 2. The determination of the beam parameters is carried out by integration over the 2-dimensional WDF plot as demonstrated in Fig.4.6. The

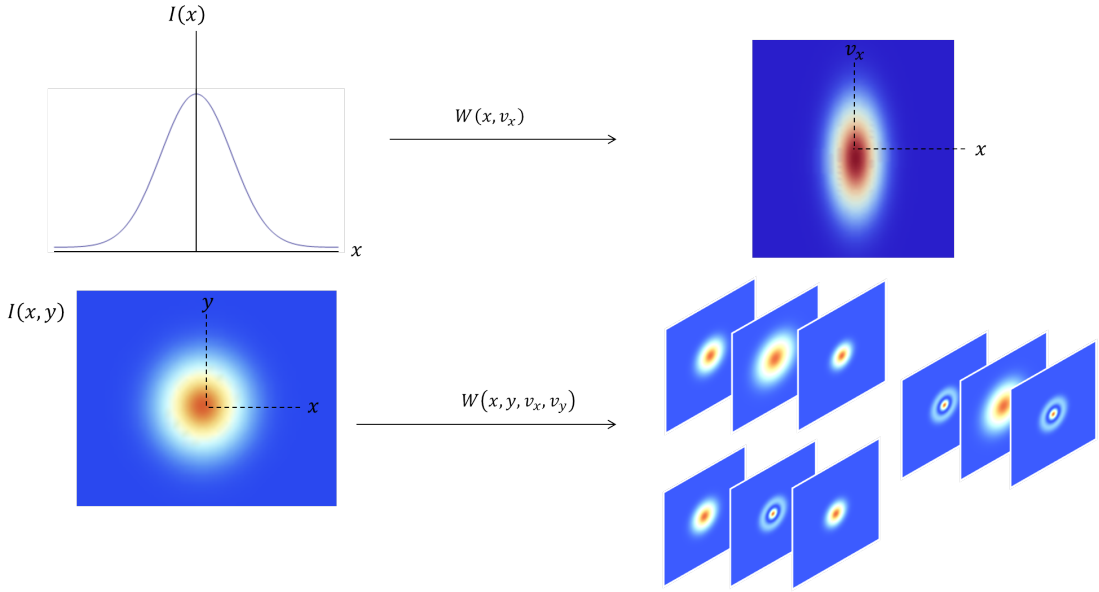


FIGURE 4.5: Transformation of a 1-dimensional and a 2-dimensional function into 2-dimensional and 4-dimensional WDF distributions respectively.

respective intensity distributions are obtained from the equations:

$$\begin{aligned} I(x) &= \frac{1}{2\pi}\int W(x,v)dv, \\ I(v) &= \frac{1}{2\pi}\int W(x,v)dx. \end{aligned} \tag{4.16}$$

To characterise general beams we employ the method of beam moments to calculate beam parameters which include the beam width, divergence, curvature, and from these parameters we can calculate the beam quality factor. Depending on the astigmatism of the beam, we can extract up to 16 beam moments from the WDF from which we can determine various other characterisation parameters like the astigmatism factor [3].

4.3.1 First order moments

From the first order moments we can determine the beam centre in a similar way to that of pure paraxial light beams. Given a paraxial light beam $u(\mathbf{r}) = u(x, y)$ whose

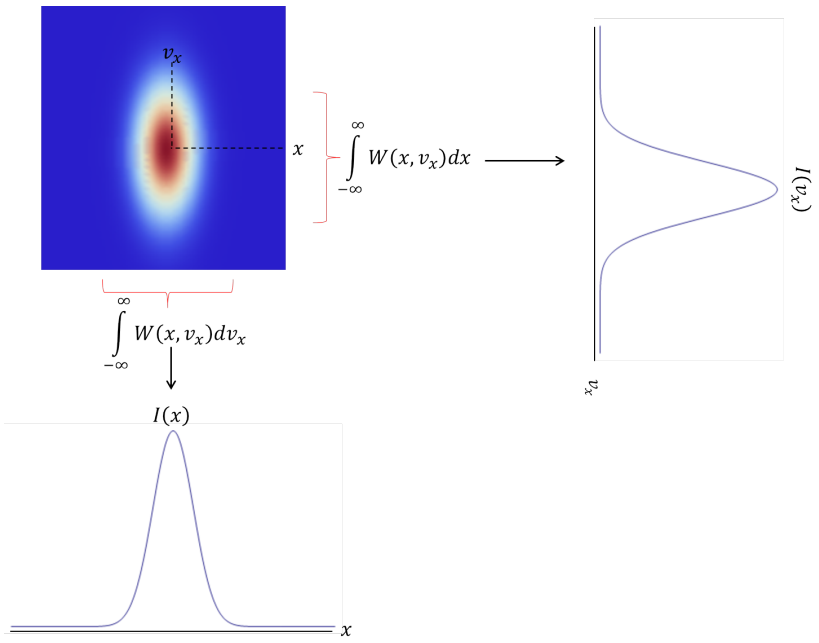


FIGURE 4.6: Integration of the WDF.

WDF is given by $W(\mathbf{r}, \mathbf{v}) = W(x, y, v_x, v_y)$, the first order moments are given by:

$$\begin{aligned} \bar{x} &= \frac{1}{2\pi P} \int\int\int\int x W(x, y, v_x, v_y) dx dy dv_x dv_y, \\ \bar{y} &= \frac{1}{2\pi P} \int\int\int\int y W(x, y, v_x, v_y) dx dy dv_x dv_y, \end{aligned} \tag{4.17}$$

and

$$\begin{aligned} \bar{v}_x &= \frac{1}{2\pi P} \int\int\int\int v_x W(x, y, v_x, v_y) dx dy dv_x dv_y, \\ \bar{v}_y &= \frac{1}{2\pi P} \int\int\int\int v_y W(x, y, v_x, v_y) dx dy dv_x dv_y, \end{aligned} \tag{4.18}$$

where the power distribution P is given by the equation:

$$P = \int\int\int\int W(x, y, v_x, v_y) dx dy dv_x dv_y. \tag{4.19}$$

The beam centre in the spatial domain is thus given by the coordinates $(\bar{x}, \bar{y})$ and in the spatial frequency domain is given by the coordinates $(\bar{v}_x, \bar{v}_y)$.

4.3.2 Second order moments

The beam width, divergence and curvature for the WDF are obtained from the second order moments [56, 3]. Using marginal distributions as demonstrated in Fig.4.6, the beam width in both transverse directions is obtained from the equations:

$$\begin{aligned} w_x^2 &= \frac{2}{\pi P}\int\int\int\int (x-\bar{x})^2 W(x,y,v_x,v_y)dxdydv_xdv_y, \\ w_y^2 &= \frac{2}{\pi P}\int\int\int\int (y-\bar{y})^2 W(x,y,v_x,v_y)dydxdv_xdv_y, \end{aligned} \tag{4.20}$$

and the beam divergence is obtained from the equations:

$$\begin{aligned} \theta_x^2 &= \frac{2\lambda^2}{\pi P}\int\int\int\int (v_x-\bar{v}_x)^2 W(x,y,v_x,v_y)dydxdv_xdv_y, \\ \theta_y^2 &= \frac{2\lambda^2}{\pi P}\int\int\int\int (v_y-\bar{v}_y)^2 W(x,y,v_x,v_y)dydxdv_xdv_y. \end{aligned} \tag{4.21}$$

To determine the beam curvature we use the relation:

$$R_{x,y} = \frac{w_{x,y}^2}{(w_{x,y}\theta_{x,y})} \tag{4.22}$$

and thus we can calculate it from determining the mixed second order moments:

$$\begin{aligned} (w_x\theta_x)^2 &= \frac{2}{\pi P}\int\int\int\int (x-\bar{x})(v_x-\bar{v_x})W(x,y,v_x,v_y)dxdydv_xdv_y, \\ (w_y\theta_y)^2 &= \frac{2}{\pi P}\int\int\int\int (y-\bar{y})(v_y-\bar{v_y})W(x,y,v_x,v_y)dxdydv_xdv_y. \end{aligned} \tag{4.23}$$

4.4 Beam quality factor

The beam quality factor of the WDF is calculated from the second order moments. The calculation is similar to that of the pure paraxial wave function and it uses the beam width, curvature and divergence. Assuming we are evaluating a general

astigmatic beam, the beam quality factor is given by:

$$\begin{aligned} M_x^2 &= \frac{k}{2}\sqrt{\langle w_x^2\rangle\langle\theta_x^2\rangle - \langle w_x\theta_x\rangle^2}, \\ M_y^2 &= \frac{k}{2}\sqrt{\langle w_y^2\rangle\langle\theta_y^2\rangle - \langle w_y\theta_y\rangle^2}. \end{aligned} \tag{4.24}$$

4.5 Summary

In this chapter we studied the WDF and how it can be used to characterise light of varying coherence. The WDF is important in the description and characterisation of partially coherent beams. Using beam moments we can characterise the marginal distributions obtained from the WDF which in theory are supposed to be a representation of the underlying beam's near and far field distributions. Using the marginal distributions we can uniquely identify some beams by calculating the beam quality, this method is especially useful in identifying modes and mode superposition of known Hermite-Gaussian and Laguerre-Gaussian functions. In the next chapter we simulate the generation of the WDF and characterisation of various beams.

5 Simulations

5.1 Simulations

In this chapter we demonstrate the theoretical generation and characterisation of various paraxial beams. We characterise beams using the field function method and the WDF using beam moments. The simulations are carried out using the MATLAB ®and Wolfram Mathematica ®software.

5.1.1 Sampling

Sampling is a significant part of computer simulations, continuous functions are evaluated at discrete points that are a generated on a fixed sample interval [79, 80, 81, 82, 83]. Let $f(x)$ be a continuous function defined on a domain $x \in \mathbb{R}$ such that $x = [x_1, x_2, \ldots, x_N]$. In the computational generation of $f(x)$, each $x_n \in x$ is defined as:

$$x_n = n\delta \tag{5.1}$$

where $n = 1, 2, 3, \ldots, N$ and δ is a fixed spacing between the points x_n as demonstrated in Fig.5.1, N is an finite number that represents the number of points in the interval. The function $f(x)$ is thus defined on a finite interval x characterised by a

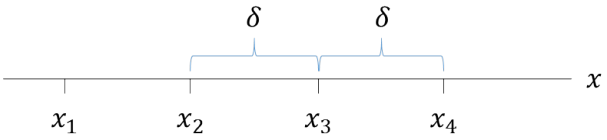


FIGURE 5.1: The domain of points x with a spacing of δ

spacing δ such that:

$$f(x) = [f(x_1), f(x_2), \ldots, f(x_N)] \tag{5.2}$$

We demonstrate the process of sampling using the Fourier transform and inverse Fourier transform of a discrete signal $f(x)$ as proposed in the texts [80, 81, 84, 85].

Let $f(x)$ denote a signal that is defined on a spatial domain x, the Fourier transform [80] of $f(x)$ is given by the equation:

$$\begin{aligned}\tilde{f}(u) &= \mathcal{F}\{f(x)\} \\ &= \int_{-\infty}^{\infty} f(x)\exp(-i2\pi ux)dx\end{aligned} \tag{5.3}$$

and the inverse Fourier transform of $\tilde{f}(u)$ gives us the original function:

$$f(x) = \int_{-\infty}^{\infty} \tilde{f}(u)\exp(i2\pi ux)du \tag{5.4}$$

where dx and du denote the spacing in the x and u domains respectively, u is the spatial frequency domain. Eq.5.3 can be defined using discrete point sampling as:

$$\begin{aligned}\tilde{f}(u_m) &= \mathcal{F}\{f(x_n)\} \\ &= \sum_{n=-\infty}^{\infty} f(x_n)\exp(-i2\pi u_m x_n)(x_{n+1} - x_n)\end{aligned} \tag{5.5}$$

where $m, n \in \mathbb{Z}^+$ and:

$$u_m = [u_1, u_2, \ldots, u_M]. \tag{5.6}$$

Since computational simulations can only work with a finite number of points, we replace ∞ by a large number N such that:

$$\tilde{f}(u_m) = \lim_{N\to\infty} \sum_{n=-N}^{N} f(x_n)\exp(-i2\pi u_m x_n)(x_{n+1} - x_n) \tag{5.7}$$

We know that $x_n = n\delta$, then the sampling spacing in the spatial frequency domain u is related to the spatial sampling spacing by:

$$\delta_u = \frac{1}{N\delta} \tag{5.8}$$

and thus the points in the spatial frequency domain are given by:

$$\begin{aligned} u_m &= m\delta_u \\ &= m\frac{1}{N\delta} \end{aligned} \tag{5.9}$$

We use a Cartesian grid system and so we sample from negative to positive numbers and for N points we obtain the equation:

$$\begin{aligned} \tilde{f}\left(\frac{m}{N\delta}\right) &= \mathcal{F}\{f(n\delta)\} \\ &= \sum_{n=-N/2}^{N/2-1} f(n\delta)\exp(-i2\pi mn/N)\delta, \end{aligned} \tag{5.10}$$

the number of points ends at $N/2-1$ instead of $N/2$ because we we take into consideration the point 0. Since $n \in \mathbb{Z}^+$, the indices n can only take positive values and so sampling from $-N/2$ is invalid and so we need to shift the whole sampling interval by $N/2$ points to the positive side of the interval.

We define a new integer n' that is a shift of the sampling interval and allows us to sample from $n = 1$, the function $f(n\delta)$ can now be defined by:

$$f_{n'} = \begin{cases} f[(n' + N/2)\delta] & \text{for} \quad n' = 1, 2, \ldots N/2 + 1 \\ f[(n' - N - 2)\delta] & \text{for} \quad n' = N/2 + 2, N/2 + 3, \ldots, N. \end{cases} . \tag{5.11}$$

Rearranging the spatial sampling interval results in the spatial frequency domain rearrangement, we denote the new sampling integer in the spatial domain as m' and the Fourier transform is thus given by:

$$\tilde{f}_{m'} = \delta \sum_{n=1}^{N} f_{n'} \exp[-i2\pi(m' - 1)(n' - 1)/N]. \tag{5.12}$$

The inverse Fourier transform is then given by

$$f_{n'} = \frac{1}{N\delta} \sum_{n=1}^{N} \tilde{f}_{m'} \exp[i2\pi(m' - 1)(n' - 1)/N]. \tag{5.13}$$

Given a two dimensional function $f(x, y)$ such that $x, y \in \mathbb{R}$, the domain points are defined by:

$$\begin{aligned} x &= n_x \delta_x, \\ y &= n_y \delta_y \end{aligned} \tag{5.14}$$

We present an example (Fig.5.2) using MATLAB ®for the generation of the Fourier transform of the Gaussian function:

$$f(x) = \sqrt{\frac{2}{\pi w_0^2}} \exp\left(- \frac{x^2 + y^2}{w_0^2} \right) \tag{5.15}$$

The simulation code is given by:

n = 2^8;

delta = $2 * 10^-3$;

deltaf = 1/(n*delta);

v = (-n/2:(n/2)-1);

x = delta*v;

u = deltaf*v;

ux = v*deltaf;

w = 0.015;

lambda = $633 * 10^-9$;

k = 2*pi/lambda;

f = $\sqrt{\frac{2}{\pi w_0^2}} \exp\left(- \frac{x^2+y^2}{w_0^2} \right)$;

ftff = fftshift(fft(f))*delta;

the Fourier transform is applied using the built-in MATLAB fft(f) function.

5.1.2 Field function

The field function method is demonstrated by generating and characterising a Laguerre-Gaussian(LG) beam as an example using a MATLAB ®program. The function is

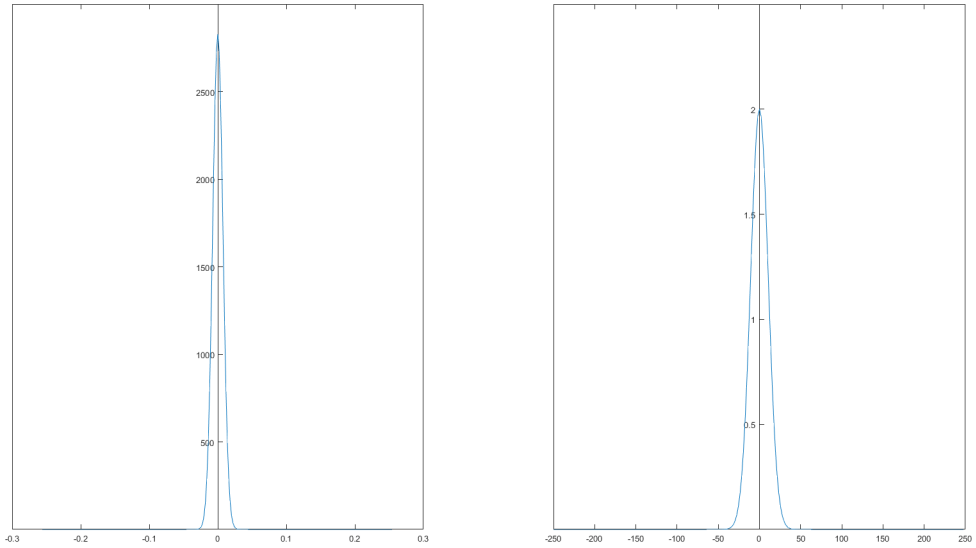


FIGURE 5.2: The function $f(x)$ and the Fourier transform $f(u)$ generated using MATLAB ®

given by:

$$\begin{aligned} \mathrm{LG}_p^{\ell}(r, w, \phi) = \sqrt{\frac{2p!}{\pi w_0^2 (p + |\ell|)!}} \left(\frac{\sqrt{2}r}{w_0}\right)^{|\ell|} L_p^l \left(\frac{2r^2}{w_0^2}\right) \\ \times \exp\left(-\frac{r^2}{w_0^2}\right) \exp(i\ell\phi), \end{aligned} \tag{5.16}$$

where $r = \sqrt{x^2 + y^2}$, w_0 is the beam waist size and:

$$\phi = \arctan\left(\frac{x}{y}\right). \tag{5.17}$$

Simulation

The simulation of the field function method is carried out using custom functions for the LG modes. We define a real domain:

$$\begin{aligned} x &= [x_1, x_2, \ldots, x_N], \\ y &= [y_1, y_2, \ldots, y_N], \end{aligned} \tag{5.18}$$

where

$$\begin{aligned} x_n &= n\delta. \\ y_m &= m\delta. \end{aligned} \tag{5.19}$$

We set N as a power of 2 i.e $N = 2^7$ and $\delta = 2 \times 10^{-6}$ is the spacing of the domain. We generate a 2-dimensional meshgrid using the x and y domains at which the LG function is defined on:

$$(x, y) = \begin{bmatrix} (x_1, y_1) & (x_2, y_1) & \dots & (x_n, y_1) \\ (x_1, y_2) & (x_2, y_2) & \dots & (x_n, y_2) \\ \vdots & \vdots & \ddots & \vdots \\ (x_1, y_m) & (x_2, y_m) & \dots & (x_n, y_m) \end{bmatrix} \tag{5.20}$$

such that $n = m$. The LG function in Eq.5.16 is then evaluated as:

$$f(x, y) = \begin{bmatrix} f(x_1, y_1) & f(x_2, y_1) & \dots & f(x_n, y_1) \\ f(x_1, y_2) & f(x_2, y_2) & \dots & f(x_n, y_2) \\ \vdots & \vdots & \ddots & \vdots \\ f(x_1, y_m) & f(x_2, y_m) & \dots & f(x_n, y_m) \end{bmatrix} \tag{5.21}$$

where we have defined the parameters:

$$\begin{aligned} w_0 &= 0.015\text{m}, \\ \lambda &= 633 \times 10^{-9}, \\ p &\in \mathbb{R}, \\ \ell &\in \mathbb{R}. \end{aligned} \tag{5.22}$$

To determine the divergence of the beam we used the built in MATLAB®Fourier transform function given by Eq5.2 and we defined the Fourier variable u as:

$$u_n \quad = n\tfrac{1}{N\delta} \tag{5.23}$$

We characterised the beams using beam moments. The first order moments were determined from:

$$\begin{aligned}
\langle x\rangle &= \frac{1}{P}\int_{\infty}^{\infty}\int_{\infty}^{\infty} x|f(x,y)|^2 dxdy,\\
\langle y\rangle &= \frac{1}{P}\int_{\infty}^{\infty}\int_{\infty}^{\infty} y|f(x,y)|^2 dxdy,\\
\langle v_x\rangle &= \frac{1}{P}\int_{\infty}^{\infty}\int_{\infty}^{\infty} v_x|\tilde{f}(v_x,v_y,)|^2 dv_x dv_y,\\
\langle v_y\rangle &= \frac{1}{P}\int_{\infty}^{\infty}\int_{\infty}^{\infty} v_y|\tilde{f}(v_x,v_y)|^2 dv_x dv_y.
\end{aligned} \tag{5.24}$$

and the second order moments:

$$\begin{aligned}
\langle w_x^2\rangle &= \frac{1}{P}\int_{\infty}^{\infty}\int_{\infty}^{\infty} [x-\langle x\rangle]^2]|f(x,y)|^2 dxdy,\\
\langle w_y^2\rangle &= \frac{1}{P}\int_{\infty}^{\infty}\int_{\infty}^{\infty} [y-\langle y\rangle]^2]|f(x,y)|^2 dxdy,\\
\langle \theta_x^2\rangle &= \frac{4\lambda^2}{\pi P}\int_{\infty}^{\infty}\int_{\infty}^{\infty} [v_x-\langle v_x\rangle]^2|\tilde{f}(v_x,v_y)|^2 dv_x dv_y,\\
\langle \theta_y^2\rangle &= \frac{4\lambda^2}{\pi P}\int_{\infty}^{\infty}\int_{\infty}^{\infty} [v_y-\langle v_y\rangle]^2|\tilde{f}(v_x,v_y)|^2 dv_x dv_y.
\end{aligned} \tag{5.25}$$

the beam quality factor was then determined from the equations:

$$\begin{aligned}
M_x^2 &= \frac{\pi^2}{\lambda^2}\langle w_x^2\rangle\langle \theta_x^2\rangle,\\
M_y^2 &= \frac{\pi^2}{\lambda^2}\langle w_y^2\rangle\langle \theta_y^2\rangle.
\end{aligned} \tag{5.26}$$

Some of the single coherent mode results obtained from the simulation are presented in Fig.5.3. The single mode beams were simulated and the characterisation results were as expected for the various Laguerre-Gaussian modes, the fundamental Gaussian beam waist was set to $w_0 = 2.1mm$ and the subsequent characterisation results obtained in the simulation adhere to the expected beam width and beam quality factor:

$$\begin{aligned}
w_{pl} &= w_0\sqrt{2p+|\ell|+1},\\
M^2 &= 2p+\ell+1
\end{aligned} \tag{5.27}$$

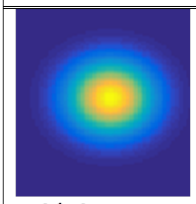
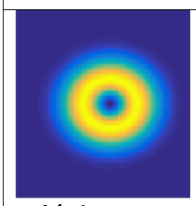
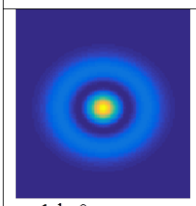
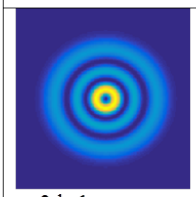
	Mode	$w_{calculated}$	$w_{expected}$	$M^2_{calculated}$	$M^2_{expected}$
a)	 p=0,l=0	2.31mm	2.31mm	1	1
b)	 p=0,l=1	3.27mm	3.27mm	2	2
c)	 p=1,l=0	4.0mm	4.0mm	3	3
d)	 p=2,l=1	5.66mm	5.66mm	6	6

FIGURE 5.3: Generated single mode beams, their beam width, divergence and beam quality factor.

We also generated multi-mode beams that are presented in Fig.5.4 where the expected M^2 is given by the equation:

$$\mathrm{M}_e^2 = \sum_n c_n[2p + \mathrm{abs}(l) + 1], \tag{5.28}$$

where c_n is the weighting of each nth mode and the beam width is also obtained in a similar weighted manner. The beam width and beam quality factor for the mode superpositions Fig.5.4(a)&(c) were obtained as expected. The mode superposition in Fig.5.4(b) exhibits a distortion in its intensity profile and the parameter results vary in each transverse direction due to a singularity in the phase that arises when we superimpose a vortex and a Gaussian beam, the singularity manifests as a hole in the intensity distribution [86].

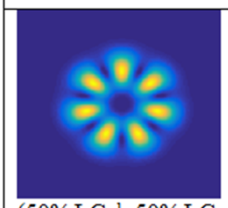
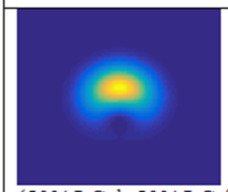
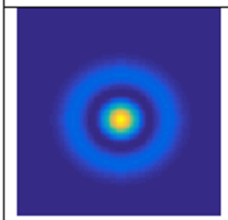
	Mode	w_x	w_y	M^2_x	M^2_y	$M^2_{expected}$
a)	 (50% LG_0^1, 50% LG_0^{-5})	4.90 mm	4.90 mm	4.5	4.5	4.5
b)	 (50% LG_0^1, 50% LG_0^0)	2.83 mm	2.31 mm	1.2247	1.2247	1.5
c)	 (33.33% LG_0^0, 33.33% LG_1^0, 33.33% LG_2^0)	3.10 mm	3.10 mm	3	3	3

FIGURE 5.4: Generated multi-mode mode beams, their beam width and beam quality factor which is given by $\mathrm{M}_e^2 = \sum_n c_n[2p + \mathrm{abs}(l) + 1]$ in both transversal directions.

5.2 WDF

The WDF generation and characterisation is separated into two sections, the generation of 1-dimensional LG modes and the generation of 2-dimensional LG modes.

5.2.1 1D WDF generation

We define the Laguerre-Gaussian function in 1-dimension using the equation:

$$\mathrm{LG}_p^{\ell}(x, w, \phi) = \sqrt{\frac{2p!}{\pi w_0^2 (p + |\ell|)!}} \left(\frac{\sqrt{2}x}{w_0}\right)^{|\ell|} L_p^l\left(\frac{2x^2}{w_0^2}\right) \exp\left(-\frac{x^2}{w_0^2}\right), \tag{5.29}$$

and the WDF is defined as:

$$\mathrm{W}(x, w) = \int f(x + s/2) f^*(x - s/2) e^{-ius} ds. \tag{5.30}$$

The sample space is defined as before, we create an x domain:

$$x = [x_1, x_2, \ldots, x_N] \tag{5.31}$$

such that the LG modes are defined as:

$$f(x) = [f(x_1), f(x_2), \ldots, f(x_N)]. \tag{5.32}$$

The WDF is generated using Fourier shift method [48]. Given a function $f(x)$, a shift s to the domain of $f(x)$ is introduced by the equation:

$$f(x \pm s) = \mathcal{F}^{-1}\{\mathcal{F}\{f(x)\} e^{\pm ius}\}, \tag{5.33}$$

where u is the frequency coordinate. The process starts with an element-wise shift on the domain of f by a constant s which is given by:

$$f(\bar{x} \pm s) = [f(x_1 \pm s), f(x_2 \pm s), ..., f(x_N \pm s)]. \tag{5.34}$$

Let s represent a vector of shifts, for each value $s_i \in s$, $i \in [1, N]$ we have a vector of the function f such that:

$$f(\bar{x} \pm s_i) = [f(x_1 \pm s_i), f(x_2 \pm s_i), ..., f(x_N \pm s_i)]. \tag{5.35}$$

The shifted function $f(x \pm s)$ across the domain s is given by:

$$f(\bar{x} \pm s) = \begin{bmatrix} f(x_1 \pm s_1) & f(x_2 \pm s_1) & \cdots & f(x_N \pm s_1) \\ f(x_1 \pm s_2) & f(x_2 \pm s_2) & \cdots & f(x_N \pm s_2) \\ \vdots & \vdots \ddots & \cdots & \vdots \\ f(x_1 \pm s_N) & f(x_2 \pm s_N) & \cdots & f(x_N \pm s_N) \end{bmatrix}. \tag{5.36}$$

The shift is introduced into the LG modes by means of an inverse Fourier transform such that:

$$\mathcal{F}^{-1}\{\mathcal{F}\{f(x)\}e^{-ius}\} = \begin{bmatrix} f(x_1 - s_1) & f(x_1 - s_2) & \cdots & f(x_1 - s_N) \\ f(x_2 - s_1) & f(x_2 - s_2) & \cdots & f(x_2 - s_N) \\ \vdots & \vdots \ddots & \cdots & \vdots \\ f(x_N - s_1) & f(x_N - s_2) & \cdots & f(x_N - s_N) \end{bmatrix}. \tag{5.37}$$

The WDF is then generated as a 2-dimensional function:

$$W(x, s) = \begin{bmatrix} W(x_1, v_1) & W(x_1, v_2) & \cdots & W(x_1, v_N) \\ W(x_2, v_1) & W(x_2, v_2) & \cdots & W(x_2, v_N) \\ \vdots & \vdots \ddots & \cdots & \vdots \\ W(x_N, v_1) & W(x_N, v_2) & \cdots & W(x_N, v_N) \end{bmatrix}. \tag{5.38}$$

The WDF was characterised using the following equations:

$$\begin{aligned} \langle x \rangle &= \frac{1}{P} \int_{\infty}^{\infty} \int_{\infty}^{\infty} xW(x, s) dx ds, \\ \langle v \rangle &= \frac{1}{P} \int_{\infty}^{\infty} \int_{\infty}^{\infty} vW(x, s) dx ds \end{aligned} \tag{5.39}$$

and the second order moments:

$$\begin{aligned}\langle w^2\rangle &= \frac{1}{P}\int_{\infty}^{\infty}\int_{\infty}^{\infty}[x-\langle x\rangle]^2]W(x,v)dxdv,\\ \langle \theta^2\rangle &= \frac{4\lambda^2}{\pi P}\int_{\infty}^{\infty}\int_{\infty}^{\infty}[v-\langle v\rangle]^2W(x,v)dxds,\end{aligned} \tag{5.40}$$

where we determined the beam quality factor using the equation:

$$M^2 = \frac{\pi^2}{\lambda^2}\langle w_x^2\rangle\langle \theta_x^2\rangle. \tag{5.41}$$

Some of the results obtained from the WDF generation given above are listed in Fig.5.5. For some modes the beam quality factor obtained from the WDF is slightly off the expected beam quality factor, we simulated and characterised pure 1-dimensional modes and the results are comparable. The difference between the obtained beam quality factor and the expected beam quality factor may be due to the partitioning of the 2-dimensional beam from which we obtain the 1-dimensional beam.

5.2.2 2-dimensional WDF generation

The WDF generation of coherent 2-dimensional LG beams is carried out as follows. We define a 2-dimensional LG function $f(x,y)$ such that:

$$f(x,y) = \begin{bmatrix} f(x_1,y_1) & f(x_2,y_1) & \dots & f(x_n,y_1)\\ f(x_1,y_2) & f(x_2,y_2) & \dots & f(x_n,y_2)\\ \vdots & \vdots & \vdots\ddots & \vdots\\ f(x_1,y_m) & f(x_2,y_m) & \dots & f(x_n,y_m)\end{bmatrix} \tag{5.42}$$

We then generate the WDF of each column $f(y)_{xn}$ and obtain an array of sections of the WDF given by;

$$W(y,s) = [W(y,s)_{x1}, W(y,s)_{x2}, \dots, W(y,s)_{xN}] \tag{5.43}$$

The same procedure is repeated for each row of $f(x,y)$ and we get the WDF sections:

$$W(x,s) = [W(x,s)_{y1}, W(x,s)_{y2}, \dots, W(x,s)_{yN}], \tag{5.44}$$

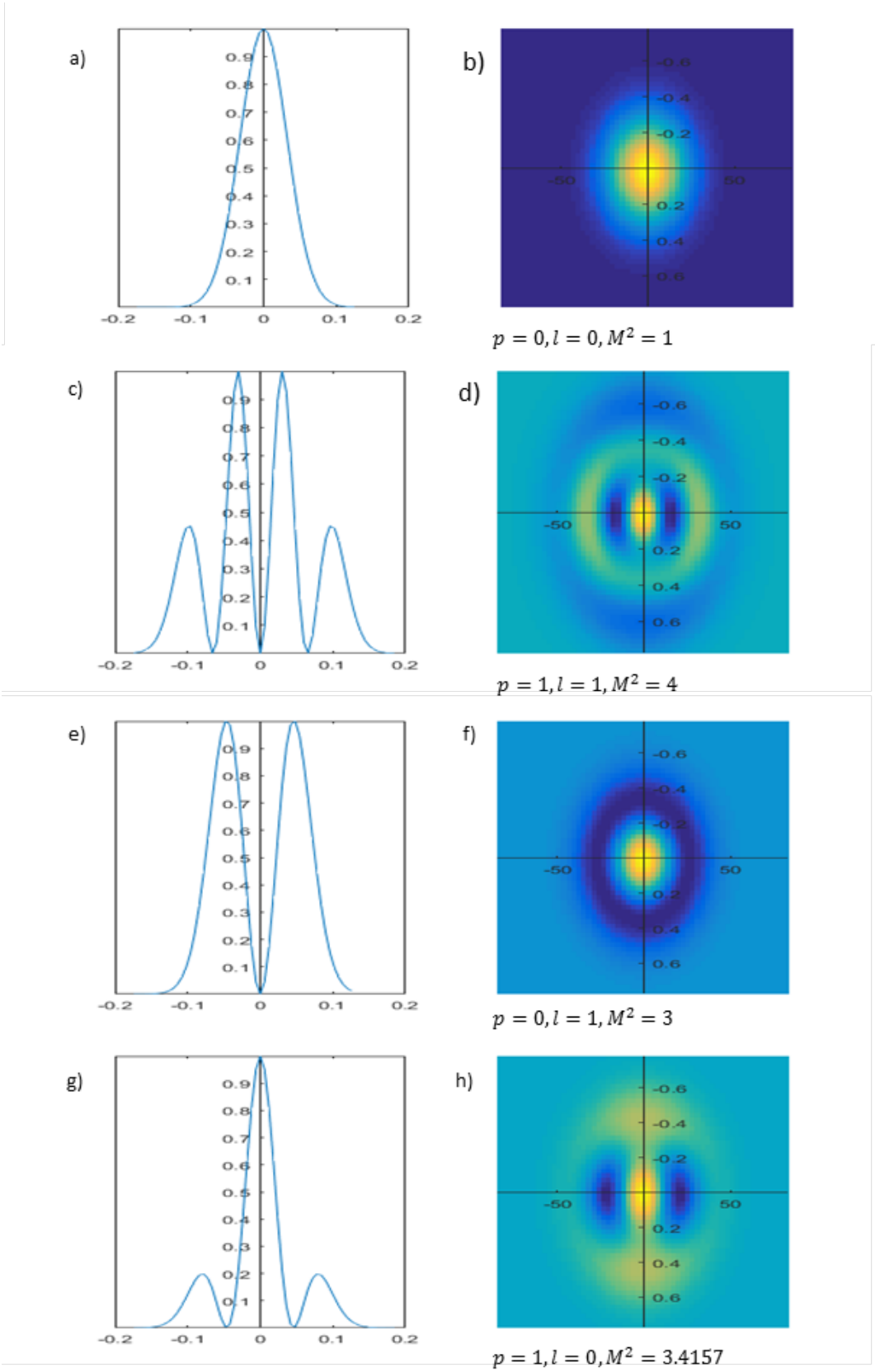


FIGURE 5.5: 1-dimensional LG beams transformed into 2-dimensional WDF plots

such that each WDF section is given by:

$$W(x,s)_{xn} = \begin{bmatrix} W(x_1,s_1) & W(x_1,s_2) & \cdots & W(x_1,s_N) \\ W(x_2,s_1) & W(x_2,s_2) & \cdots & W(x_2,s_N) \\ \vdots & \vdots\ddots & \cdots & \vdots \\ W(x_N,s_1) & W(x_N,s_2) & \cdots & W(x_N,s_N) \end{bmatrix}_{xn} \tag{5.45}$$

The characterisation was carried out as follows. The first order moments were determined from the equations:

$$\begin{aligned} \langle x\rangle &= \frac{1}{P}\int_\infty^\infty\int_\infty^\infty\int_\infty^\infty\int_\infty^\infty xW(x,y,v_x,v_y)dxdydv_xdv_y, \\ \langle y\rangle &= \frac{1}{P}\int_\infty^\infty\int_\infty^\infty\int_\infty^\infty\int_\infty^\infty yW(x,y,v_x,v_y)dxdydv_xdv_y, \\ \langle v_x\rangle &= \frac{1}{P}\int_\infty^\infty\int_\infty^\infty\int_\infty^\infty\int_\infty^\infty v_xW(x,y,v_x,v_y)dxdydv_xdv_y,, \\ \langle v_y\rangle &= \frac{1}{P}\int_\infty^\infty\int_\infty^\infty\int_\infty^\infty\int_\infty^\infty v_yW(x,y,v_x,v_y)dxdydv_xdv_y,. \end{aligned} \tag{5.46}$$

And the second order moments

$$\begin{aligned} \langle w_x^2\rangle &= \frac{1}{P}\int_\infty^\infty\int_\infty^\infty\int_\infty^\infty\int_\infty^\infty [x-\langle x\rangle]^2]W(x,y,v_x,v_y)dxdydv_xdv_y, \\ \langle w_y^2\rangle &= \frac{1}{P}\int_\infty^\infty\int_\infty^\infty\int_\infty^\infty\int_\infty^\infty [y-\langle y\rangle]^2]W(x,y,v_x,v_y)dxdydv_xdv_y, \\ \langle \theta_x^2\rangle &= \frac{4\lambda^2}{\pi P}\int_\infty^\infty\int_\infty^\infty\int_\infty^\infty\int_\infty^\infty [v_x-\langle v_x\rangle]^2W(x,y,v_x,v_y)dxdydv_xdv_y, \\ \langle \theta_y^2\rangle &= \frac{4\lambda^2}{\pi P}\int_\infty^\infty\int_\infty^\infty\int_\infty^\infty\int_\infty^\infty [v_y-\langle v_y\rangle]^2W(x,y,v_x,v_y)dxdydv_xdv_y, \end{aligned} \tag{5.47}$$

the beam quality factor was then determined from the equations:

$$\begin{aligned} M_x^2 &= \frac{\pi^2}{\lambda^2}\langle w_x^2\rangle\langle\theta_x^2\rangle, \\ M_y^2 &= \frac{\pi^2}{\lambda^2}\langle w_y^2\rangle\langle\theta_y^2\rangle. \end{aligned} \tag{5.48}$$

Below we present results of the 4-dimensional WDF generated from 2-dimensional LG modes. Each 4-dimensional WDF is given in Fig.5.6 using a 2-dimensional section since we cannot plot a 4-dimensional function. The sectional generation yielded the desired WDF results for single mode beams, the beam quality factors were obtained as a) and b) p =1 & ℓ =1, M^2=4. c) and d) p =0 & ℓ =0, M^2=1. e) and f)

p =1 & ℓ =0, M^2=3. We also notice that the calculated beam quality factors are exactly what we expect with no slight differences due to generating the WDF using a 2-dimensional beam instead of a 1-dimensional one.

5.2.3 Partially coherent beams

The characterisation of partially coherent light was carried out using a Gaussian-Schell model beam given by the mutual coherence function

$$\Gamma(x,s,\sigma) = \frac{1}{2}ce\left|\sqrt{\frac{2}{\pi w_0^2}}\right|^2 \exp\left(-\frac{2x^2}{w_0^2} - \frac{s^2}{2w_0^2\sigma^2}\right) \tag{5.49}$$

where σ is the degree of coherence, $c = 3 \times 10^1$1mm/s, $w_0 = 1$mm and $e = 8.85 \times 10^{-9}$F/mm. Using Eq.5.49, we generated Gauss-Schell beams of different coherence degree, we then transformed and characterised them using the WDF and beam moments.

The generated partially coherent beams and their corresponding WDFs are presented in Fig.5.7. From the results we notice that the pure fundamental case where the degree of coherence $\sigma = 1$ results in the expected beam quality factor $M^2 = 1$. The beam quality factor gradually gets large as σ approaches zero, the increase in the beam quality factor is a result of increased divergence due to increasing fluctuations in the phase, the beam quality factor approaches ∞ as the degree of coherence approaches zero.

5.3 Summary

In this chapter we simulated the generation of the WDF for various coherent and partially coherent beams. Using the beam quality factor we characterised coherent

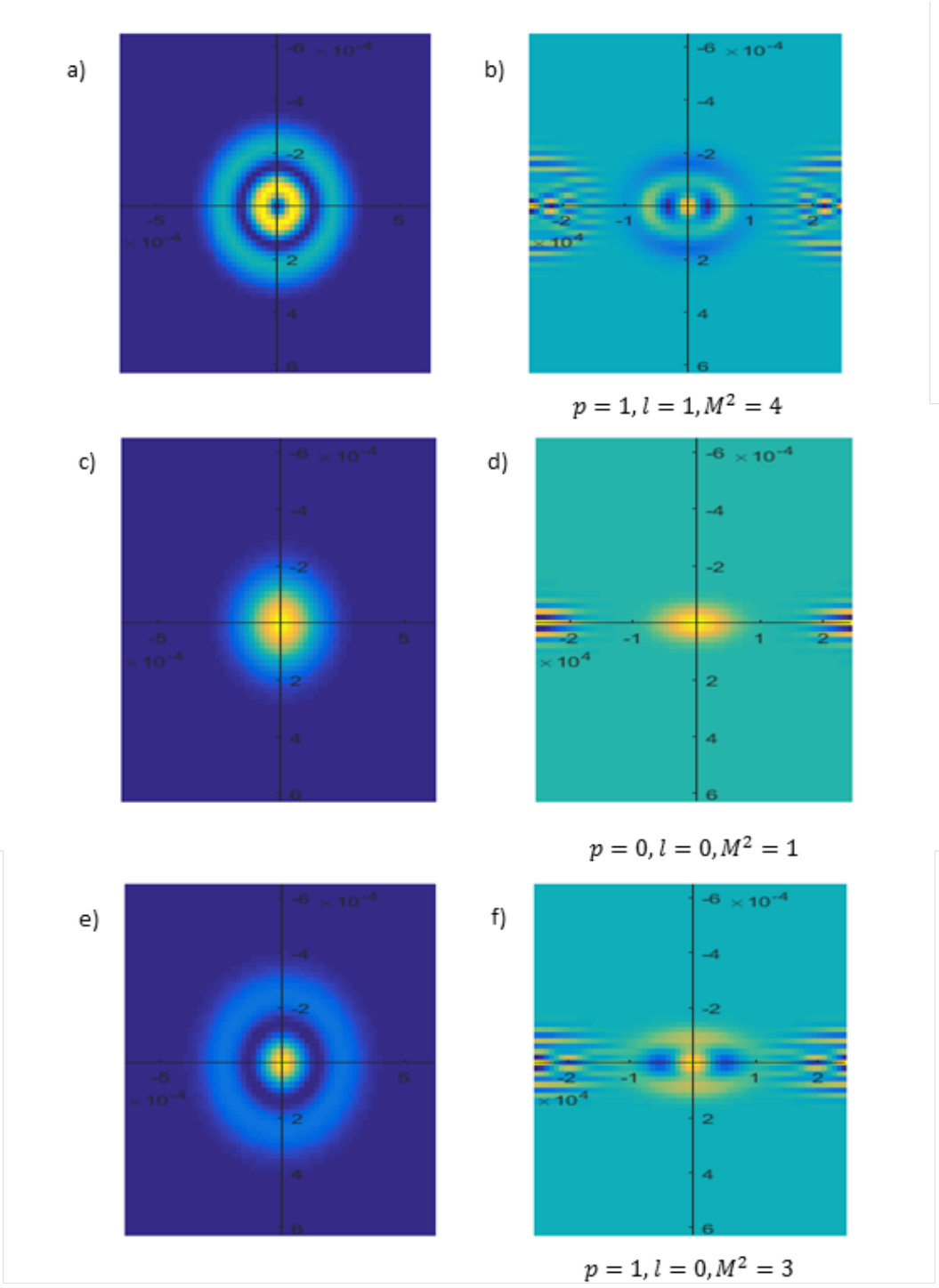


FIGURE 5.6: 2-dimensional LG beams (left) and their corresponding 2-dimensional WDF centre section plots (right).

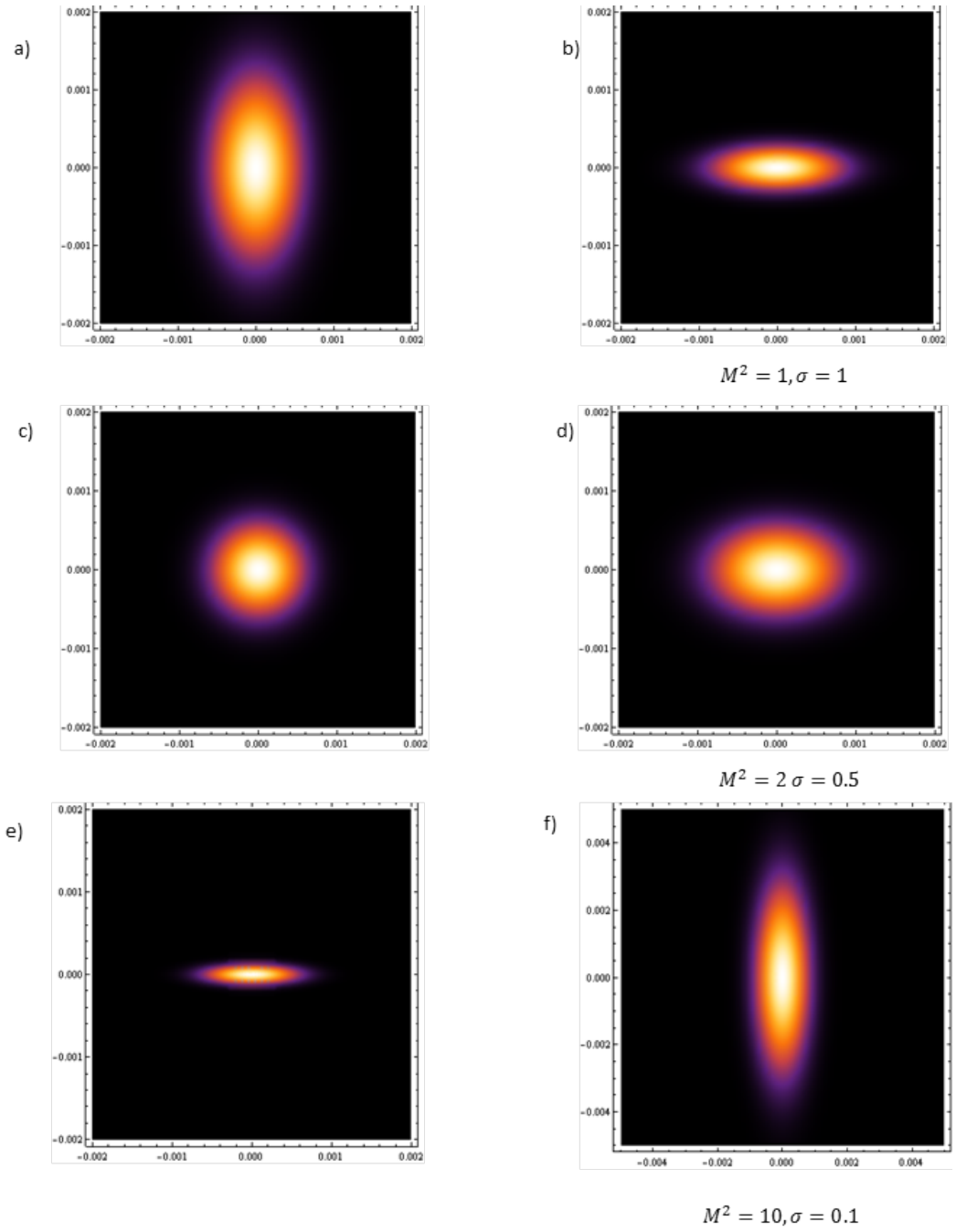


FIGURE 5.7: Gaussian-Schell model beams (left) and their corresponding WDF plots (right).

single mode beams and superpositions of various modes, we also characterised partially coherent beams using the Gauss-Schell model and the results were obtained as expected. The WDF was generated for 1-dimensional and 2-dimensional beams, excluding a few cases whose slight differences can be explained, the resulting marginal distributions yielded the desired results which are comparable to the characterisation results obtained from the pure field functions. The theoretical results obtained in this chapter verify the use of the WDF as a general approach to the characterisation of light beams. In the next chapter we investigate various experimental methods employed in generating the WDF for real physical beams.

6 Experiments

6.1 Introduction

Various authors have generated the Wigner Distribution Function (WDF) experimentally as a means to characterise beams using parameters such as the beam quality factor and the degree of coherence. The experimental generation of the WDF is important especially for the characterisation of partially coherent light as the mutual coherence function can be obtained indirectly from the WDF [87] [72]. The WDF has been experimentally generated for various other purposes for coherent and partially coherent beams including the determination of propagation parameters and studying the changes in beam parameters in interaction with optical elements [88].

A key aspect in the experimental generation of the WDF is finding a method that takes into account and accommodates the increase in dimension while generating the full WDF of a beam. As mentioned previously, the WDF is a $2n$-dimensional distribution of an n-dimensional beam and so generating a 4-D WDF of a 2-D beam requires a sectional method [89]. The WDF can be interpreted as a coordinate shift of the light field and a Fourier transform of the shift coordinate, this has resulted in the formulation of methods such as the inverse Radon transform . A different method to this treats the WDF as a linear spatial coordinate shift that is paired with an exponential modulation of the light field using the k-vector, from both these methods the WDF can be successfully generated experimentally as demonstrated by the results obtained in the literature [90, 91]. One of the direct experimental methods of obtaining the WDF is by performing a real physical shift on the beam using a steering optical element such a steering mirror, this results in a coordinate shift of the beam. One of various ways to achieve the exponential modulation of the shifted product in the WDF is to perform a set of angular shifts along with the

linear coordinate shifts [72, 88]. A Fourier transform can also be applied on one of the coordinates of a symmetrical beam to obtain the WDF [89, 92, 93]. The Radon transform is another useful indirect method of obtaining the WDF, a Radon transform is generated by recording various 1-dimensional intensity distributions of the light field and analytically transforming them using the inverse Radon transform [87, 91].

In this chapter we will review various experimental methods that are used to obtain the WDF and perform an experimental simulation of one of the methods. We will use the beam parameter results obtained from the simulation and compare them to expected theoretical results.

6.2 Review of experimental methods

Obtaining a full 4-dimensional WDF from a physical 2-dimensional beam requires the partitioning of the beam into sections from which the WDF can be generated. Taking sections of the beam is advantageous when one is dealing with symmetric light fields, a single 2-dimensional WDF plot is enough to characterise the underlying field since the results from one axis can be extended to the other [3]. Performing transformations on a light beam in one transverse direction and/or sectioning are common in the generation of the WDF, the experiments reviewed in this section use at least one of these methods.

Sectioning a light beam into a set of 1-dimensional beams requires the use of some sort aperture that only allows a section of the beam to pass through it and blocking the rest of the beam. Various experimental set-ups employ this method including the *scan-slit* method presented in [89] by K. H. Brenner and A. W. Lohmann, the set-up uses a slit that scans across the entire beam and generates a WDF from each section of the beam as demonstrated in Fig.6.1.

To use as a slit, the set-up of this experiment (Fig.6.2) contains a screen that transmits a slit section of the of a real beam described by a function $u(x, y)$ and the

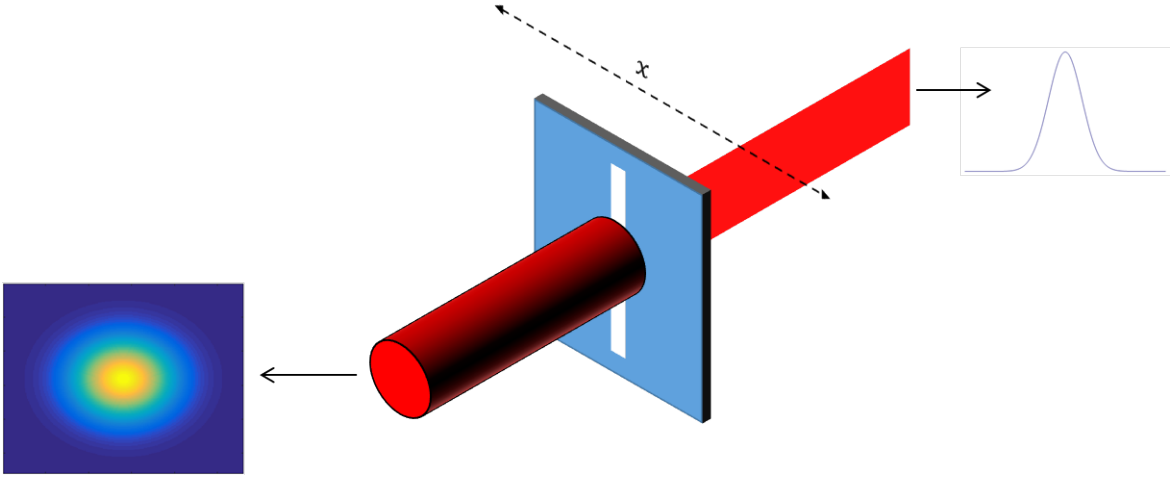


FIGURE 6.1: The scanning of a beam using a slit

output is obtained as a 1-dimensional function $u(x)$, the aim with employing the transparency is to generate the function:

$$F(x,s) = u\left(x + \frac{1}{2}y\right)u\left(x - \frac{1}{2}y\right). \tag{6.1}$$

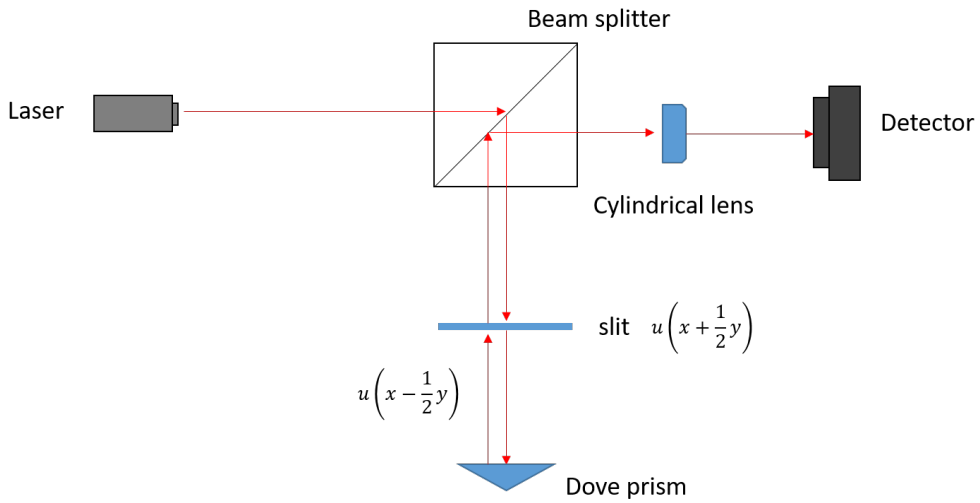


FIGURE 6.2: The scanning transparency setup

The function $F(x,y)$ is generated by rotating the transparency by an angle θ using

the coordinate matrix transformation:

$$\begin{aligned}\begin{bmatrix} x \\ y \end{bmatrix} &= \begin{bmatrix} x_0 \\ y_0 \end{bmatrix}^t \begin{bmatrix} \cos\theta & -\sin\theta \\ \sin\theta & \cos\theta \end{bmatrix} \\ &= \begin{bmatrix} x_0\cos\theta - y_0\sin\theta \\ x_0\sin\theta + y_0\cos\theta \end{bmatrix},\end{aligned} \tag{6.2}$$

and we can obtain the function $u(x - 1/2y)$ by setting $\cos\theta = 1$ and $\sin\theta = 1/2$, the angle θ is then $\theta \approx 26.6^o$. The transparency is irradiated with the beam of light $u(x, y)$ and the output is obtained as $u(x - 1/2y)$, the output is inverted by a Dove prism such that:

$$u(x - 1/2y) \longleftrightarrow u(x + 1/2y). \tag{6.3}$$

The beam $u(x+1/2y)$ is again passed through the transparency to form the product $u(x-1/2y)u(x+1/2y)$, this product is then Fourier transformed along the y coordinate using a cylindrical lens. Each shift intensity is recorded by a detector and some of the results are presented in Fig.6.3.

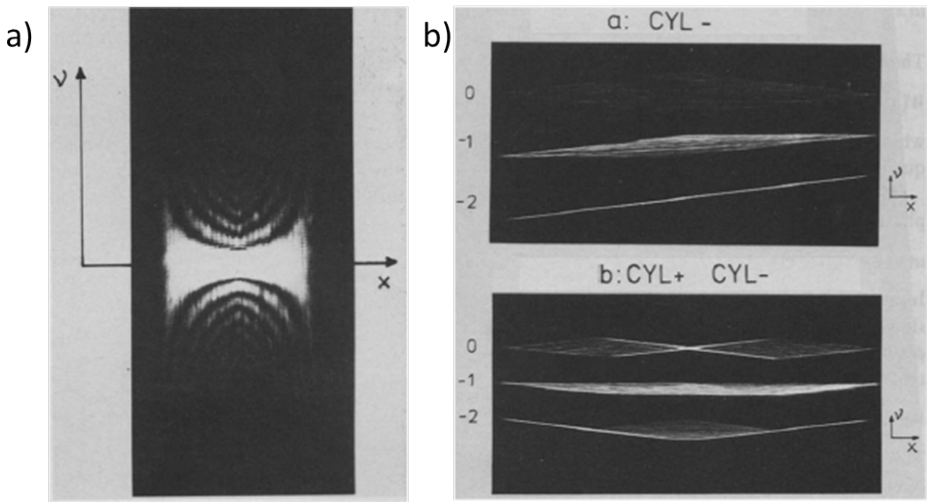


FIGURE 6.3: a) The WDF of a slit. b) The WDF a. a cylindrical lens and b. half positive and negative lenses, both generated using a hologram as complex objects. Image courtesy of K. H. Brenner and A. W. Lohmann [89]

Both real and complex objects were used to generate the WDF and in the case of

of a complex object, the transparency is replaced by a hologram because now the product, $u(x-1/2y)u^*(x+1/2y)$, has a conjugate term. A hologram inherently contains a conjugate of the encoded field.

Another WDF sectional generation method is demonstrated by Jagus J. *et al* in [87]. Sectioning of the beam in this experiment is achieved by attaching a slit on a detector, the detector records 1-dimensional intensity distributions of the field that are used to generate the WDF and characterise it using the beam quality factor and global coherence factor. The experiment makes use of the inverse Radon transform, the Radon transform is an intergration method that uses rays to measure the intensity of a distribution based on the interaction of the rays with the distribution [94]. In the paper [91], Eppich B. and Reng N. concluded that the WDF can be determined from the inverse Radon transform of a finite number of intensity plots recorded along the propagation axis of the beam. To generate the WDF, a beam $u(x,y)$ is passed through a lens of focal length f and several 1-dimensional intensity distributions are recorded by the detector with a slit attached to it along the propagation axis. The positions z_k at which the intensity distributions $I(x,z_k)_k$ are recorded is determined by a parameter α_k pre-experiment, this parameter corresponds to a set of angles in the WDF intensity distribution. The set of parameters α contains a set of equidistant angles α_k as demonstrated in Fig.6.4 where the angles are at least 135^o and are given by:

$$\alpha_k = \arctan\left(\frac{z_k - z_0}{z_R}\right), \tag{6.4}$$

where z_R the Rayleigh range. The complete set of intensity distributions is represented by $I(\tilde{x},\tilde{\alpha})$ where $\tilde{x} = x/w_k$, $\tilde{\alpha}_k = \alpha_k/w_k$ and $w_k = w_0/\cos\alpha_k$, w_0 is the beam waist. From the inverse Radon transform of $I(\tilde{x},\tilde{\alpha})$ we obtain the WDF $F(x,u)$.

The experimental method was used to characterise aberrated laser beams produced by a Nd:YVO_4 laser with a pump power of $6.2W$ ($M^2 = 1.16$) (a) and $18W$ ($M^2 = 1.52$)(b) (Fig.6.5).

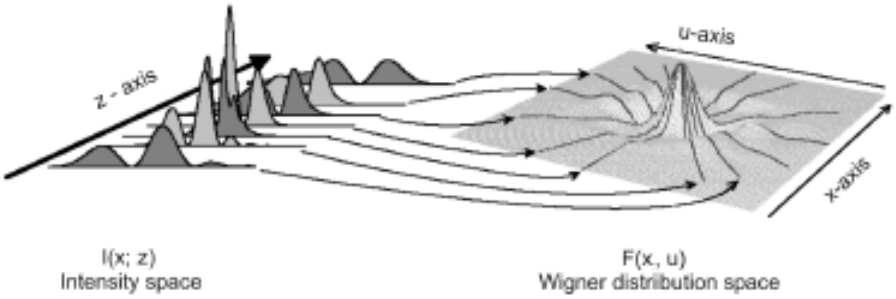


FIGURE 6.4: The Wigner distribution function whose section are obtained by several intensity distributions of the beam. Image courtesy of Jagus J. *et al* [87]

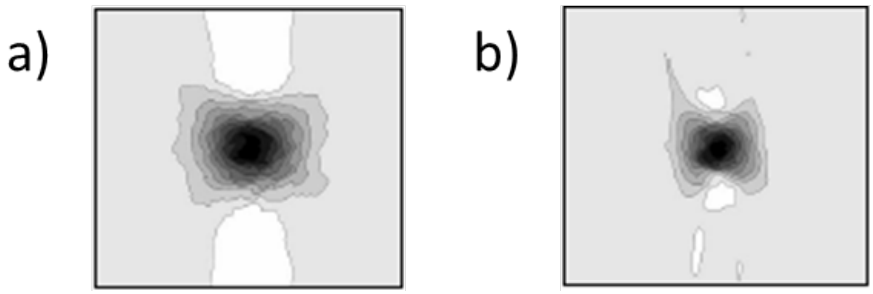


FIGURE 6.5: Generated WDF distributions. Image courtesy of Jagus J. *et al* [87]

Mukamel E. *et al* in [90] demonstrate an interferometric method that uses numerical integration instead of a slit, the experimental setup employs a shift and tilt technique by using a steering mirror. The experiment is based on rewriting the form of the equation of the WDF, given a light beam $u(x)$, the WDF of $u(x)$ is:

$$W(x,k) = \frac{1}{\pi^2}\int \langle u(x+\varepsilon)u^*(x-\varepsilon)\rangle \exp(2ik\varepsilon)d\varepsilon. \tag{6.5}$$

The above equation (Eq.6.5) can be rewritten as:

$$W(x,k) = \frac{1}{\pi^2}\langle \int u(x+\varepsilon)\exp(ik\varepsilon)[u(x-\varepsilon)\exp(-ik\varepsilon)]^*\rangle d\varepsilon, \tag{6.6}$$

where $\langle\cdot\rangle$ is the average operator, ε is the shift variable and k is the spatial frequency variable.

The function $u(x+\varepsilon)\exp(ik\varepsilon)$ is interpreted as a spatial shift of the function $u(x)$ by a quantity ε and an angular tilt by a quantity $k\varepsilon$ of the shifted beam $u(x+\varepsilon)$. The

WDF is then an overlap of two fields that are spatially shifted and angularly tilted, the overlap is obtained using a beam splitter. The WDF generation in this format is implemented using the interferometric set-up depicted in Fig.6.6. A real physical light beam $u(x, y)$ is incident on a steering mirror, the steering mirror is controlled to shift and tilt (angular shift) the beam in the x-direction. In each instance the beam is shifted by ε and tilted by $k_x\varepsilon$ where $k_x = 2\lambda/x$ and we obtain the function $u(x+\varepsilon)\exp(ik\varepsilon)$. The shifted plus tiled beam is then divided by a beam splitter into two beams which are directed to different ends of a Dove prism. The Dove prism rotates each beam by 90^o such that the total rotation is 180^o for both beams. The two beams then recombine at the beam splitter, they are then focused by a lens and their intensity is recorded by the detector. The detector records a set of planes $u(x, y)$ for each shift ε, to obtain a function in x and k, the planes are integrated along the y coordinate.

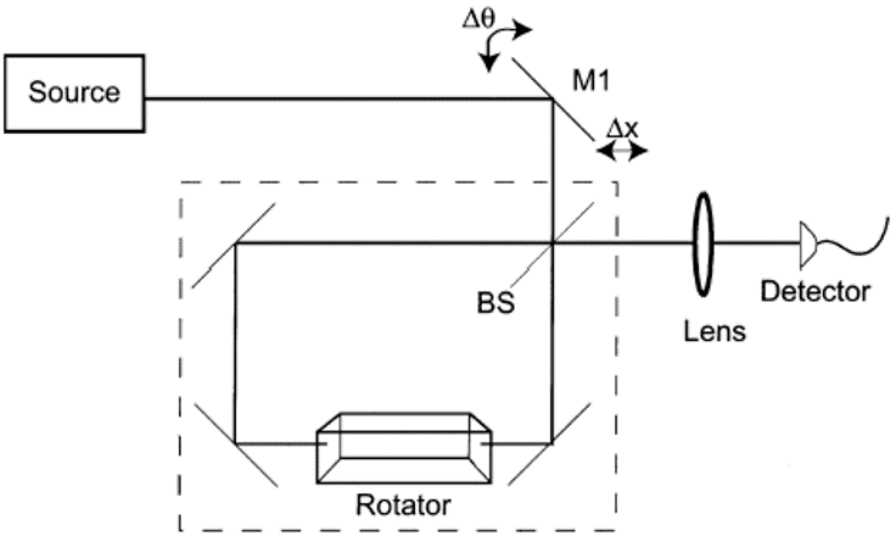


FIGURE 6.6: Interferometric WDF generation setup

The detector records the intensity:

$$\begin{aligned} I &= \left|u(x+\varepsilon)\exp(ik\varepsilon) + [u(x-\varepsilon)\exp(-ik\varepsilon)]^*\right|^2 \\ &= |u(x+\varepsilon)\exp(ik\varepsilon)|^2 + |[u(x-\varepsilon)\exp(-ik\varepsilon)]^*|^2 \\ &+ |u(x+\varepsilon)\exp(ik\varepsilon)[u(x-\varepsilon)\exp(-ik\varepsilon)]^*|^2 \\ &= I_1 + I_2 + I_{1,2} \end{aligned} \tag{6.7}$$

where:

$$\begin{aligned} I_1 &= |u(x+\varepsilon)\exp(ik\varepsilon)|^2, \\ I_2 &= |[u(x-\varepsilon)\exp(-ik\varepsilon)]^*|^2, \\ I_{1,2} &= |u(x+\varepsilon)\exp(ik\varepsilon)[u(x-\varepsilon)\exp(-ik\varepsilon)]^*|^2 \end{aligned} \tag{6.8}$$

The WDF is then determined using the equation:

$$I_{1,2} = \frac{\pi^2 \cos\varphi}{2} W(x,k). \tag{6.9}$$

Some results obtained from the experiment are presented in Fig.6.7 for a partially coherent collimated Gaussian beam (a), a slightly divergent Gaussian beam (b) and a Gaussian beam reflected off a glass wedge. The WDFs (a) and (b) were also found to have a degree of coherence $K^2 = 1.02$.

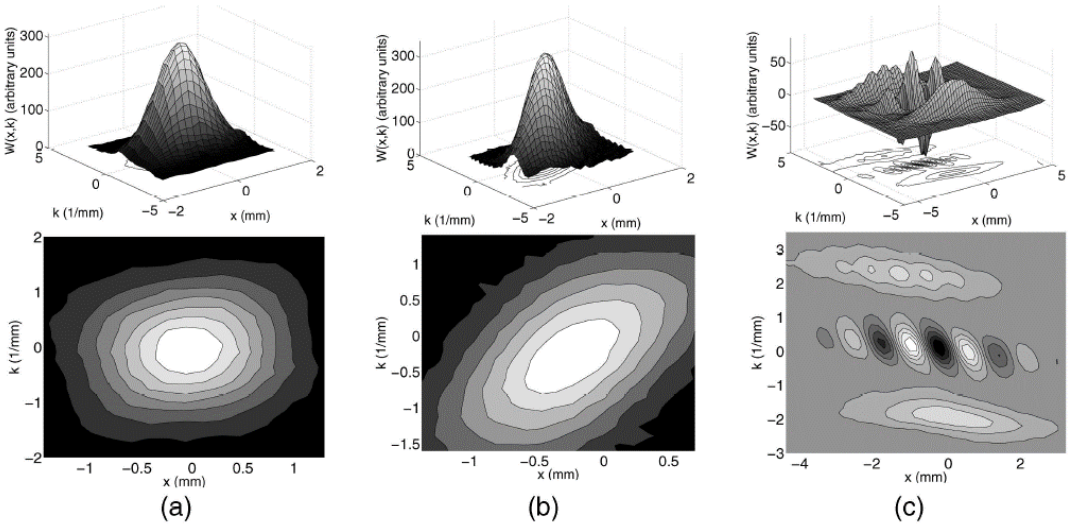


FIGURE 6.7: Interferometric WDF generation results. Image courtesy of Mukamel E. *et al* [90]

A similar shift method is employed on beams that are sectioned using an aperture in the papers [78, 72]. Instead of an entire beam shift, a slit/aperture is used instead to partition the beam into sections that are then transformed by shifting and tilting in the experimental setup (Fig.6.8).

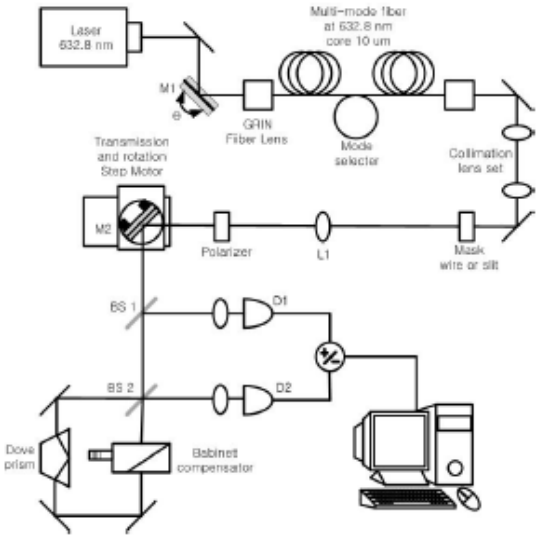


FIGURE 6.8: Sectional interferometric WDF generation. Image courtesy of Lee C. H. *et al et al* [72]

In the next chapter we present characterisation results we obtained from an experimental simulation of the interferometric WDF generation method and compare them to theoretical results.

6.3 Experimental simulation

We tested the WDF interferometric method on Laguerre Gaussian modes. From each beam we generated and determined the beam width, beam divergence and beam quality factor and compared the results to the results we obtained from the theoretical generation of the WDF. The steps followed in the simulation are as follows:

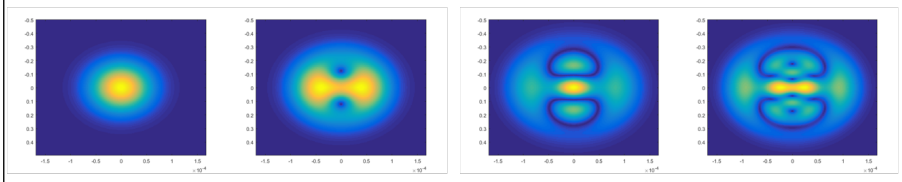
- We generate an LG beam.
- We apply n shifts on the beam by shifting the domain by a quantity $\mathbf{s}$. This process produces n planes, each shifted by $s_i \in \mathbf{s}$.
- The tilt on each plane is achieved by modulating each plane by a function $\exp(i\mathbf{ks})$.
- Each beam is then passed through a beam splitter that sends the two replicas of the beam to different ends of a Dove prism.
- The dove prism rotates the beams by 90^o each in opposite directions.

- The beams exit the Dove prism and are recombined in the beam splitter.
- The two rotated beams are then detected by a camera. The detected intensity contains the term $I_{1,2}$ which is used to determine the WDF.

Theoretically, using marginal distributions obtained from the WDF, we get similar results to those obtained from the field function characterisation. We generated and characterised the beams in Fig.6.9. The simulation was carried out using MATLAB

Simulation results

Generated WDF



$l = 0, p = 0$ $l = 1, p = 0$ $l = 1, p = 1$ $l = 1, p = 1$

Mode(l,p)	n	$w(m)$	$\theta(mrad)$	M^2
0,0	280	8.0306×10^{-5}	0.0026	1.0337
1,0	250	1.1293×10^{-4}	0.0036	2.0451
0,1	250	1.4620×10^{-4}	0.0043	3.1507
1,1	250	1.6736×10^{-4}	0.0046	4.0295

Expected results

Mode	$w_0(m)$	$\theta(mrad)$	M^2
LG_0^0	8.0×10^{-5}	0.0025	1
LG_0^1	1.1314×10^{-4}	0.0036	3
LG_1^0	1.3856×10^{-4}	0.0044	2
LG_1^1	1.6×10^{-4}	0.0050	4

FIGURE 6.9: Results obtained from the experimental simulation and the expected theoretical results

and there are a couple of notes on some of the parameters used for the simulation. The fundamental Gaussian waist size and the pixel size were kept constant throughout the simulation, the grid points were varied for specific modes for which we will indicate on the results due to fluctuations in the resultant beam divergence. The results obtained from the experiment simulation negligibly vary from the theoretical results and are given in Fig.6.9 (expected results) where w is the beam waist, θ the beam divergence, n the number of grid points used and M^2 the beam quality factor. By varying the number of grid points we managed to get as close as possible to the exact WDFs for the various beams, the differences are negligible. By using the same

parameters in the analysis, we can analyse data obtained from a physical setup and characterise it with reasonable accuracy.

The simulation of the experimental generation of the WDF is important in that it allows us to predict the results we can obtain from the experiment and to confirm that the experimental method works. In this chapter we explored the common sectional methods used to generate the WDF, using transparencies, the inverse Radon transform and an interferometric method. The interferometric generation method was simulated and the results show negligible variance from the theory obtained results. The experimental simulation shows comparable results to what we expect from theoretical generation of the WDF, the differences in the results are negligible and can be minimized by choosing the optimal grid and pixel sizes. In the next chapter we explore the physical generation of the WDF by performing the interferometric experiment.

7 Experiment and future work

7.1 Introduction

In this initial work we generated the WDF experimentally as outlined by Mukamel *et.al* in [90]. The experiment followed a similar scheme to the simulated experiment from which we obtained comparable results to theory and the results obtained will be improved by taking into consideration recommendations explained in conclusion.

The experiment requires a combination of physical shifting (s) and tilting ($u_x s$) techniques with the aim of obtaining the product:

$$F(x,s) = E\big(x+\frac{1}{2}s\big)E\big(x-\frac{1}{2}s\big)\exp(-iu_x s), \tag{7.1}$$

for an optical field $E(x)$. The product $F(x,s)$ is then integrated with respect to the shifting variable s to obtain a WDF $W(x,u_x)$. The experiment focused on the generation and characterisition of WDFs of a Gaussian and vortex beams which were generated using the Laguerre-Gaussian equation cited in [95] encoded digitally on a phase-only SLM screen. The SLM encodes information using pixels on the SLM screen with a pixel size of 8.8μm, the pixel size is used as a basis for the set of shifts employed in generating the WDF. The experiment was carried out by enlarging, using a 10x objective, and collimating a laser beam produced by an He:Ne laser with a wavelength of 633nm to ensure we have a big enough beam to cover the SLM screen. As demonstrated in Fig.7.1, a mirror that is positioned at a distance 500mm from the laser is used to project the laser beam onto the objective. The resultant beam propagates through a pair of (40mm and 500mm) lenses and is projected onto the SLM screen as an enlarged beam. The enlarged beam is characterised by a flat wave-front and can be approximated as a plane wave over the entire SLM screen.

The SLM screen was digitally encoded with phase patterns of a Gaussian and vortex beams, the screen was irradiated with the collimated oncoming beam such that at the Fourier plane we obtained the physical encoded Gaussian and vortex beams.. The beams are then focused on a steering mirror and sent into the interferometric set-up (Fig.7.1). The steering mirror directs the beam into the interferometric set-up which is split by a 50:50 intensity beam splitter to create two copies which are manipulated to generate the WDF.

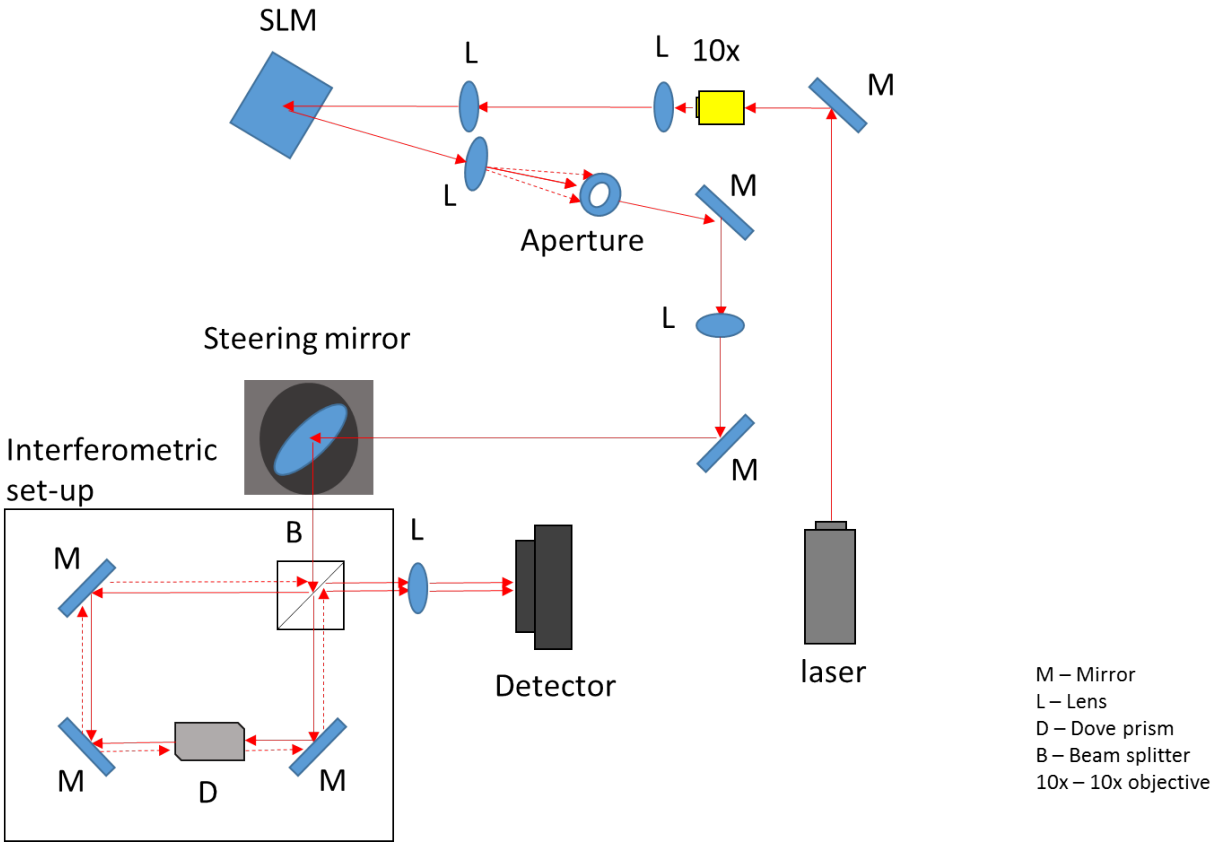


FIGURE 7.1: The WDF generation experimental set-up

7.1.1 Interferometric set-up

The steering mirror is mounted on a translation stage that allows for a vertical (y), a horizontal (x) and also a horizontally angular shift $(\theta_x) = u_x s$, it can be adjusted to shift and tilt an incoming beam in the μm and μrad regions. The

interferometric set-up employs a dove prism through which the two beams split by the beam splitter undergo a total πrad rotation. Achieving a WDF of good resolution was of huge importance in the experiment, the clarity of the generated WDF is directly proportional to the size of the set of position and angular shifts. Due to equipment constraints, a set of size 40 was chosen for the set:

$$\mathbf{s} = \{s | s \in [-200\mu m, 200\mu m]\}, \tag{7.2}$$

in steps of 10 μm. And the angular shift set of size 11 was:

$$\theta = \{\theta_s | \theta_s \in [-0.0045\text{rad}, 0.0040\text{rad}]\}, \tag{7.3}$$

in steps of 0.0007rad. A combination of the shifts and tilts from the experiment are demonstrated in Fig.7.2.

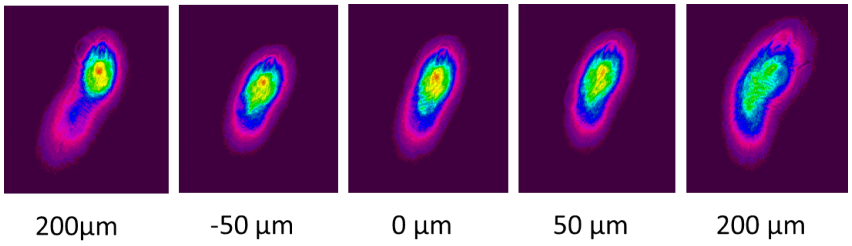


FIGURE 7.2: Position shifting the two Gaussian beams of opposite orientation at 0rad angular shift

The shifting and tilting processes coupled with the axis rotation inside the dove prism results in the two beams drifting away from each other simultaneously in the horizontal and vertical directions. We first generated the WDF of a Gaussian beam whose WDF plot is demonstrated in Fig.7.3. The initial generation was carried out using a smaller position shift set of size 20 and angular shift size of 4, the resultant WDF was a plot of very low resolution and only a small portion of the expected WDF mapping. Increasing the size of the position shift and angular shifts to 40 and 11 respectively improved the recovered beam width 0.105mm from 0.0442mm, at an expected beam width of 1.5mm.

The same process was repeated for a vortex beam generated in a similar process as the Gaussian beam using an SLM. The shift and tilt images are as shown in Fig.7.4

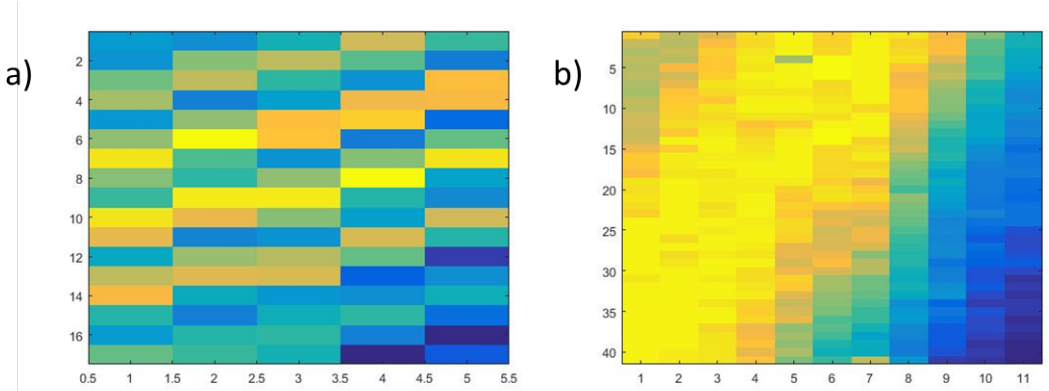


FIGURE 7.3: Experimentally generated WDFs of a Gaussian beam for a positional and angular shift set size of a) 20 and 4, b) 40 and 11, respectively.

where the vortex beam demonstrates a similar horizontal plus vertical drift as we approach the end of the shift and tilt sets.

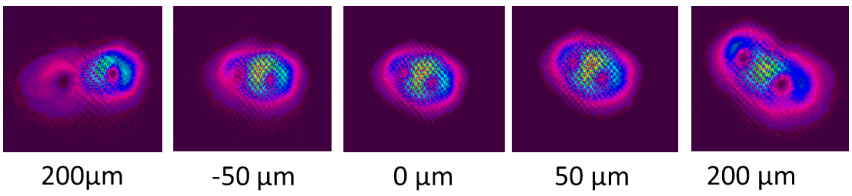


FIGURE 7.4: Position shifting the two vortex beams of opposite orientation at 0rad angular shift

The recovered WDF using a set size of 40 (position shift) and 11 (angular shift) was found as shown in Fig.7.5 for a starting beam width of 1.5mm, the recovered WDF was found to have a beam width of 0.105mm and a beam quality of 1.5×10^{-6}, both a fraction of the expected beam width (1.5mm) and beam quality factor(1).

Fig.7.5a is a fraction of Fig.7.5b which could just be a line across the centre, a better figure can be obtained by increasing the positional and angular shifts. Both the positional and angular shift sets were set at 200 points which was also the set size of the beam domain, from this simulation we obtained a beam width of 2.1mm and a beam quality factor of 2.1 which are comparable to the expected vortex beam parameters of a starting Gaussian waist size of 1.5mm. We also simulated a experiment using the actual experiment sets and we obtained a beam width of 0.13mm and beam quality factor of 1.82×10^{-6} which are comparable to the experimental results.

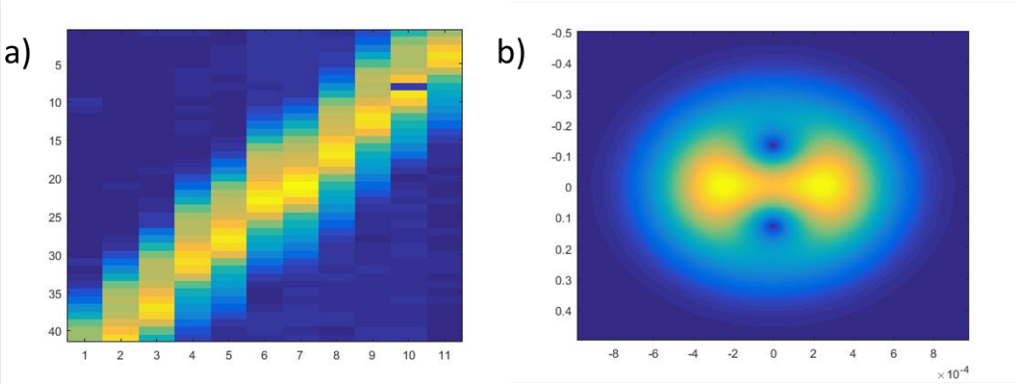


FIGURE 7.5: a) The experimentally generated WDF of a vortex beam b) The expected WDF of a vortex beam.

7.2 Summary and discussion

In this chapter we generated the WDF of a Gaussian beam and a vortex beam using a tilt-shift experiment. The results obtained were found to be a fraction of the results we expect, for the Gaussian beam we obtained a beam width and beam quality factor of 0.105mm and 1.5×10^{-6} versus the expected 1.5mm beam width and beam quality factor of 1. On the vortex beam we obtained a beam width of 0.13mm instead of 2.12mm and a beam quality factor of 1.82×10^{-6} instead of 2. Better results can be achieved by increasing the number of positional and angular shifts as demonstrated (Fig.7.5) in the simulation of the experiment in which we used a shift set size equal to the domain used to generate the beam. For future work we plan to find better ways to structure our positional and angular shifts. One of the main reasons we worked with the sets we worked with was because of limitations in equipment. For the size of the beams we generated, the mirrors in the interferometric set-up were not big enough to accommodate a broader set of shifts, beyond a certain number of shifts the beam would fall off the mirrors completely. Other ideas that can be explored to increase the number of shifts are using smaller beams or decrease the steps between shifts. We also plan to experimentally generate and characterise the WDF of a partially coherent beam.

8 Conclusion

We explored the Wigner Distribution Function (WDF) as a means to better the characterisation process of arbitrary beams of varying coherence. In Chapter 1 we introduced the fundamentals of wave and laser theory. Laser devices generally produce a beam of light concentrated on a small area that does not expand much over a certain distance. These beams of light can be described using paraxial approximation which is derived from wave theory. The generation of a laser beam requires 3 main processes namely absorption, spontaneous emission and stimulated emission, all of which depend on the the ability of the population of atoms in the gain medium of a laser resonator to absorb and emit photons. We also gave a brief formulation of the fundamental Gaussian beam and higher order beams, mainly the Laguerre-Gaussian beams in circular symmetry and the Hermite-Gaussian beams in rectangular symmetry.

The characterisation of general beams was explored in chapter 2. The propagation and interaction of light rays with optical systems informs the propagation and interaction of the fundamental Gaussian beam with optical systems. We explored parameters of the Gaussian beam in both the theoretic and physical context, the beam width, divergence and the radius of curvature. These parameters are used to identify the order of the Laguerre-Gaussian and Hermite-Hermite Gaussian beams using the beam quality factor. The beam quality factor is a measure of how the beam width of some higher order mode deviates from that of the fundamental Gaussian mode in free space propagation. Beam moments are used to denote beam parameters which are obtained by applying the 2σ method of integrating the area under the intensity distribution, this method can be used to calculate the beam centre and beam width in the spatial and Fourier planes.

The underlying theory of partially coherent beams is explained using probability theory in Chapter 3. The changes in intensity a partially coherent beam undergoes over a specific period of time are random. A measure of this randomness is important in describing partially coherent beams and the degree of coherence is used as a measure of the randomness. In this chapter we introduced the mutual coherence function which is a general description of light that takes into account coherence effects, the mutual coherence function allows us to characterize a partially coherent beam using beam moments. The Gauss-Schell model beam was also introduced as an example of a partially coherent beam.

Phase-space optics is a field in optics that unifies geometric and space optics while retaining the unique features of each concept. In Chapter 4 we introduced the Wigner Distribution Function (WDF) which is a phase-space function that combines the spatial and propagation properties of a beam. The WDF is convenient for the characterisation of partially coherent beams because it takes into account the statistical features of a beam and employs the mutual coherence function. Beam moments are applied to a single WDF plot to obtain the beam parameters needed to calculate the beam quality factor.

In Chapter 5 we carried out simulations using the theoretical expressions for the WDF for characterisation tests and the results showed comparable accuracy to the expected results. The simulations were tested for a variety of coherent beams including the fundamental Gaussian beam and the vortex beam. For the partially coherent case we generated and characterised Gauss-Schell model beams of varying coherence.

Our preliminary WDF experimental simulation results in Chapter 6 obtained from a set of coherent Laguerre-Gaussian beams and also a partially coherent Gauss-Schell model beam were similar to results obtained in Chapter 5, proving that the WDF is an effective characterisation method. To generate the WDF experimentally with real physical beams requires a set of techniques to mitigate the increase in dimension including the Radon-transform method and the various sectional generation methods

[89, 87, 91]. We employed a sectional method to generate the WDF of both a Gaussian beam and vortex beam. The results obtained from our experiment highlighted the need for a better means to obtain a broader positional and angular shift set, the set we employed in our experiment generated a low resolution WDF. A better resolution was obtained by increasing the set. The simulated experiment using a broader set of positional and angular shifts showed comparable results to what we expect for our said beams.

Bibliography

[1] Melvin Lax, William H Louisell, and William B McKnight. "From Maxwell to paraxial wave optics". In: *Physical Review A* 11.4 (1975), p. 1365.

[2] Max Born and Emil Wolf. *Principles of Optics: Electromagnetic Theory of Propagation, Interference and Diffaction of Light*. Pergamon Press, 1959.

[3] Norman Hodgson and Horst Weber. *Laser Resonators and Beam Propagation: Fundamentals, Advanced Concepts, Applications*. Vol. 108. Springer, 2005.

[4] Max Born and Emil Wolf. *Principles of optics: electromagnetic theory of propagation, interference and diffraction of light*. Elsevier, 2013.

[5] Dennis G Zill. *Differential equations with boundary-value problems*. Nelson Education, 2016.

[6] Anthony E Siegman and Robert C Hilborn. *Lasers*. 1998.

[7] Bahaa EA Saleh, M Carl Teich, and E Bahaa Saleh. *Fundamentals of photonics*. Vol. 22. Wiley New York, 1991.

[8] Pablo Vaveliuk, Beatriz Ruiz, and Alberto Lencina. "Limits of the paraxial approximation in laser beams". In: *Optics letters* 32.8 (2007), pp. 927–929.

[9] Krishnan Thyagarajan and Ajoy Ghatak. *Lasers: fundamentals and applications*. Springer Science & Business Media, 2010.

[10] Miguel A Porras, Javier Alda, and Eusebio Bernabeu. "Complex beam parameter and ABCD law for non-Gaussian and nonspherical light beams". In: *Applied optics* 31.30 (1992), pp. 6389–6402.

[11] Herwig Kogelnik and Tingye Li. "Laser beams and resonators". In: *Proceedings of the IEEE* 54.10 (1966), pp. 1312–1329.

[12] Jean-Pierre Guigay. "On Fresnel diffraction by one-dimensional periodic objects, with application to structure determination of phase objects". In: *Journal of Modern Optics* 18.9 (1971), pp. 677–682.

[13] George B Thomas et al. *Thomas' Calculus: Early Transcendentals*. Pearson Boston, 2010.

[14] James Stewart. *Calculus*. Cengage Learning, 2011.

[15] Anthony E Siegman. "Defining the effective radius of curvature for a nonideal optical beam". In: *IEEE Journal of Quantum Electronics* 27.5 (1991), pp. 1146–1148.

[16] Emil Wolf. "New theory of partial coherence in the space–frequency domain. Part I: spectra and cross spectra of steady-state sources". In: *JOSA* 72.3 (1982), pp. 343–351.

[17] Vasudevan Lakshminarayanan, María L Calvo, and Tatiana Alieva. *Mathematical Optics: Classical, Quantum, and Computational Methods*. CRC Press, 2012.

[18] PA Bélanger. "Beam propagation and the ABCD ray matrices". In: *Optics letters* 16.4 (1991), pp. 196–198.

[19] Ajoy K Ghatak. *Contemporary optics*. Springer Science & Business Media, 2012.

[20] Philip E Ciddor. "Refractive index of air: new equations for the visible and near infrared". In: *Applied optics* 35.9 (1996), pp. 1566–1573.

[21] P Schiebener et al. "Refractive index of water and steam as function of wavelength, temperature and density". In: *Journal of physical and chemical reference data* 19.3 (1990), pp. 677–717.

[22] W Hou and R Thalmann. "Accurate measurement of the refractive index of air". In: *Measurement* 13.4 (1994), pp. 307–314.

[23] Michael P Schellekens et al. "Measurements of the refractive index of air using interference refractometers". In: *Metrologia* 22.4 (1986), p. 279.

[24] Nicolaas Bloembergen and PS Pershan. "Light waves at the boundary of nonlinear media". In: *Physical Review* 128.2 (1962), p. 606.

[25] Tae Moon Jeong, Do-Kyeong Ko, and Jongmin Lee. "Generalized ray-transfer matrix for an optical element having an arbitrary wavefront aberration". In: *Optics letters* 30.22 (2005), pp. 3009–3011.

[26] I Moreno et al. "Teaching Fourier optics through ray matrices". In: *European journal of physics* 26.2 (2005), p. 261.

[27] Jeffrey A Davis and Roger A Lilly. "Ray-matrix approach for diffractive optics". In: *Applied optics* 32.2 (1993), pp. 155–158.

[28] Michael W Sasnett and Timothy J Johnston. "Beam characterization and measurement of propagation attributes". In: *Laser Beam Diagnostics*. Vol. 1414. International Society for Optics and Photonics. 1991, pp. 21–33.

[29] Simin Feng and Herbert G Winful. "Physical origin of the Gouy phase shift". In: *Optics letters* 26.8 (2001), pp. 485–487.

[30] Taco D Visser and Emil Wolf. "The origin of the Gouy phase anomaly and its generalization to astigmatic wavefields". In: *Optics Communications* 283.18 (2010), pp. 3371–3375.

[31] Ricardo Borghi and Massimo Santarsiero. "M 2 factor of Bessel–Gauss beams". In: *Optics letters* 22.5 (1997), pp. 262–264.

[32] Degang Deng et al. "Far-field intensity distribution and M 2 factor of hollow Gaussian beams". In: *Applied optics* 44.33 (2005), pp. 7187–7190.

[33] N Passilly, G Martel, and K Aït-Ameur. "Beam propagation factor of truncated laguerre—gauss beams". In: *Journal of Modern Optics* 51.15 (2004), pp. 2279–2286.

[34] J Martin Bland and Douglas G Altman. "Statistics notes: measurement error". In: *Bmj* 313.7059 (1996), p. 744.

[35] Orazio Svelto and David C Hanna. *Principles of lasers*. Vol. 4. Springer, 1998.

[36] I-IOf Standardization. "ISO 11146-2". In: *ISO/TC* 172 (2005).

[37] D Wright et al. "Laser beam width, divergence and beam propagation factor—an international standardization approach". In: *Optical and Quantum Electronics* 24.9 (1992), S993–S1000.

[38] Ari T Friberg and Ronald J Sudol. "Propagation parameters of Gaussian Schell-model beams". In: *Optics Communications* 41.6 (1982), pp. 383–387.

[39] John T Foley and MS Zubairy. "The directionality of Gaussian Schell-model beams". In: *Optics Communications* 26.3 (1978), pp. 297–300.

[40] Jennifer C Ricklin and Frederic M Davidson. "Atmospheric turbulence effects on a partially coherent Gaussian beam: implications for free-space laser communication". In: *JOSA A* 19.9 (2002), pp. 1794–1802.

[41] Larry C Andrews and Ronald L Phillips. *Laser beam propagation through random media*. Vol. 1. SPIE press Bellingham, WA, 2005.

[42] Nikola V Krylov. *Introduction to the theory of random processes*. Vol. 43. American Mathematical Soc., 2002.

[43] Athanasios Papoulis and Unnikrishna S Pillai. *Probability, random variables, and stochastic processes*. Tata McGraw-Hill Education, 2002.

[44] Joseph L Doob. *Stochastic processes*. Vol. 7. 2. Wiley New York, 1953.

[45] Steven E Shreve. *Stochastic calculus for finance II: Continuous-time models*. Vol. 11. Springer Science & Business Media, 2004.

[46] William A Gardner. *Introduction to Random Processes: with applications to signals and systems*. Macmillan Publishing Company, 1986.

[47] Howard Anton. *Elementary linear algebra*. John Wiley & Sons, 2010.

[48] Bhagwandas P Lathi. *Signal processing and linear systems*. Oxford university press New York, 1998.

[49] Seymour Lipschutz and Marc Lipson. *Schaum's outline of theory and problems of linear algebra*. Erlangga, 2001.

[50] Tomohiro Shirai, Olga Korotkova, and Emil Wolf. "A method of generating electromagnetic Gaussian Schell-model beams". In: *Journal of Optics A: Pure and Applied Optics* 7.5 (2005), p. 232.

[51] Bryan Hennelly, Jorge Ojeda-Castañeda, and Markus Testorf. *Phase Space Optics: Fundamentals and Applications*. 2009.

[52] Martin J Bastiaans. "A frequency-domain treatment of partial coherence". In: *Journal of Modern Optics* 24.3 (1977), pp. 261–274.

[53] Martin J Bastiaans. "Signal description by means of a local frequency spectrum". In: *Transformations in Optical Signal Processing*. Vol. 373. International Society for Optics and Photonics. 1984, pp. 49–63.

[54] Eugene Wigner. "On the quantum correction for thermodynamic equilibrium". In: *Physical review* 40.5 (1932), p. 749.

[55] A Walther. "Radiometry and coherence". In: *JOSA* 58.9 (1968), pp. 1256–1259.

[56] Tatiana Alieva et al. "Wigner distribution moments for beam characterization". In: *Mathematical Optics: Classical, Quantum, and Computational Methods* (2012), p. 13.

[57] Martin J Bastiaans. "The Wigner distribution function applied to optical signals and systems". In: *Optics communications* 25.1 (1978), pp. 26–30.

[58] David L Andrews. *Photonics, Volume 1: Fundamentals of Photonics and Physics*. Vol. 2. John Wiley & Sons, 2015.

[59] Mingui Sun et al. "Elimination of cross-components of the discrete pseudo Wigner distribution via image processing". In: *Acoustics, Speech, and Signal Processing, 1989. ICASSP-89., 1989 International Conference on.* IEEE. 1989, pp. 2231–2233.

[60] Gabriel Cristóbal, Consuelo Gonzalo, and Julián Bescós. "Image filtering and analysis through the Wigner distribution". In: *Advances in Electronics and Electron physics.* Vol. 80. Elsevier, 1991, pp. 309–397.

[61] John L Semmlow and Benjamin Griffel. *Biosignal and medical image processing.* CRC press, 2014.

[62] Azeddine Beghdadi and Béatrice Pesquet-Popescu. "A new image distortion measure based on wavelet decomposition". In: *Signal Processing and Its Applications, 2003. Proceedings. Seventh International Symposium on.* Vol. 1. IEEE. 2003, pp. 485–488.

[63] Martin J Bastiaans et al. *Wigner distribution in optics.* 2009.

[64] Daniela Dragoman. "Applications of the Wigner distribution function in signal processing". In: *EURASIP Journal on Advances in Signal Processing* 2005.10 (2005), p. 264967.

[65] Yao Li, George Eichmann, and Michael Conner. "Optical Wigner distribution and ambiguity function for complex signals and images". In: *Optics communications* 67.3 (1988), pp. 177–179.

[66] WH Carter and E Wolf. "Coherence and radiometry with quasihomogeneous planar sources". In: *JOSA* 67.6 (1977), pp. 785–796.

[67] EW Marchand and E Wolf. "Radiometry with sources of any state of coherence". In: *JOSA* 64.9 (1974), pp. 1219–1226.

[68] L Mandel and E Wolf. "Spectral coherence and the concept of cross-spectral purity". In: *JOSA* 66.6 (1976), pp. 529–535.

[69] L Mandel. "Concept of cross-spectral purity in coherence theory". In: *JOSA* 51.12 (1961), pp. 1342–1350.

[70] Martin J Bastiaans. "Wigner distribution function applied to partially coherent light". In: *Laser Beam Characterization* (1993), pp. 65–87.

[71] Miguel A Alonso. "Wigner functions in optics: describing beams as ray bundles and pulses as particle ensembles". In: *Advances in Optics and Photonics* 3.4 (2011), pp. 272–365.

[72] Chang-Hyuck Lee et al. "Analysis of Propagating Beam Transverse-mode Evolution by Using the Wigner Distribution Function". In: *Journal of the Korean Physical Society* 56.6 (2010), pp. 1781–1786.

[73] R Gase. "Representation of Laguerre-Gaussian modes by the Wigner distribution function". In: *IEEE journal of quantum electronics* 31.10 (1995), pp. 1811–1818.

[74] Rui-Pin Chen, Hong-Ping Zheng, and Chao-Qing Dai. "Wigner distribution function of an Airy beam". In: *JOSA A* 28.6 (2011), pp. 1307–1311.

[75] Gal Shabtay, David Mendlovic, and Zeev Zalevsky. "Proposal for optical implementation of the Wigner distribution function". In: *Applied optics* 37.11 (1998), pp. 2142–2144.

[76] Richard Bamler and Helmut Glünder. "The Wigner distribution function of two-dimensional signals coherent-optical generation and display". In: *Journal of Modern Optics* 30.12 (1983), pp. 1789–1803.

[77] Nikola Subotic and Bahaa EA Saleh. "Generation of the Wigner distribution function of two-dimensional signals by a parallel optical processor". In: *Optics letters* 9.10 (1984), pp. 471–473.

[78] Chang-Hyuck Lee, Yoonshik Kang, and Jaewoo Noh. "Measurement of coherence and beam parameter of a propagating laser beam by using wigner distribution function measurement". In: *Applied Physics Express* 2.3 (2009), p. 032402.

[79] Zabih Ghassemlooy, Wasiu Popoola, and Sujan Rajbhandari. *Optical wireless communications: system and channel modelling with Matlab®*. CRC press, 2012.

[80] Jason Daniel Schmidt. "Numerical simulation of optical wave propagation with examples in MATLAB". In: SPIE Bellingham, Washington, USA. 2010.

[81] Ting-Chung Poon and Taegeun Kim. *Engineering Optics with MATLABÂ®*. World Scientific Publishing Co Inc, 2006.

[82] William H Press. *Numerical recipes 3rd edition: The art of scientific computing*. Cambridge university press, 2007.

[83] Peter J Acklam. "MATLAB array manipulation tips and tricks". In: *Statistics Division* (2000).

[84] Joseph W Goodman. *Statistical optics*. John Wiley & Sons, 2015.

[85] Ronald N Bracewell. *The Fourier transform and its applications*. Vol. 31999. McGraw-Hill New York, 1986.

[86] Angela Dudley et al. "Implementing digital holograms to create and measure complex-plane optical fields". In: *American Journal of Physics* 84.2 (2016), pp. 106–112.

[87] Jarosław Jaguś, Jan K Jabczyński, and Waldemar Żendzian. "Application of Wigner transform for characterization of aberrated laser beams". In: *14th Slovak-Czech-Polish Optical Conference on Wave and Quantum Aspects of Contemporary Optics*. Vol. 5945. International Society for Optics and Photonics. 2006, p. 594519.

[88] Walter D Furlan, Carlos Soriano, and Genaro Saavedra. "Opto-digital tomographic reconstruction of the Wigner distribution function of complex fields". In: *Applied optics* 47.22 (2008), E63–E67.

[89] K-H Brenner and AW Lohmann. "Wigner distribution function display of complex 1D signals". In: *Optics Communications* 42.5 (1982), pp. 310–314.

[90] Eran Mukamel et al. "Direct measurement of the spatial Wigner function with area-integrated detection". In: *Optics letters* 28.15 (2003), pp. 1317–1319.

[91] Bernd Eppich and Norbert Reng. "Measurement of the Wigner distribution function based on the inverse Radon transformation". In: *Proc. SPIE*. Vol. 2375. 1995, pp. 261–268.

[92] G Nemes. "Measuring and handling general astigmatic beams". In: *Laser Beam Characterization* (1993), pp. 325–358.

[93] Alejandro Cámara et al. "Phase space tomography reconstruction of the Wigner distribution for optical beams separable in Cartesian coordinates". In: *JOSA A* 26.6 (2009), pp. 1301–1306.

[94] Peter Toft. "The Radon transform. Theory and implementation". In: (1996).

[95] Christian Schulze et al. "Modal analysis of beams emerging from a multicore fiber using computer-generated holograms". In: *SPIE LASE*. International Society for Optics and Photonics. 2011, 79142H–79142H.